THE ROLE OF HORMONE-SENSITIVE LIPASE AND KIAA1363 IN LIPID METABOLISM OF MOUSE PERITONEAL MACROPHAGES

Mag. Marlene Buchebner
Institute of Molecular Biology and Biochemistry
Center of Molecular Medicine, Medical University of Graz

Dissertation submitted at the Medical University of Graz
for the degree of Doctor of medical science (Dr. scient. med.)

Graz, Juli 2009

Acknowledgement

This doctoral thesis was performed at the Institute of Molecular Biology and Biochemistry at the Medical University of Graz within the GEN-AU project (Genomics of Lipid-associated Disorders - GOLD) supported by the Austrian Federal Ministry of Science and Research and a project supported by the Austrian Science Fund FWF (P19186). First of all I want to thank my great supervisor **Prof. Dr. Dagmar Kratky** for giving me the possibility to compose my doctoral thesis at the Medical University of Graz under her strong support. Furthermore, I want to thank Prof. Gerhard Kostner and Prof. Sanja Levak-Frank for their encouragement and critical discussions.

Special thanks go to my colleagues for their fruitful discussions and excellent working climate, especially to Nora Rathke, Thomas Pfeifer, Adelheid Kratzer, Prakash Chandak, Sascha Obrowsky, Anton Ibovnik, Silvia Povoden and Elisabeth Stanzer.

Moreover, I thank my collaborators Achim Lass, Isabella Hindler, Dagmar Kolb, Renate Schreiber and Heimo Wolinski for their experimental help and assistance.

Last but not least I thank my parents, Manfred, my sister and my friends for their moral encouragement and conversations in good as well as in bad times.

For my parents

AFFIDAVIT

I hereby declare that this doctoral thesis has been written independently and completely on my own and without any assistance from third parties.
Furthermore, I confirm that no sources have been used in the preparation of this thesis other than those indicated in the thesis itself.

Graz, July 2009

_____

Mag. Marlene Buchebner

Summary

Atherosclerosis is the most common cause for stroke and cardiovascular disease in westernized societies. Different cell types including monocytes, smooth muscle cells and macrophages play a central role in this multifactorial disease. Macrophages are able to take up modified low density lipoprotein via scavenger receptors and store tremendous amounts of cholesteryl esters (CE) in lipid droplets leading to foam cell formation, which is one of the earliest and important step in the initiation and progression of atherosclerosis. Foam cells are able to mobilize massive lipid deposition by the action of a neutral CE hydrolase. Due to the importance of this enzyme activity in macrophages and conflicting publications over 40 years I compared the lipolytic activities of two suggested neutral CE hydrolases in mouse peritoneal macrophages: hormone-sensitive lipase (HSL) and KIAA1363.

First I determined the gene expression profiles of these two genes in several mouse tissues and cells in regard to any sex-specific differences in macrophages and foam cells by quantitative real time PCR. Furthermore, the enzyme activities against CE, triglycerides, diglycerides and acetyl monoalkylglycerol ether (AcMAGE) in COS-7 cells overexpressing HSL and KIAA1363 were investigated. Whereas HSL cleaved all substrates, KIAA1363 was only able to hydrolyze AcMAGE *in vitro*. For *in vivo* studies, HSL- deficient and KIAA1363-deficient mice were used. I found nearly abolished neutral CE hydrolase activity in all cells and tissues of HSL-deficient mice and reduced AcMAGE hydrolase activities in macrophages and some tissues of KIAA1363- deficient mice. Moreover, I could show that HSL is localized in the cytosol and next to lipid droplets. In macrophages KIAA1363 gene expression is influenced by lipopolysaccharide stimulation.

The results demonstrate the functional presence of HSL as a neutral CE hydrolase in murine macrophages but, due to the unchanged lipid content in macrophages of HSL- deficient mice, another mechanism, other compartments and/or other enzymes cooperate with HSL to regulate CE levels in macrophages *in vivo*. In contrast, KIAA1363 might be an important AcMAGE hydrolase in MPM, but does not hydrolize CE *in vitro* or *in vivo*.

Zusammenfassung

Atherosklerose ist die häufigste Ursache für Schlaganfall und kardiovaskuläre Erkrankungen in der westlichen Welt. In dieser multifaktoriellen Erkrankung spielen verschiedene Zelltypen (wie zum Beispiel Monozyten, Makrophagen und glatte Muskelzellen) eine zentrale Rolle. Arterielle Makrophagen sind in der Lage modifizierte Lipoproteine über verschiedene Rezeptoren aufzunehmen und speichern überschüssiges Cholesterin als Cholesterinester (CE) in Lipidtröpfchen. Dadurch kommt es zur sogenannten „Schaumzellbildung", die eine der ersten und wichtigsten Ereignisse in der Entstehung der Atherosklerose darstellt. Neutrale CE-Hydrolasen hingegen können die gespeicherten CE hydrolysieren und in Folge mobilisieren und so der Schaumzellbildung entgegen wirken. Durch die Wichtigkeit dieser Enzymaktivität in Makrophagen und die widersprüchlichen Publikationen auf diesem Gebiet in den letzten vierzig Jahren habe ich in dieser Arbeit die unterschiedlichen lipolytischen Aktivitäten der hormonsensitiven Lipase (HSL) und KIAA1363 untersucht.

Zuerst bestimmte ich das Expressionsmuster beider Kandidatengene in verschiedenen Geweben der Maus mittels quantitativer PCR und habe dabei auch auf geschlechtsspezifische Unterschiede geachtet. Weiters untersuchte ich die CE-, Triglyzerid-, Diglyzerid-, Retinolester (RE)-, und Acetyl-monoalkylglyzerinether (AcMAGE)-Hydrolaseaktivitäten von Zelllysaten mit überexprimierter HSL und KIAA1363. HSL spaltete alle Substrate, während KIAA1363 nur RE und AcMAGE hydrolysieren konnte. Für *in vivo* Versuche wurden HSL- und KIAA1363-defiziente Mäuse verwendet. Zellen und Gewebe von HSL-defizienten Mäusen zeigten fast keine neutrale CE-Hydrolaseaktivität, wobei KIAA1363-defiziente Mäuse reduzierte AcMAGE-Hydrolaseaktivität in Makrophagen und einigen Geweben aufwiesen. Ausserdem konnte ich in dieser Arbeit die Lokalisation der HSL im Cytosol und in der Nähe von Lipidtröpfchen im Makrophagen nachweisen und zeigen, dass die Genexpression von KIAA1363 durch Lipopolysaccharidstimulation beeinflusst wird.

Die Resultate zeigen, dass HSL eine, wenn gleich auch nicht die einzige, neutrale CE-Hydrolase im Mausmakrophagen ist. Im Vergleich dazu spielt KIAA1363 eine Rolle als AcMAGE-Hydrolase in den Peritonealmakrophagen der Maus, diesem Enzym ist es aber nicht möglich CE *in vitro* oder *in vivo* zu hydrolysieren.

Contents

1. Introduction

1.1 Atherosclerosis

Atherosclerosis comes from the Greek words athero, designing paste and sclerosis, which means hardness. It is a multifactorial disease and the primary cause of heart disease and stroke in westernized societies. In the year 2006 about 37 % of all deaths in Austria were caused by cardiovascular disease (3). Atherosclerosis typically begins in early adolescence and is a syndrome affecting medium and large blood vessels. This process leads to deposits of cholesterol, cellular waste products, calcium and other material built up in the inner lining of the artery. These atheromatous plaques develop in the arteries, leading to endothelial dysfunction, chronic inflammatory response and interfere with the blood flow (Figure 1). Furthermore, vulnerable plaques can suddenly rupture, leading to death of the tissues fed by the artery in several minutes. One of the most common events is a thrombus of a coronary artery, causing myocardial infarction. If the same process takes part in an artery to the brain, stroke is frequently occuring that is even more harmful. A thrombus could also happen in vessels to all the other organs, it is a body-wide process.

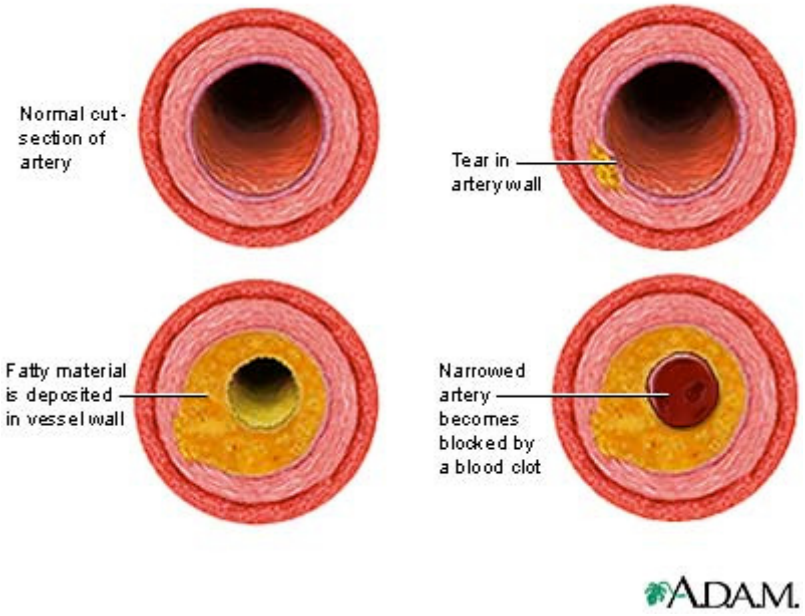

Figure 1: Different cut sections of arteries with atherosclerotic lesions (1). The deposition of fatty material in the development of atherosclerosis leads to narrowing of the artery and therefore reducing the blood flow until total blockage.

Various anatomic, physiological, behavioral, and environmental risk factors for atherosclerosis are known (4). One of the most common problems for the risk of

atherosclerosis is the metabolic syndrome, defined as a combination of medical disorders including diabetes, dyslipoproteinemia, high blood pressure and obesity. But also a sedentary lifestyle, a fatty nutrition, too much stress, and tobacco smoking can intensify the risk of atherosclerosis.

1.1.1 The role of macrophages in atherosclerosis

Plasma lipoproteins and macrophages play critical roles in the initiation and progression of atherosclerotic lesions. The major cellular event is the fatty streak formation underlying the endothelium, due to the recruitment of macrophages and their subsequent uptake of LDL-derived cholesterol (5). The oxidation of LDL is influenced by the inducible nitric oxide synthase (iNOS) (6), produced by macrophages and endothelial cells, as well as 15-lipoxygenase (15-LO) (7). The recruitment of monocytes to lesion-prone sites in the intima of large arteries is regulated by cell adhesion molecules that are expressed on the surface of endothelial cells in response to inflammatory stimuli. The most important adhesion molecule is vascular cell adhesion molecule-1 (VCAM-1), due to its increased expression on endothelial cells over lesion-prone areas and its pattern of regulation by pro-inflammatory stimuli (8). E selectin, P selectin as well as inter-cellular adhesion molecule 1 (ICAM-1) appear also to play a role in monocyte recruitment (9, 10). The migration of monocytes can be stimulated either directly by modified LDL (11) or modified LDL can induce the expression of chemotactic molecules by endothelial cells, such as monocyte chemotactic protein 1 (MCP-1) (5) or CCR2, which is the receptor of MCP-1 (12). LDL can be modified non-enzymatically (e.g. proteoglycans, glycosylation) or by enzymatic actions (e.g. lipases, oxygenases) (11). *In vivo* mainly the oxidative modification of LDL (oxLDL) occurs and can lead to a higher susceptibility of LDL to other types of modifications (e.g. lipid modifications, aggregation) (reviewed in (13). LDL can also be modified *in vitro*, e.g. the most studied form is acetylated LDL (acLDL) (14), which are hardly formed under *in vivo* conditions and is mainly taken up by macrophages with the SR-B1 (15). After migration of monocytes to the intima of vessel walls, they differentiate to macrophages by stimulation with the macrophage colony stimulating factor (M-CSF). These macrophages permanently take up the excess of cholesterol within the modified LDL particles via the scavenger receptors A, B1 and CD36 (16). Macrophages handle this huge amount of cholesterol by storing it as cholesteryl esters (CE) in lipid droplets (LD); this process is called foam cell formation. Foam cells are able to remove cholesterol, when extracellular acceptors, like high density lipoprotein (HDL) or apolipoprotein A1 (Apo-A1), are present (Figure 2).

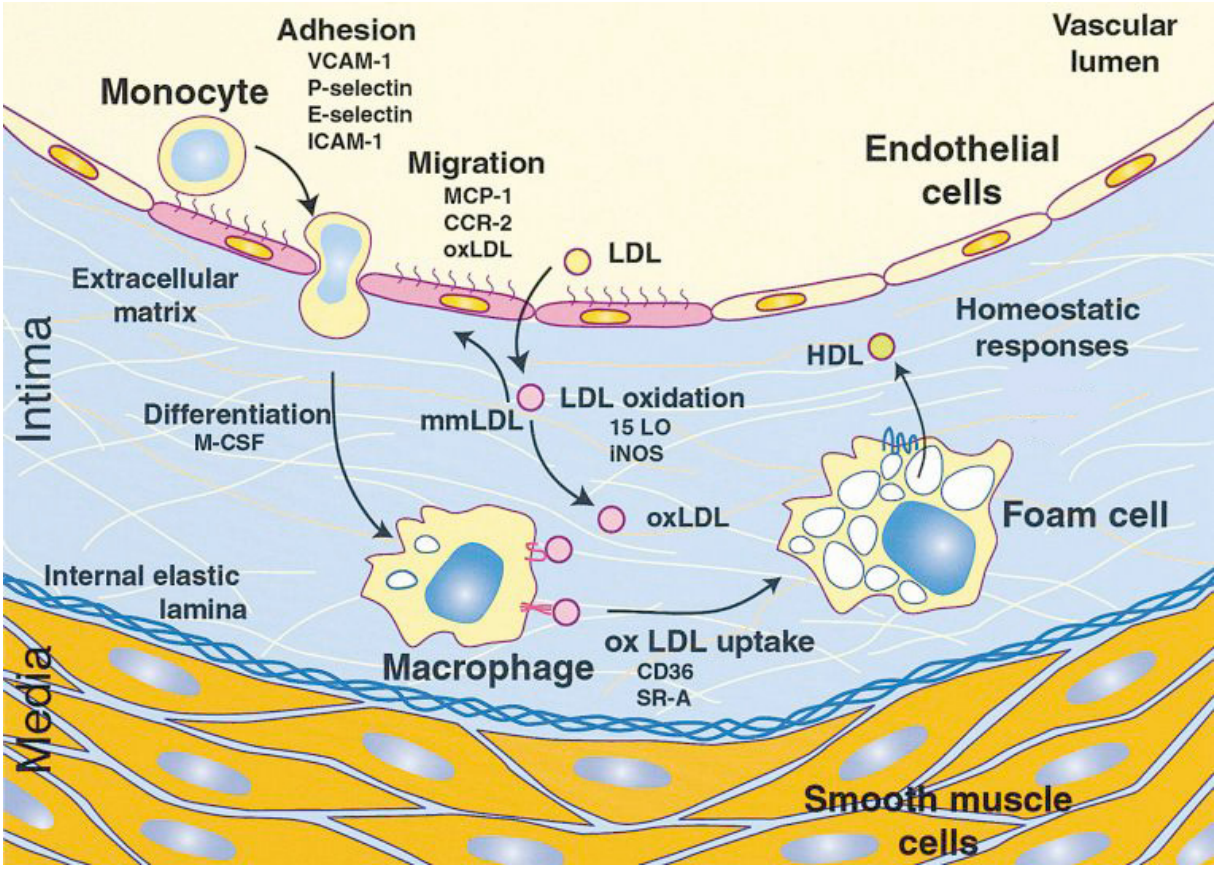

Figure 2: Initiating events in the development of fatty streak lesions (2). Monocytes are recruited to the intima, differentiate to macrophages and take up an excess of LDL-derived cholesterol by scavenger receptors. Lipid loaden macrophages (foam cells) remove cholesterol by transporting it to extracellular acceptors (here: HDL).

The initial step in the transition from a fatty streak to the complex lesion is the immigration of smooth muscle cells into the subendothelial space (Figure 3). These cells are also able to take up modified lipoproteins, leading to foam cell formation and, moreover, to the development of the fibrous cap by secreting extracellular matrix proteins (17). Furthermore, a chronic inflammatory process is established by interactions between foam cells, T-cells and smooth muscle cells. Activated lesional T cells express both Th1 and Th2 cytokines (18). Similarly, macrophages, endothelial cells and smooth muscle cells are stimulated based on their expression of MHC class II molecules and numerous inflammatory products (e.g. tumor necrosis factor α (TNF-α), interleukin 6 (IL-6) and MCP-1). Interferon γ (IFN γ) (19) and Interleukins (IL) also contribute to atherogenesis. IL-4 exerts both anti-atherogenic as well as pro-atherogenic effects. Together, these factors lead to the progression of atherosclerotic plaques, (Figure 1).

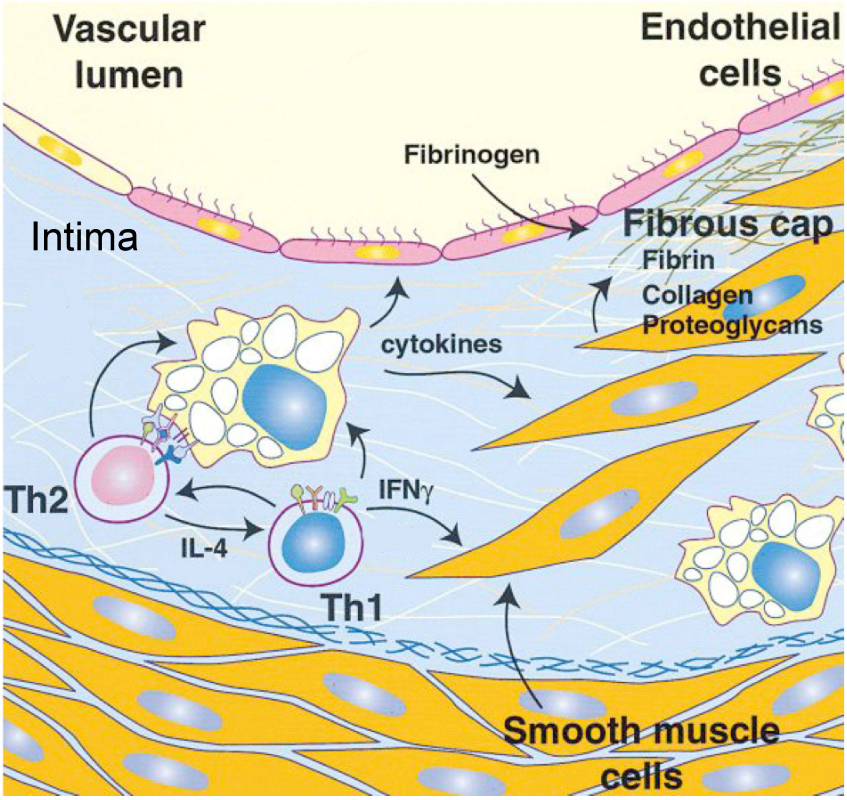

Figure 3: Atherosclerotic lesion progression (2). Macrophages interact with T cells (Th1 and Th2) and due to the release of chemokines, smooth muscle cells are recruited to the intima. They produce extracellular matrix proteins that form the fibrous plaque.

1.2 Role of lipid metabolism in atherogenesis

Lipids are fat-soluble naturally-occurring molecules, such as fats, oils, waxes, sterols, fat-soluble vitamins (such as vitamins A, D, E and K), fatty acids (FA) and their derivates, and others. The most important biological functions of lipids are energy storage, to be components of cell membranes and they play an important role as signalling molecules.

1.2.1 Cholesterol

Cholesterol is the principal synthesized sterol in mammals; cholesterol is found in cell membranes and is the precursor for steroid hormones and bile acids (20-22). In cell membranes, cholesterol is required for the membrane permeability and fluidity and is situated in the phospholipid (PL) bilayer (23).

In normal cells the highest concentration of cholesterol is found in the plasma membrane. The reminder is distributed decreasingly between lysosomal, golgi and endoplasmic reticulum (ER) membranes (24).

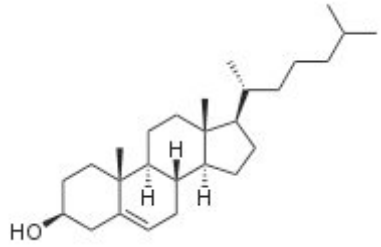

Figure 4: Structure of cholesterol. The body of cholesterol consists of a series of fused rings, which make the molecule quite rigid. At the one end of the planar ring system cholesterol has a hydroxyl group and at the other end a hydrocarbon tail. These hydrophilic and hydrophobic poles determine the positioning of the molecule within the lipid bilayer.

Dietary cholesterol in mammalian cells can be obtained through *de novo* synthesis (~70%) or through dietary uptake (~30%). Cholesterol from both sources is transported through the circulation in lipoprotein particles. Healthy cells maintain a complex balance between cholesterol synthesis, uptake, transport, and efflux. Excessive cholesterol is toxic for cells and contributes to several diseases, notably cardiovascular diseases.

1.2.1.1 Cholesterol biosynthesis

Cholesterol biosynthesis takes mainly place in the ER, but also in peroxisomes and the plasma membrane. The acetyl-coenzyme A (CoA) utilized for cholesterol biosynthesis is derived from an oxidation reaction in the mitochondria and is transported to the cytoplasm. For all reduction reactions NADPH is required as a cofactor. Two moles of acetyl-CoA are condensed in a reversal of the thiolase reaction, forming acetoacetyl-CoA. Acetoacetyl-CoA and a third mole of acetyl-CoA are converted to 3-hydroxy-3-methylglutaryl-CoA (HMG-CoA) by the action of HMG-CoA synthase (HMGCS). HMG-CoA is converted to mevalonate by HMG-CoA reductase, (HMGCR) at the ER. This reaction catalyzed by HMGCR is the rate limiting step of cholesterol biosynthesis and is the target of many statins, which are cholesterol lowering drugs (25, 26). Mevalonate is then activated by three successive phosphorylation steps yielding 5-pyrophosphomevalonate. In addition to activating mevalonate, the phosphorylations maintain its solubility, since otherwise it is insoluble in water. After phosphorylation, an ATP-dependent decarboxylation produces isopentenyl pyrophosphate (IPP), an activated isoprenoid molecule. IPP is in equilibrium with its isomer dimethylallyl pyrophosphate (DMPP). Of one molecule IPP and one molecule DMPP geranyl pyrophosphate (GPP) is generated. GPP further condenses with another IPP molecule to yield farnesyl pyrophosphate (FPP). Finally, squalene synthase catalyzes the head-to-tail condensation of two molecules of FPP to squalene. Squalene undergoes a two step cyclization to produce lanosterol. Through a series of 19 additional reactions, lanosterol is converted to cholesterol (Figure 5). The 3'OH group of cholesterol can be esterified with FA to CE which is stored in LD.

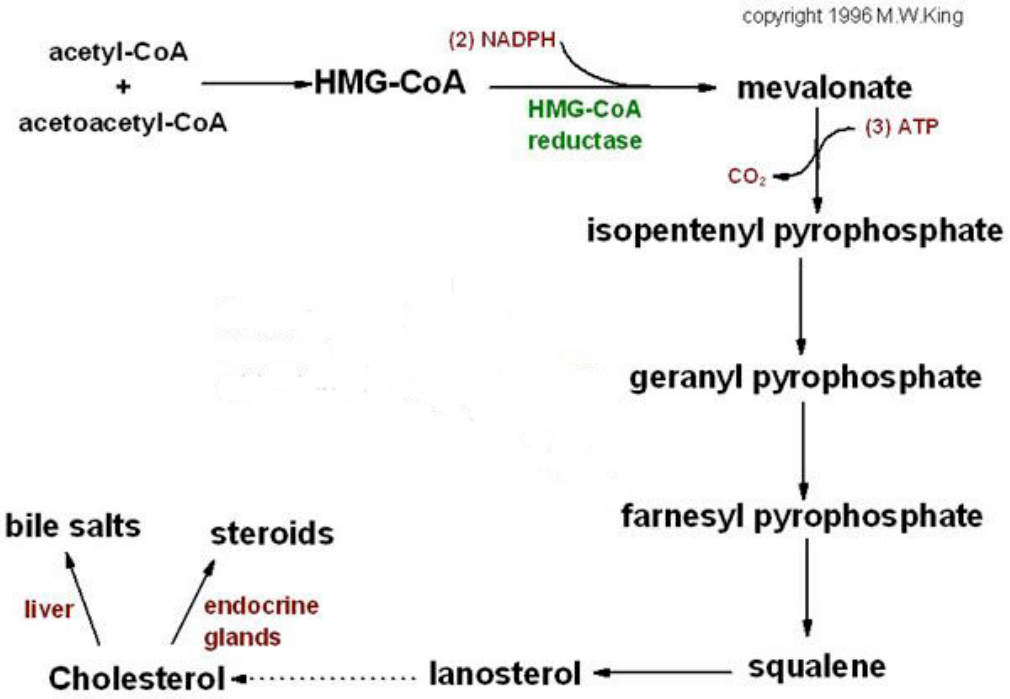

Figure 5: Pathway of cholesterol biosynthesis (27).

1.2.1.2 Regulation of cholesterol biosynthesis

Cells require a large amount of energy for the cholesterol biosynthesis. Thus, this mechanism is regulated by several processes to amend cholesterol from biosynthesis with dietary absorbed cholesterol. As already mentioned above, HMGCR catalyzes the synthesis of mevalonate, which is a crucial intermediate in the formation of sterols and non-sterol isoprenoid compounds (28). HMGCR has three regulatory mechanisms: i) repression of transcription, ii) control of degradation and iii) covalent modification.

i) The repression of transcription of the HMGCR gene by sterols is a well established process (29-31). For example, cholesterol (endogenous cholesterol delivered by plasma lipoproteins or dietary cholesterol delivered by chylomicrons) can repress the gene transcription, dependent upon a short regulatory sequence in the 5`-flanking region of the gene. When this sequence is altered, HMGCR transcription becomes constitutive and there is no suppression by sterols anymore (31).

ii) HMGCR is also controlled by degradation of the enzyme, an event that is dependent upon its association with the ER (32-36). High levels of cholesterol and its derivatives increase the

rate of degradation, possibly by increasing the rate of transport of the membrane-bound enzyme to the site of degradation.
iii) Short term control is affected by covalent modifications: HMGCR is an interconvertible enzyme that is inactivated by phosphorylation. Several hormones are involved in the regulation of HMGCR as needed in fasting, feeding, growth, and development (e.g. insulin stimulates HMGCR production by dephosphorylation of the enzyme (37), whereas glucagon leads to phosphorylation of the protein (38)).

Cholesterol homeostasis is regulated on the transcriptional level by sterol regulatory element binding proteins (SREBPs). SREBPs belong to the family of basic helix-loop-helix-leucine zipper transcription factors, consisting of three members, SREBP-1a, -1c and -2 (39, 40). SREBPs activate the expression of at least 30 genes involved in the synthesis of cholesterol and lipids. They are synthesized as precursor proteins in the ER (41, 42), where they form a complex with SREBP cleavage activating potein (SCAP) that escorts SREBP to the Golgi. In the presence of cholesterol this complex is localized at the ER (43), because SCAP is bound to Insig-1 or Insig-2 (44), which are ER retention proteins. Insig-1 is also able to bind HMGCR, thereby leading to degradation of the enzyme in the ER (45). With cholesterol depletion, the SCAP/SREBP complex appears in vesicles budding from the ER membranes (46) and translocates to the Golgi (47-49). During the transport to the Golgi, the ER vesicle membrane bound site-1 protease (S1P) is activated (50). After incorporation of the complex into the Golgi membrane site-2 protease (S2P) is required to cleave SREBP into the mature nuclear SREBP (nSREBP) form (51). The active nSREBP migrates to the nucleus and binds to a sterol-responsive element (SRE), thus regulating genes belonging to cholesterol synthesis as well as FA synthesis and lipogenesis, TG and PL synthesis, and glucose metabolism.

Three SREBP isoforms activate different genes. Whereas SREBP-1a and -1c influence predominantely FA synthesis, SREBP-2 action favors cholesterol synthesis (52).

1.2.2 Fatty acids (FA)

FA are the simplest lipids and more than 100 different forms have been identified in various species. They are classified into saturated (without any carbon-carbon double bound) and unsaturated (with at least one carbon-carbon double bound) FA. Unsaturated FA are subdivided in monounsaturated FA having one double bond and polyunsaturated FA with more than one double bound. The most abundant monounsaturated FA is oleate, consisting of

18 carbons and a double bond between C9 and C10 (C18:1). Linoleate is a polyunsaturated FA consisting of 18 carbons and 2 double bounds (C18:2).

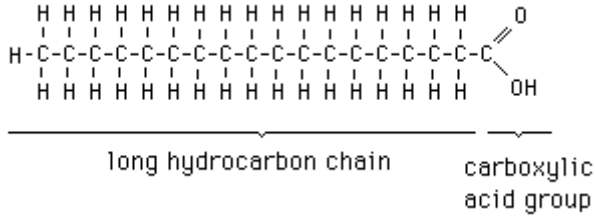

Figure 6: Essential features of a fatty acid with a long hydrocarbon chain and a carboxylic acid group

FA are an important source of energy, since FA oxidation yields more energy than the oxidation of proteins or carbohydrates. In cells, FA are components of more complex lipids, because an excess of FA is toxic to the cells and could disrupt membranes. Thus, FA are generally stored as neutral lipids in TG. Furthermore, they are components of cell membranes, are involved in the regulation of gene expression and can function as signaling molecules (53, 54). Long chain FA (C16 and above) are insoluble in water and in the plasma, where they are transported either esterified in TG-rich lipoproteins, or in a non-esterified form loosely bound to albumin or specific FA binding proteins.

1.2.2.1 FA synthesis

FA synthesis takes place in the cytosol of all species. In mammals, it occurs mainly in liver cells and adipocytes, but also in the central nervous system and lactating mammary gland. Acetyl-CoA from the mitochondria is necessary to build the main substrate malonyl-CoA. This rate-limiting reaction is catalyzed by the regulatory key enzyme acetyl-CoA carboxylase (ACC), which is under tight short term control. ACC is regulated by the endproduct palmitoyl-CoA as well as by covalent modifications (phosphorylation/dephosphorylation) influenced by hormones. Six molecules of malonyl-CoA and one molecule of acetyl-CoA then interact sequentially with fatty acid synthase (FAS) to yield the final product palmitate, a 16 carbons long fatty acyl group (C16:0). FAS is a multifunctional enzyme complex with seven activities (55). Palmitate is typically modified to other FA. Also FA from dietary sources are often modified either by elongation to produce long-chain FA or by desaturation to create unsaturated FA (Figure 7).

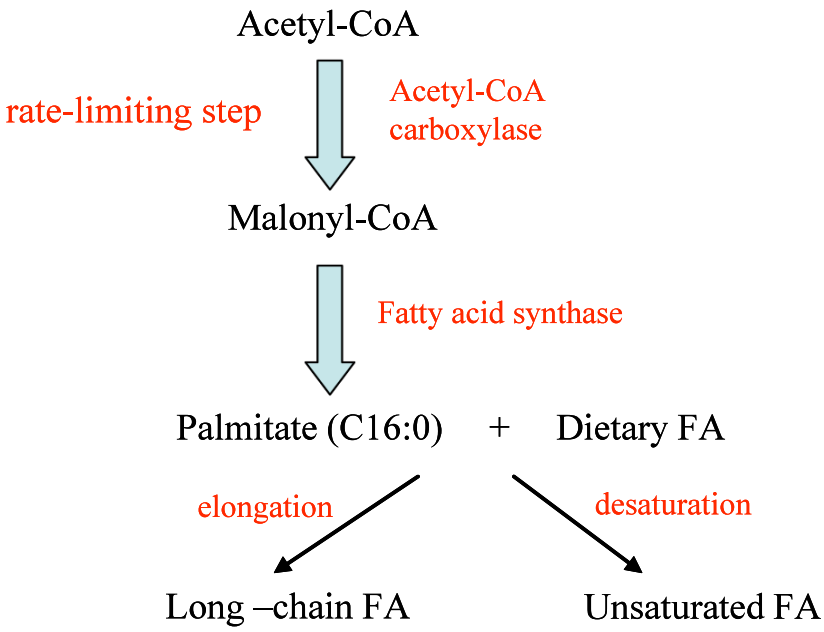

Figure 7: Synthesis of FA. The substrate for FA synthesis is acetyl-CoA. Acetyl-CoA is carboxylated to malonyl-CoA by a rate-limiting step, catalyzed by acetyl-CoA carboxylase. In seven following reactions effected by the multifunctional enzyme fatty acid synthase complex, palmitate (C16:0) is generated. Palmitate as well as dietary FA can be further modified to long-chain FA by elongation or unsaturated FA by desaturation.

FA are stored in different cell types as hydrophobic TG in LD. TG are composed of 3 FA esterified to glycerol, a three-carbon sugar alcohol. In Figure 8 the anabolic and catabolic pathways of TG in adipocytes are shown (56). In the catabolic pathway, several enzymes (adipose triglyceride lipase [ATGL], hormone sensitive lipase [HSL], mono acylglycerol lipase [MGL]) work together to breakdown TG into glycerol and non-esterified FA (NEFA). CGI-58, bound to perilipin on adiposomes, acts as ATGL cofactor (57). Intermediates of this pathway may also be recycled for PL and TG synthesis. NEFA, bound to serum albumin, are transported through the bloodstream to other tissues, mainly muscles and liver, where they are used as energy source. At the target cells, NEFA are taken up passively and get bound to fatty acid binding protein (FABP) for further elongation, desaturation or β-oxidation for energy production. The oxidation of TG is regulated at several levels, but primarily by substrate availability, which in turn is controlled hormonally.

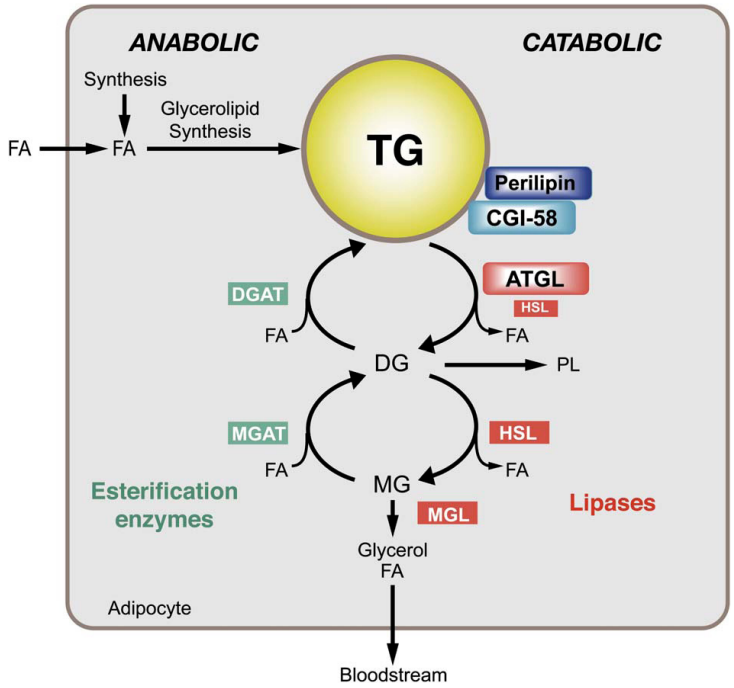

Figure 8: Model of anabolic and catabolic pathways that regulate TG levels in adipocytes (56). In the catabolic pathway TG are hydrolized by several lipases (adipose triglyceride lipase [ATGL], hormone sensitive lipase [HSL], monoacylglycerol lipase [MGL]) into glycerol and FA. CGI-58, which acts as cofactor for ATGL, is bound to perilipin on the adiposome. In the anabolic pathway FA are esterified by acyl- CoA: monoacylglycerol acyltransferase (MGAT) and acyl- CoA: diacylglycerol acyltransferase (DGAT) to diacylglycerol (DG) and triglycerids (TG).

In the anabolic pathway, FA derived from cellular uptake, *de novo* synthesis, or lipolytic hydrolysis of TG are esterified to diacylglycerol (DG) and TG by acyl-CoA: monoacylglycerol acyltransferase (MGAT) and acyl-CoA: diacylglycerol acyltransferase (DGAT) for the storage in LD.

1.2.3 Lipoprotein metabolism

Since lipids are not soluble in water, they can not be transported in the blood or lymph as free molecules. Therefore, lipids assemble with phospholipids (PL) and amphipathic lipid binding proteins to form lipoproteins. Lipoproteins consist of a hydrophobic core containing TG and CE and a hydrophilic surface containing a layer of amphipathic molecules, such as cholesterol, phospholipids and proteins (Figure 9). Large lipoprotein particles contain a number of different lipid binding proteins, called apolipoproteins (apo). The most important apo is apo-B100, which is firmly bound to very-low-density lipoproteins (VLDL), intermediate density lipoproteins (IDL), and low-density lipoproteins (LDL). ApoB-48 is the dominant apo present only on chylomicrons. Apo have a variety of functions, including modulation of certain enzymes involved in lipid mobilization and interaction with cell surface receptors.

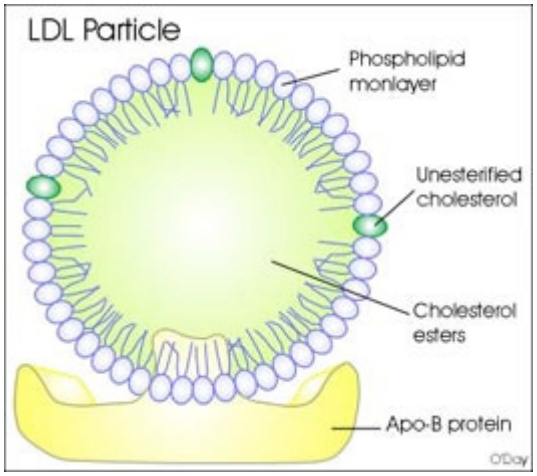

Figure 9: Low density lipoprotein (LDL) particle (58). The LDL particle consists of approximately 40 % CE, 20 % protein, 20 % PL and 10 % TG.

Lipoprotein metabolism has a key role in atherogenesis. It involves the transport of lipids, particularly cholesterol and TG, in the blood. The intestine absorbs dietary fat and packages it into TG-rich chylomicrons, which are transported to peripheral tissues through the blood. In muscle and adipose tissues, lipoprotein lipase (LPL) breaks down chylomicrons, and FA enter these tissues. The chylomicron remnants are subsequently taken up by the liver. The liver loads lipids onto apoB and secretes VLDL, which undergo lipolysis by LPL to form LDL. LDL are then taken up by the liver by the LDL receptor (LDLR), as well as through other pathways. In contrast, high-density lipoproteins (HDL) are generated by the intestine and the liver through the secretion of lipid-free apoA-I (Figure 10).

In the reverse cholesterol transport, ApoA-I recruits cholesterol from these organs through the actions of the transporter ABCA1, forming nascent HDL. This protects apoA-I from being rapidly degraded in the kidneys. In the peripheral tissues, nascent HDL particles promote the efflux of cholesterol from tissues, including from macrophages, through the action of ABCA1. Mature HDL activates this efflux through ABCG1. In macrophages, the production of ABCA1 and ABCG1 is regulated by the liver X receptor (LXR). Free cholesterol (FC) in nascent HDL is esterified to CE by lecithin cholesterol acyltransferase (LCAT), to a mature HDL. The cholesterol in HDL is returned to the liver both directly through uptake by the receptor SR-BI and indirectly by transfer to LDL and VLDL through the cholesteryl ester transfer protein (CETP), which is absent in mice. The lipid content of HDL is altered by the enzymes hepatic lipase and endothelial lipase and by the transfer proteins CETP and phospholipid transfer protein (PLTP), affecting HDL catabolism (Figure 10).

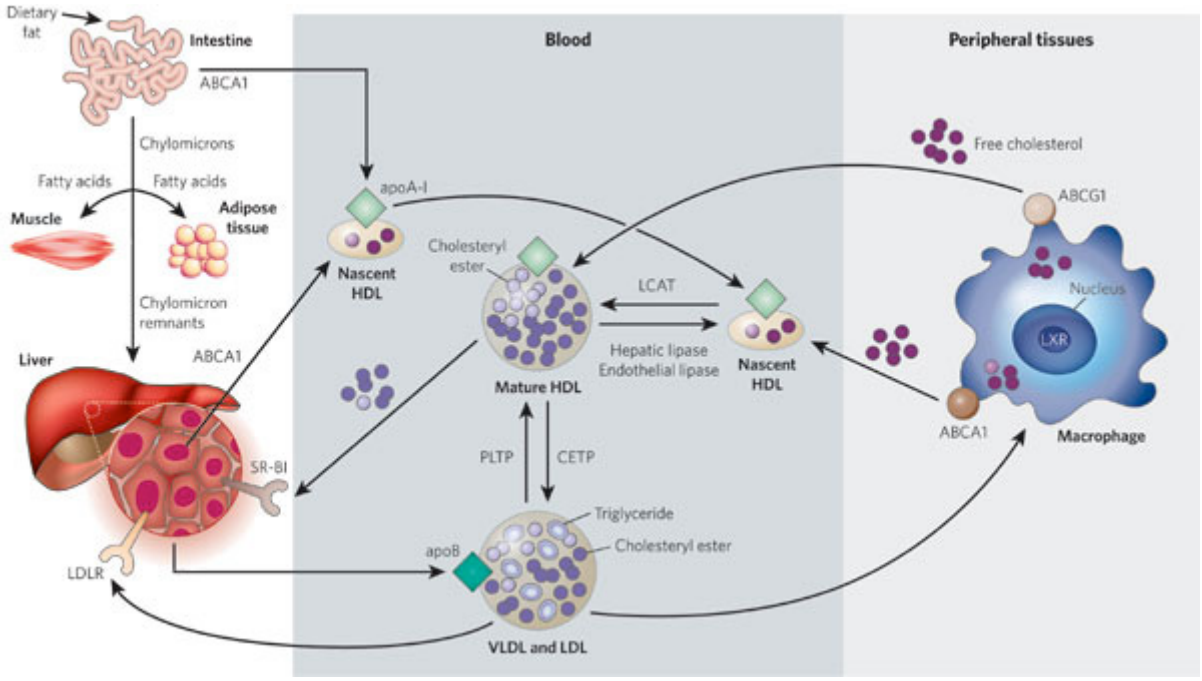

Figure 10: Overview of cholesterol and TG metabolism in the body (59).

1.2.4 Intracellular cholesterol transport

The intracellular transport and distribution of cholesterol within cells is important for normal physiology. Many fundamental aspects of intracellular cholesterol movements are not well understood. The first initial step in the cholesterol uptake of a cell is binding of LDL to the specific LDL receptor on the surface of the cell (60, 61). LDLR bound to the LDL particle is then internalized by a clathrin-coated pit. In the cell the coated vesicles rapidly fuse with lysosomes, where an receptor releases the LDL particle due to the acid pH. While the receptor is recycled and transported back to the cell surface (21), LDL is degraded in the lysosome into amino acids, FA and FC through the action of lysosomal acid lipase (LAL) (Figure 11). After efflux from the late endosomes and lysosomes, cholesterol can be delivered to various other organelles, mostly to the ER and the plasma membrane. FC recycled back to the plasma membrane may be critical in FC efflux from the cells (62). Transport to the ER is necessary for important negative feedback pathways (52) and for cholesterol esterification (63). The feedback pathways are described in 1.2.1.2. A part of FC is converted at the mitochondria to 27-hydroxycholesterol, which is important for the sterol efflux of macrophages (64).

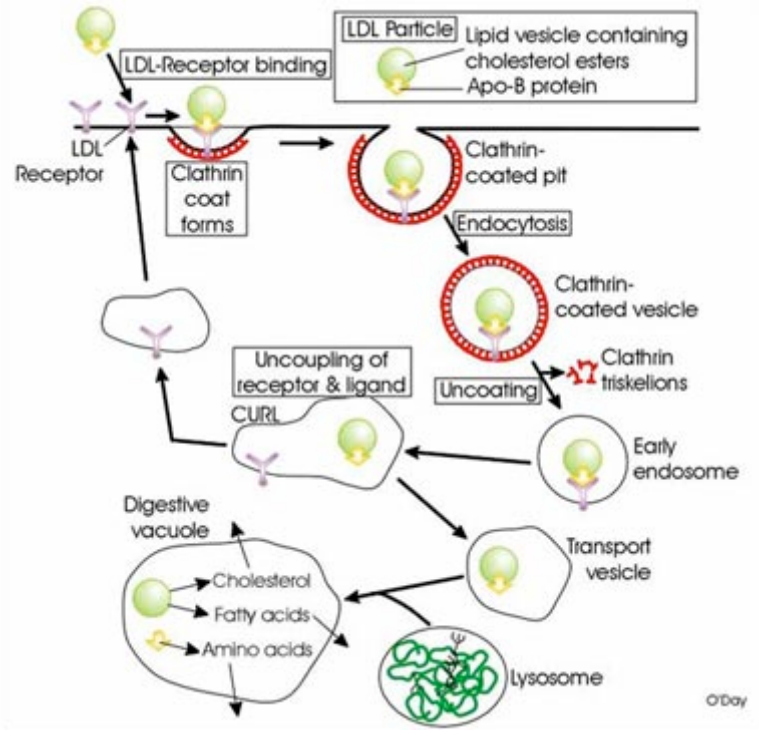

Figure 11: Receptor mediated endocytosis of LDL (58).

In macrophages, cholesterol esterification is a very important process in atherogenesis. At the ER, FC is esterified to CE by acyl-CoA:cholesterol acyltransferase-1 (ACAT-1) to prevent FC accumulation (63) (Figure 12).

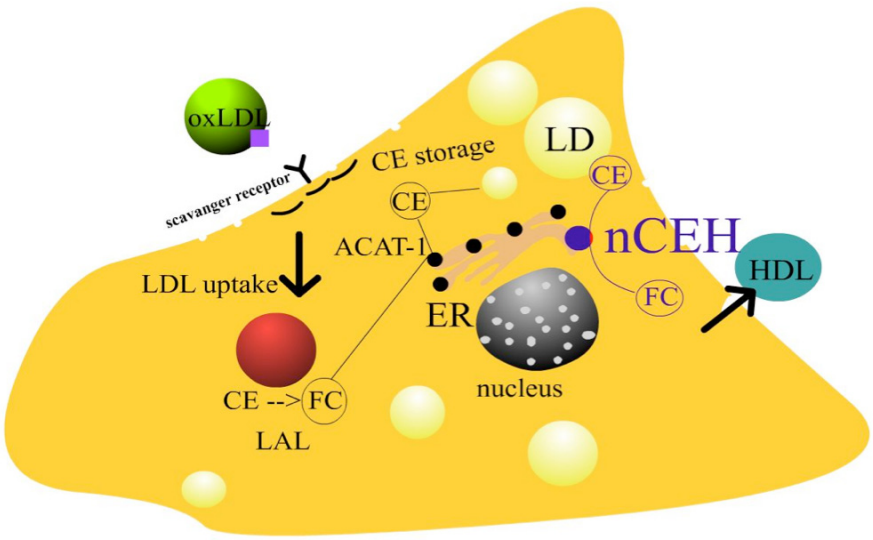

Figure 12: Intracellular cholesterol transport.

Finally CE can be rehydrolyzed by a cytoplasmic neutral CE hydrolase (nCEH). This "cholesteryl ester cycle" goes on continuously, but the ratio of CE hydrolysis to cholesterol

esterification is increased during cholesterol efflux from cells. FC resulting from this hydrolysis is available for efflux, because an excess of FC in cells is cytotoxic and can lead to apoptosis (65).

1.3 Retinoids

1.3.1 Retinoids (Vitamin A and its metabolites)

Retinoids are crucial for nearly all forms of life. They are necessary to maintain immunity, reproduction, embryogenesis and normal cell proliferation and differentiation (66). Retinoids include retinol (ROH, most useable form of vitamin A), retinal (RALD, aldehyde form), retinoic acid (RA, acid form) and retinyl ester (RE, ester form). RA acts as ligand for the transcription factor retionid X receptor (RXR) and therefore regulates many genes which are involved in several mechanisms.

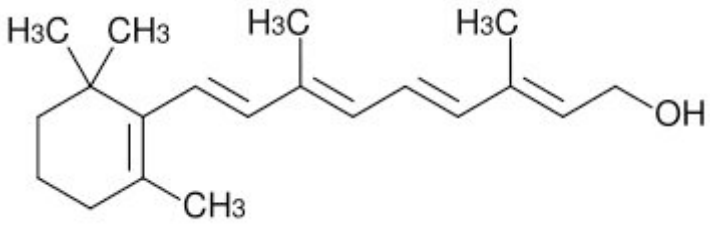

Figure 13: The structure of retinol, the most common dietary form of vitamin A. All forms of vitamin A have a beta-ionone ring to which an isoprenoid chain is attached. This structure is essential for vitamin activity. The orange pigment of carrots - beta-carotene - can be represented as two connected retinyl groups, which are used in the body to contribute to Vitamin A levels. The retinyl group, when attached to a specific protein, is the only primary light absorber in visual perception, and the compound name is related to the retina of the eye.

Vitamin A deficiency is a public health problem in more than 120 countries all over the world. This disease is characterized by several ocular features (xerophthalmia) and an impaired resistance to infections. Vitamin A deficiency is associated with defects in both the innate and adaptive immune systems (11-20). This disease impairs innate immunity by impeding normal regeneration of mucosal barriers damaged by infection and by diminishing the function of neutrophils, macrophages and natural killer cells.

1.3.2 Body retinoid metabolism

Dietary RE are hydrolyzed in the intestinal lumen by the pancreatic TG lipase and phospholipase B into retinoids, which are taken up by enterocytes (67). In enterocytes retinoids are esterified by the lecithin retinol acyltransferase (LRAT) (68) into RE, which are then incorporated into chylomicrons (69). As mentioned above, cylomicrons are secreted into the lymph and move into the general circulation where they shrink in chylomicron remnants.

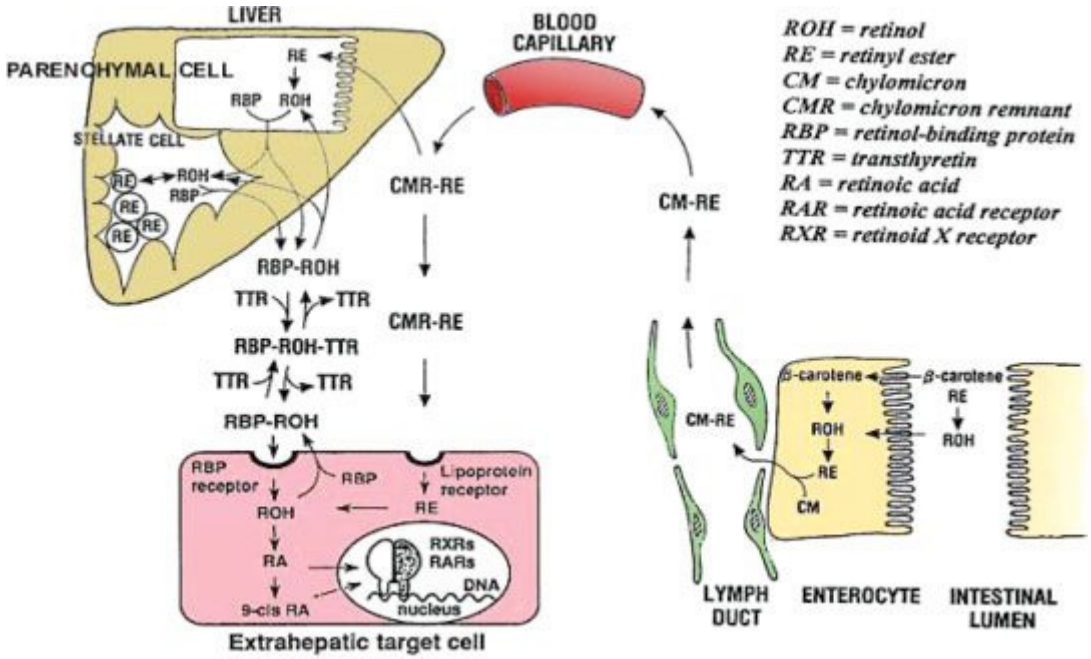

Figure 14: Major pathways for retinoid transport in the body (70). Dietary retinoids are carried through the body via chylomicrons as RE. Most of them are absorbed by hepatocytes and stored as RE in stellate cells, the primary retinol storing cells. Extrahepatic cells are also able to take up RE or RBP bound retinol. Moreover they store RE in LD or RA interact with nuclear receptors to regulate genes.

The chylomicron remnants are mainly cleared by hepatocytes of the liver. In hepatocytes, the RE are hydrolyzed and retinol either binds to retinol binding protein (RBP) followed by secretion of retinol-RBP into plasma (69) or is translocated to the stellate cells for storage (71). In these primary retinoid storing cells, ROH is esterified by LRAT into RE. Extrahepatic tissues (e.g. adipose tissue) are also able to take up RE from chylomicrons or RBP-bound ROH facilitated by the lipoprotein lipase (72). In extrahepatic cells, retinoids are stored as RE in LD or RA acts as a transcriptional ligand for nuclear receptors.

1.3.3 Retinoic acid synthesis in macrophages

Macrophages are able to take up RE and ROH via chylomicron remnants. Within the cell, RE are hydrolyzed in early endosomes. One part of this ROH leaves the cell, another part is oxidized to RA acid and a third fraction is esterified again into RE for temporary storage in LD (73). Within the cell, RA is produced from ROH (vitamin A) via a two-step enzymatic pathway that oxidizes ROH to RALD and furthermore to RA (Figure 15).

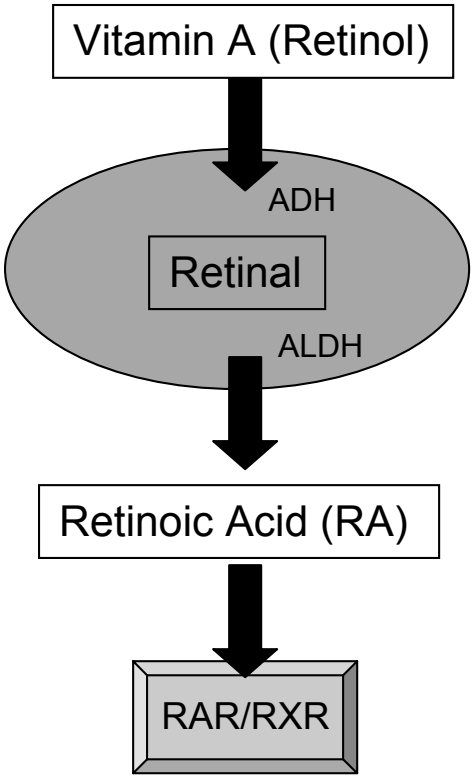

Figure 15: Intracellular RA synthesis.

Oxidation of ROH to RALD requires several alcohol dehydrogenases (ADH-1, -4, -5), whereas oxidation of RALD to RA is dependent on the activity of retinal dehydrogenases, which is generally believed to be the critical and rate-limiting step in the biosynthesis of all-trans RA. The transcriptional activities of RA are mediated through its binding to retinoid nuclear receptors such as RA receptor (RAR) and the retinoid X receptor (RXR) (74). These receptors form heterodimers (RAR/RXR) or homodimers (RXR/RXR) and are known to regulate more than 500 genes. Recent studies have shown that RXR is also able to

heterodimerize with other nuclear receptors like peroxisome proliferator-activated receptors (PPAR), vitamin D receptor, LXR, and farnesoid X receptor (75-77).

1.4 Hormone sensitive lipase (HSL)

HSL is a serine hydrolase, which is expressed in multiple tissues and possesses lipolytic activities against p-nitrophenyl esters (78), monoacylglycerol (MG), DG, TG, CE (79), RE (80), and steroid esters (81). HSL mainly exists as a homodimer, although the monomeric form also shows enzyme activity. The single polypeptide with a molecular mass of 84 kDa comprises three major domains: a catalytic domain, a regulatory domain encoding several phosphorylation sites and an N-terminal domain involved in protein-protein and protein-lipid interactions (Figure 16). The catalytic domain consists of a structural α/β hydrolase fold found in many other lipases (82).

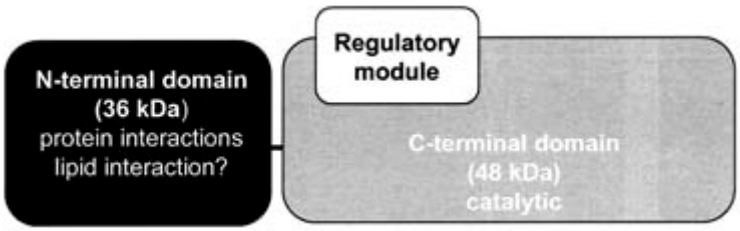

Figure 16: Suggested structural domains of HSL (83).

Three isoforms of HSL have been identified, ranging in tissue distribution and size from 84 to 130 kDa (84-86).

1.4.1 Regulation of HSL

The regulation of HSL depends on several mechanisms, including reversible phosphorylation by a number of different protein kinases, translocation to different sites within the cell and interaction with proteins via the N-terminal region (87).

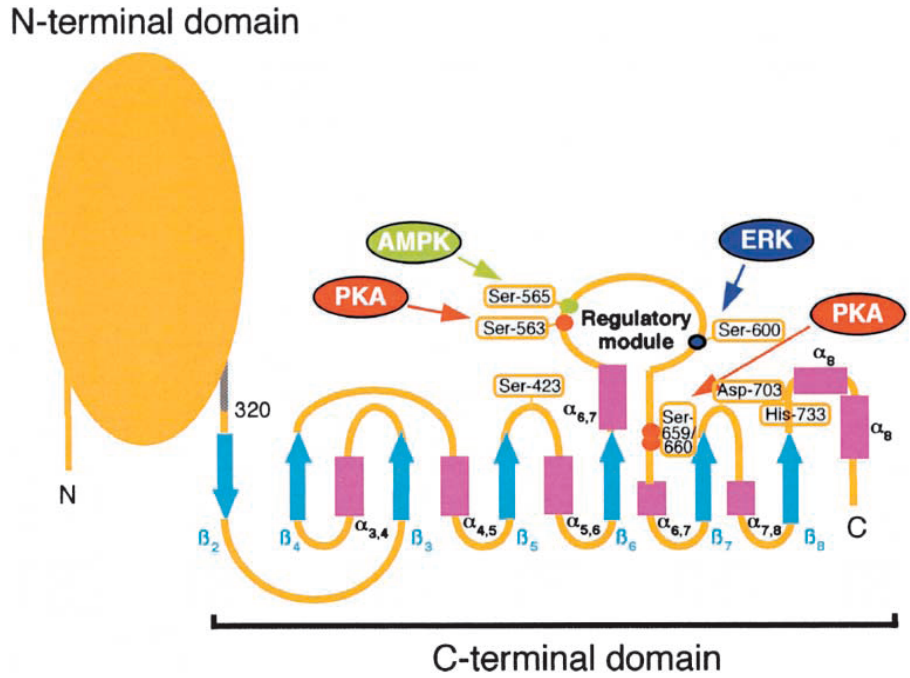

Figure 17: Schematic structure of rat HSL (88). The C-terminal domain consists of an α/β hydrolase structure and the catalytic triad. The regulatory module in the C-terminal domain contains important serine residues that can be phosphorylated by different kinases.

The activity of HSL towards TG, CE and RE seems to be regulated by reversible phosphorylation, whereas hydrolytic activities against DG, MG and water-soluble substrates is unaffected by phosphorylation (89). Several phosphorylation sites (serine residues) exist on the polypeptide (Figure 17). A number of kinases are able to phosphorylate HSL on different serine (Ser) residues (e.g. the AMP-activated protein kinase (AMPK) (Ser565) or the cAMP dependent protein kinase A (PKA) (Ser563 *in vivo*, Ser659 and Ser660 *in vitro*)). In adipose tissue, which is the most investigated tissue regarding HSL regulation, the binding of agonists to the β-adrenergic receptors coupled to adenylate cyclase via the stimulatory G-protein, leads to an increased production of cAMP and activation of PKA. Furthermore, through PKA phosphorylation, HSL is translocated from the cytosol to LD (90), which can be monitored as an increased lipolytic activity against TG and CE. Perilipin A, a LD-associated protein is also required for the translocation of HSL to the LD upon stimulation. Very recently it was shown from Shen et al., that HSL can form a physical interaction with a N-terminal and a C-terminal region of Perilipin A (91). Catecholamines are important stimulators of lipolysis, while insulin is the most important anti-lipolytic hormone. Additionally, not only PKA is activated by lipolytic hormones, but also the mitogen activated protein kinase pathway and extracellular signal-regulated kinase (ERK) (Ser600). Activation of the ERK pathway appears to be able to regulate adipocyte lipolysis and increases the activity of HSL (92).

HSL can also be inactivated through dephosphorylation of serine residues by protein phosphatases, such as phosphatase 2A and 2C (93).

1.4.2 The different roles of HSL

- **Macrophages**

CE hydrolysis in macrophages has been studied for more than 40 years (94). In 1989, it was first reported that the neutral CE hydrolase activity in the mouse macrophage cell line WEH1 is catalyzed by HSL (95). In RAW264.7 macrophages, neutral CE hydrolase activity was nearly completely blocked with an anti-HSL antibody whereas overexpression of HSL increased CE hydrolysis in these cells (96). Adenoviral-mediated overexpression of HSL in human THP-1 macrophages resulted in complete elimination of CE stores (97). Enhanced CE hydrolysis specifically in macrophages of transgenic mice overexpressing HSL led to FC accumulation and an increased incidence and severity of aortic fatty lesions (98). These results suggested that HSL plays a major role in the hydrolysis of CE stores in macrophages. However, these findings were challenged by unchanged CE hydrolase activities and HSL-independent CE hydrolysis in MPM of HSL-deficient mice (99, 100) arguing against a dominant role of HSL as a CE hydrolase in macrophages.

- **Steroidogenic tissues**

In **adrenals** HSL is suggested to be responsible for the main nCEH activity, since adrenals of HSL-deficient mice exhibit less than 2 % nCEH compared to WT mice (101). It seems that the actions of HSL are involved in the delivery of cholesterol for steroidogenesis, since HSL deficiency resulted in a reduction in corticosterone response to the adrenocorticotropic hormone.

HSL is also expressed in testicular cells, like spermatids and spermatozoa (85), suggesting its role in sperm development and/or function. HSL deficiency leads to male sterility caused by oligospermia and **testis** of HSL null mice show no measurable nCEH activity anymore (102). Moreover, the absence of HSL in testis caused CE and DG accumulations (103). HSL is also able to hydrolyze RE (80). Thus, male sterility can arise from a disturbed retinoid metabolism and/or reduced FC, which is necessary for steroid hormone production.

Furthermore, HSL plays a role in steroidogenic tissues in female rats; it is also involved in gamete maturation and oogenesis in the **ovary** (104).

- **Adipose tissue**

For a long time HSL was considered to be the rate-limiting enzyme for the hydrolysis of TG in adipose tissue as well as non adipose tissues. HSL was believed to be the primary hormonal stimulated lipase in adipose tissue, because this enzyme is able to hydrolyze DG and TG. But these ideas changed since HSL-deficient mice were not overweight or obese (102, 103). Most interestingly, absence of HSL resulted in DG accumulation in adipose tissue, indicating that HSL is the rate-limiting enzyme in DG hydrolysis (105). These findings were confirmed when ATGL was published as a TG lipase in adipose tissue and ATGL deficient mice exhibit a severe "lipid" phenotype (106). In 2009, HSL was published as a RE hydrolase in adipose tissue by Ström et al (107). WAT and BAT of HSL-deficient mice revealed nearly no RE hydrolase activity anymore and RE levels of these mice were significantly increased, whereas ROH, RALD and RA levels were decreased (107).

- **Liver**

Recently, it was published from Sekiya et al (108) that livers from HSL-deficient mice had significantly reduced nCEH activity, but unchanged TG hydrolase activity compared to WT mice. Furthermore, after a 7 week diet supplemented with 2 % cholesterol, the authors measured significantly increased CE levels in livers of HSL-deficient mice compared to their WT littermates. Thus, they suggested that HSL is involved in hepatic CE hydrolysis. These findings were confirmed by they group of Holm (109). After feeding a high fat diet for 27 weeks, they assessed significantly elevated TC and CE levels in livers of HSL-deficient mice compared to controls in the fasted state. Moreover, they showed a downregulation of genes, which are involved in *de novo* synthesis of cholesterol, in livers of 6 month HFD-fed HSL-deficient mice. All these findings led to the consumption that HSL-deficient mice have a disturbed cholesterol homeostasis in the liver.

- **Intestine**

Grober et al suggested HSL to contribute to the DG hydrolase activity in the intestinal mucosa and to be fully responsible for the nCEH activity in all three parts of the small intestine (110).

- **Muscle**

HSL is also expressed in cardiac (111) and skeletal muscle (112). In **skeletal muscle** HSL is stimulated by catecholamines acting via β-adrenergic receptors and cAMP playing a role in energy utilization. In heart-specific overexpressing HSL mice, Suzuki et al (113) showed that

HSL controls the accumulation of TG droplets in the **cardiac muscle**. Furthermore, HSL overexpression affected the expression of several genes involved in lipid/energy metabolism, cell growth/cell cycle, and cellular antigen presentation (113).

1.4.3 Pathophysiology

In various metabolic disorders diminished HSL activity or genetic polymorphisms have been reported. For instance, HSL activity is decreased in patients with familial combined hyperlipidemia (114, 115). Varying data exist about HSL and obesity. It has been reported in obese men and women that HSL mRNA and protein expression are reduced (116). In another trial of obese middle-aged men HSL mRNA levels were higher compared to the control group (117). Thus, it awaits further investigations to link genetic variations of HSL with human disorders.

1.5 KIAA1363

KIAA1363 was first found on a list of unnotated proteins based on the human genome (118). High levels of KIAA1363 were found in human invasive breast, ovarian and melanoma cancer cell lines suggesting involvement in tumor invasiveness (119). Later, in 2005/2006, KIAA1363 was established to hydrolyze not only the endogenous substrate acetyl monoalkylglycerol ether (AcMAGE) (120), but also degrades xenobiotics such as chlorpyrifos oxon (CPO) (121). Our group found KIAA1363 in an *in silico* homology search for enzymes with an α/β hydrolase fold within the GOLD 1 project.

1.5.1 Structure of KIAA1363

KIAA1363 is an 50 kDa membrane-bound protein with two glycosylation states (45 kDa and 50 kDa). Due to the sequence, KIAA1363 belongs to the arylacetamide deacetylase (AADA) class of five members are known in humans. The enzyme consists of an α/β hydrolase fold and a Ser, His and Asp catalytic triad (122). The primary sequence of murine KIAA1363 has about 43 % homology with AADA.

1.5.2 The different roles of KIAA1363

- **AcMAGE hydrolase and detoxifying enzyme**

KIAA1363 plays a regulatory role in ether lipid metabolism. This enzyme hydrolyzes AcMAGE, the penultimate precursor in the *de novo* biosynthesis of PAF, to acetate and monoalkylglycerol ether (MAGE) in mice and cancer cell lines (Figure 19). MAGE can be further metabolized to alkyl lysophosphatidic acid (alkyl LPA). This is important in tumor cells, where KIAA1363 RNA knockdown led to decreased MAGE and alkyl LPA levels and therefore to a decrease in cancer cell migration and growth (120). KIAA1363-deficient mice revealed no obvious phenotype in comparison to WT mice (121), but it was discovered that KIAA1363 is the primary AcMAGE hydrolase in mouse brain, heart, lung, and kidney. In the brain, KIAA1363 regulates PAF levels by AcMAGE degradation in addition to PAF-acetylhydrolase (PAF-AH). PAF is important for the stimulation of neurotransmission in brain at moderate levels, but an excess of PAF is neurotoxic. KIAA1363 is also a detoxifying enzyme that hydrolyzes CPO and some other potent insecticide metabolites. Therefore KIAA1363 protects against poisoning by improved organophosphorus (OP) detoxification (121).

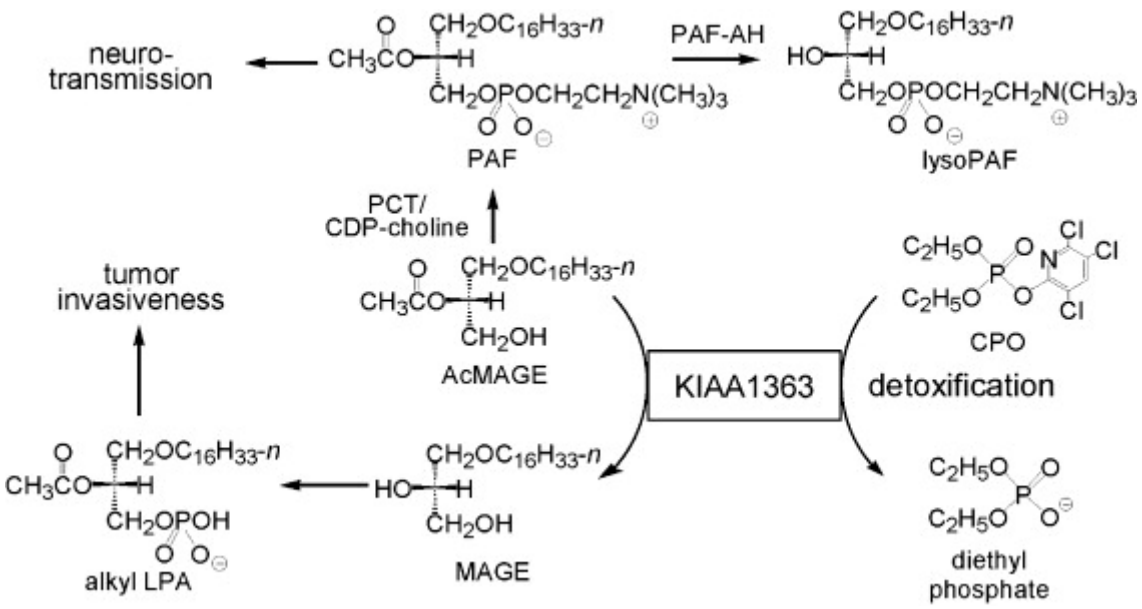

Figure 18: KIAA1363 modulates ether lipid metabolism and OP detoxification (123).

- **CE hydrolase**

Very recently it has been published by Okazaki et al (124) that KIAA1363 is the key enzyme for removing cholesterol from macrophages *in vitro*. The authors renamed KIAA1363 into neutral CE hydrolase (NCEH). An adenoviral construct of KIAA1363 was expressed in HEK293 cells and the transcribed product revealed CE hydrolase activity as well as TG hydrolase activity. The structural homology of NCEH to HSL is 22.1 %.

2. Aim of this doctoral thesis

The aim of this thesis was to elucidate the substrate specificity of the two enzymes, hormone-sensitive lipase (HSL) and KIAA1363 in mouse peritoneal macrophages (MPM) *in vivo* and *in vitro*, with particular focus on cholesteryl ester (CE) hydrolase activity.

Since foam cell formation is considered as a hallmark in early stages of atherosclerosis, many groups focussed on investigating enzymes involved in cholesterol homeostasis of macrophages and foam cells. Especially the action of a neutral CE hydrolase was addressed, because this enzyme is able to mobilize unesterified cholesterol which in turn facilitates efflux out of the cell and prevents from foam cell formation; this is actually considered as an anti-atherogenic mechanism. Two potential candidates for the hydrolysis of CE in macrophages are HSL and KIAA1363. The role of HSL as neutral CE hydrolase in macrophages was studied for more than 40 years and resulted in numerous conflicting findings. Very recently KIAA1363 was suggested to be a key enzyme removing cholesterol from murine macrophages *in vitro*. Since our group was also interested in characterizing neutral CE hydrolases in macrophages, I wanted to confirm previous work and study the role of HSL and KIAA1363 in MPM. The following points were addressed:

- Foam cell formation of MPM
- Lipolytic activities of recombinant HSL and KIAA1363
- Characterization of macrophages from HSL- and KIAA1363- deficient mice
- Generating and characterizing HSL/KIAA1363 double knockout mice
- Localization of HSL in macrophages
- Influence of LPS on KIAA1363 mRNA level and protein expression

A part of this work was summarized in the manuscript "**LIPOLYTIC ACTIVITIES OF HSL AND KIAA1363 IN MURINE MACROPHAGES"** by Buchebner et al., and submitted to the Journal of Lipid Research.

3. Materials and Methods

3.1 Materials

3.1.1 Chemicals and solutions

This chapter lists all the chemicals and solutions for cell culture experiments, molecular biology techniques and biochemical methods which were used in this thesis.

3.1.1.1 Chemicals and solutions for cell culture experiments

Table 1: Chemicals and solutions used for cell culture experiments.

chemical/solution	company
Agar	Serva
Albumin, bovine serum, fraction V	Sigma-Aldrich
Albumin, bovine serum, essentially FA free, fraction V	Sigma-Aldrich
Deoxycholic acid	Sigma
DMSO	Merck
DTT	Sigma
Dulbecco´s modified Eagle´s medium (DMEM)	Gibco
EDTA	Roth
Fetal bovine serum (FCS)	PAA
Glucose	Sigma
Human serum extract	Self made
KBr	Roth
KCl	Merck
$K_4[Fe(CN)_6]$ x 3 H_2O	Merck
$K_3[Fe(CN)_6]$	Merck
KH_2PO_4	Merck
KOH	Merck
L-cystein	Serva

LPDS	Self made
LPS	Sigma-Aldrich
NaCl	Merck
NaOH	Roth
Na-oleate	Sigma-Aldrich
PBS	Self made
Penicillin/streptomycin	Cambrex
Peptone 110	Gerbu Biochemicals
Peptone 140	Gibco
Protease inhibitor cocktail (PIC)	Sigma
Saccharose	Merck
Sodium chloride	Roth
Sodium sulfite	Merck
Sodium thioglycollate	Sigma
3 % Thioglycollate medium	Self made
Tris	Roth
Triton X-100	Merck
Trypsin	PAA

- **Isolation of LDL, VLDL and HDL:**

Low density lipoprotein (LDL) and high density lipoprotein (HDL) were isolated by gradient ultracentrifugation of human plasma. One g/l sodium acide was added to the plasma to avoid bacterial growth.

First, density of the plasma was adjusted to δ = 1.06 g/l by adding ~10 g NaCl /200 ml plasma.

Then 1 g EDTA /l and 1 g sodium acide /l were added. Fourty ml plasma were transferred into centrifugation tubes and centrifuged in an ultracentrifuge using a fixed angle rotor (Ti 60 or Ti 70.2) at 48000 rpm at 15°C for 24 h. Two phases had build up during this centrifugation: the upper containing VLDL and LDL and the lower containing Lp(a) as well as HDL. Both phases were dialysed versus distilled water for 30 min. Thereafter, the density of the LDL/VLDL phase was set to δ =1.027 g/l with NaCl. Separation of VLDL from LDL was performed by centrifugation at 48000 rpm at 15°C for 24 h. After centrifugation, VLDL was found in the upper phase, LDL in the lower phase. Approximately 18 ml of the LDL fraction were taken and density was adjusted to δ =1.063 g/l. Three ml of the LDL fraction were put

into high-speed centrifugation tubes and centrifuged for 24 h at 48000 rpm, 15°C in a swing-up (SW-41) rotor.

After centrifugation, the LDL fraction, which appeared as a yellow band about 5 mm wide in the middle of the tube, was aspirated and filtered through a crude filter into a shot on which a 40 µm acetate sterile filter (Iwaki) was attached.

HDL was isolated from the δ =1.063 g/ infranate by ultracentrifugation for 48 h at 48000 rpm, after setting the density to δ =1.21 g/l with NaBr. HDL, mostly HDL_3 floated to the top of the gradient as a yellow band. After dialysis for 48 h, HDL_3 was used for cell culture experiments.

- **Preparation of aggregated LDL (aggLDL):**

aggLDL was produced by vortexing native LDL for 2 min.

- **Preparation of acetylated LDL (acLDL):**

3.2 ml LDL were mixed with an equal amount of saturated NaCl (salt). The mixture was stirred on ice and 57.76 µl diethyl ether were added in 5.4 µl portions every 3 min. After the 3rd addition, 100 µl of 10 x PBS were added to avoid precipitation of LDL. Thereafter, the mixture was stirred for 45 min on ice. For dialysis the solution was put into a dialysis tube and dialysed against 1 x PBS for 1 h. Thereafter, another dialysis against 2 l PBS was done overnight (ON) at 4°C. After determination of TC content acLDL was covered with nitrogen gas and stored at 4°C.

- **Preparation of β-VLDL:**

Plasma of WTD- fed WT mice was pooled and centrifuged for 10 min (14000 rpm, 4°C) to remove chylomicrons on the top of the plasma. Next, a KBr gradient centrifugation was performed. The gradient was prepared as follows: 2 ml ddH_2O were pipetted into a centrifuge tube, then 3 ml density solution δ = 1.019 g/l and 3 ml density solution δ = 1.063 g/l were added. Finally, 1.3 g KBr were mixed with 4 ml plasma and transferred onto the top of the gradient. The gradient was centrifuged for 24 h at 38000 rpm (4°C), the second fraction (= β-VLDL, δ = 1.006 g/l) was transferred to a new tube and TC, FC and TG content were determined enzymatically (3.2.4.9).

- **3 % Thioglycollate medium**

17 g	Peptone 140
3 g	Peptone 110
0.25 g	L-cystein
6 g	Glucose
2.5 g	Sodium chloride
0.5 g	Sodium thioglycollate
0.1 g	Sodium sulfite
0.7 g	Agar
1000 ml	ddH_2O

Components were dissolved in ddH_2O, sterile filtrated, aliquoted and stored at -20°C.

3.1.1.2 Chemicals and solutions used for molecular biological methods

Table 2: Chemicals and solutions used for molecular biological methods.

chemical/solution	company
Agarose	Gibco
Ampicillin	Roth
Bromo phenol blue	Merck
Chloroform	Fluka
ddH_2O	Fresenius
Diethylpyrocarbonate (DEPC)	Sigma-Aldrich
DNA 100 bp ladder	Fermentas
Ethanol	Merck
Ethidium bromide	Sigma-Aldrich
Formaldehyd	Sigma-Aldrich
High-Capacity cDNA Reverse Transcription Kit	Applied Biosystems
Isopropanol	Merck
Maxi Prep Kit	Qiagen
β - Mercaptoethanol	Merck
Morpholinopropansulfonicacid (MOPS)	Roth
Primer	Invitrogen

QuantiFast™ SYBR Green PCR Kit	Qiagen
Recombinant His-tagged HSL	Thomas Pfeifer
Recombinant His-tagged KIAA1363	Achim Lass
RNAse Inhibitor	Qiagen
SDS	Serva
TAE buffer	self made
TRI-reagent	Peqlab

- **DEPC water:**

400 µl DEPC were added to 400 ml ddH_2O. The mixture was left open ON in the hood, autoclaved on the next day and stored at RT.

- **10 x MOPS buffer:**

10.5 g	MOPS
1.7 g	Na-Acetate
5 ml	0.5M EDTA
200 ml	DEPC-water

pH was set to 7 with 10 N NaOH and the volume was filled up to 250 ml with DEPC water.

- **RNA sample buffer (3 ml)**

1.44 ml	99.5 % Formamide
280 µl	10 x MOPS buffer
520 µl	37 % Formaldehyde
400 µl	DEPC water
200 µl	80 % sterile Glycerol
10 µl	Ethidium bromide

Storage at 4°C.

- **DNA sample buffer (10 ml)**

5 ml	Glycin
250 µl	40 x TAE buffer
1 granule	Bromo phenol blue
4.75 ml	dd H_2O

Storage at RT.

- **40 x TAE buffer**

193.6 g	Tris
65.5 g	Na-Acetate
14.9 g	EDTA
800 ml	ddH_20

pH was set to 7.2 with acetic acid and the volume was brought up to 1000 ml with ddH_20. Storage at RT.

3.1.1.3 Chemicals and solutions used for biochemical methods

Table 3: Chemicals used for biological methods.

chemical/solution	company
ACAT-Inhibitor 58-035	Sandoz
Acetic acid	Merck
AcLDL	Self made
Acrylamid/bisacrylamid	Sigma Aldrich
AggLDL	Self made
Ammonium persulfate (APS)	BioRad
Anti-HSL	Cell signaling Technology
Anti-KIAA1363	Benjamin Cravatt
Apo A-I	Behring Diagnostika AG
Bio-rad Protein Reagent	Bio-Rad
10 x Blot washing buffer	Self made
Boric acid	Riedel-de Haen
$CaCl_2$	Merck

Chloroform	Fluka
[1, 2 ^{3}H]Cholesterol	Hartmann Analytik
Cholesteryloleate	Sigma-Aldrich
Cholesteryl[1-^{14}C]oleate	Amersham
ddH_2O	Fresenius
2-O-dibutyryladenosine 3`,5`-cyclic monophosphate sodium salt	Sigma-Aldrich
3.5-Dichloro-2-hydroxy-benzenesulfonate	Sigma
Diethyl ether	Fluka
1,2 Diolein	Sigma
1,3 Diolein	Sigma
Dioleyl-rac-glycerol [oleoyl-1-^{14}C]	American Radiolabeled Chemicals
ECL^{TM} western-blotting detection reagents	Amersham
EDTA	Roth
Ethanol	Merck
Fast green	Serva
Filipin	Sigma
Glutaraldehyd	Merck
Glycerin	Merck
Glyceroltrioleate	Sigma-Aldrich
Glycerol tri[9,10(n)-^{3}H]oleate	Amersham
Glycin	Roth
HDL_3	Selfmade
Heptane	Merck
Hexane	Roth
Isopropanol	Merck
K_2CO_3	Sigma
KH_2PO_4	Merck
LD buffer	Self made
Lysis buffer	Self made
Metafectene™	Biontex
Methanol	Roth
$MgCl_2$	Merck

NaCl	Merck
NaN_3	Sigma
NaOH	Roth
Na- taurocholate	Fluka
Nile red	Sigma
[9,10 (n) -^{3}H] Oleic acid	Amersham
1-O-[acetyl-^{3}H(n)] PAF	Perkin Elmer
PageRuler ^{TM}	Fermentas
[9,10 (n)-^{3}H] Palmitate	Achim Lass
Phosphatidylcholine	Sigma
Phosphatidylinositol	Sigma
Phospholipase C from *Bacillus cereus*	Calbiochem
Platelet activating factor (PAF)	Sigma
P-Nitrophenylvalerate	Sigma
Polyclonal goat-anti rabbit immunoglobuline-HRP	DakoCytomation
RIPA buffer	Self made
SDS	Serva
10 x SDS-running buffer	Self made
SDS sample buffer	Self made
Selfmade anti-HSL	Thomas Pfeifer
Seperating gel buffer	Self made
Skim milk	Interspar
Stacking gel buffer	Self made
TEMED	Sigma Aldrich
Tris	Roth
Triton X-100	Merck
β-VLDL	self made
X-Gal	Roth

- **Lysis buffer**

0,1 M KH_2PO_4
1 mM EDTA
pH 7 with KOH
0,25 M Saccharose
1 M DTT
1: 2000 PIC (before use)

Storage at 4°C.

- **RIPA buffer**

50 mM KH_2PO_4
150 mM NaCl
1% Triton X-100
0,5% Deoxycholate
1: 2000 PIC (before use)

Storage at 4°C.

- **LD buffer**

50 mM Tris HCl
100 mM KCl
pH 7.4 with KOH
1: 2000 PIC (before use)

Storage at 4°C.

- **10 x SDS running buffer**

30.3 g	Tris
150.1 g	Glycin
10 g	SDS

Volume was made up with ddH_2O to 1000 ml. Storage at RT.

- **Separating gel buffer (buffer 1)**

18.2 g	Tris
4 ml	10 % SDS
80 ml	ddH_2O

The pH was set to 8.8 with HCl and the volume was filled up to 100 ml. Storage at RT.

- **Stacking gel buffer (buffer 2):**

6 g Tris were dissolved in 90 ml ddH_2O, the pH was adjusted to 6.8 with HCl and the volume was filled up to 100 ml. Storage at RT.

- **SDS sample buffer:**

2.15 g	SDS
0.76 g	Tris
45 ml	ddH_2O

The pH was set to 6.8 with HCl and 10 ml glycerol (80 %) and some granules of brom phenol blue were added. Storage at RT.

- **10 x Blot buffer:**

12.1 g	Tris
30 g	Glycin
1 mg/ml	EDTA

Volume was made up to 1000 ml with ddH_2O. Storage at RT.

- **10 x Blot washing buffer:**

5 g	Tween
90 g	NaCl
100 ml	1 M Tris HCl pH 7.4

Volume was made up to 1000 ml with ddH_2O. Storage at RT.

- **Blocking solution for microscopy:**

10 ml	PBS
500 µl	1 M Tris
0.3 %	Skin milk
0.1 %	Triton X 100

Always fresh prepared.

- **Washing buffer for microscopy:**

8 g	NaCl
3 g	Tris
0.2 g	KCl
0.147 g	$CaCl_2$

Volume was made up to 1000 ml with ddH_2O. Storage at 4°C.

3.2 Methods

3.2.1 Animals and diets

Animal experiments were performed in accordance with the standards established by the Austrian Federal Ministry of Science and Research, Division of Genetic Engineering and Animal Experiments. HSL(-/-) (103, 105) and KIAA1363(-/-) (122, 125) mice as well as littermates and C57Bl/6 mice were obtained from in-house breeding and maintained in a clean environment on a regular light-dark cycle (14 h light, 10 h dark) receiving a standard mouse chow diet (Ssniff R/M H; ssniff, Soest, Germany). KIAA1363(-/-)/HSL(-/-) mice were obtained from cross breeding of HSL(-/-) and KIAA1363(-/-) mice in our animal facility.

3.2.2 Cell culture

3.2.2.1 Cell lines

Media used for the different cell lines were supplemented with 1 % L-glutamine and 1 % streptomycin/penicillin and pre-warmed to 37°C in a water bath. All cells were grown in a humidified incubator with 5 % CO_2 at 37°C.

COS-7 (ATCC Number: CRL-1651)

COS-7 is an African green monkey kidney fibroblast-like cell line containing T antigen. Cells were cultivated in Dulbecco´s modified Eagle´s medium (DMEM) with 10 % FCS and medium was renewed 2 to 3 times per week. Cells were splitted in a subcultivation ratio of 1:4 to 1:8.

RAW264.7 (ATCC Number: TIB-71)

RAW264.7 is a male *mus musculus* macrophage cell line established from a tumor induced by Abelson murine leukemia virus. These cells are negative for surface immunoglobulin, Ia, and Thy-1.2. Routinely the cells were maintained in DMEM with 10 % FCS and medium was replaced every 2 to 3 days. For subcultivation cells were splitted in a ratio of 1:6 to 1:10.

3.2.2.2 Thawing of cells

Vials containing frozen cells were taken out of liquid nitrogen and put into a 37°C water bath until nearly thawed. Then cells were transferred into an appropriate tube containing cell

culture medium. For removal of DMSO, cells were centrifuged for 5 min at 500 x g. The cell pellet was suspended in pre-warmed medium and transferred to a new flask for cultivation.

3.2.2.3 Freezing of cells

Cells were collected in a centrifuge tube and centrifuged at 500 x g for 5 min. The supernatant was discarded and cells were suspended in an appropriate volume of cell culture medium containing 10 % DMSO. One ml aliquots of the cell suspension were put into freezing vials and stored at -20°C overnight, followed by 24 h at -70°C before the frozen vials were transferred to liquid nitrogen. Usually from one confluent T-75 flask four vials were prepared.

3.2.2.4 Splitting of cells

COS-7 cells were routinely splitted by trypsinization. Therefore, the medium was aspirated from cells and cells were washed once with pre-warmed PBS followed by incubation with 1 x trypsin EDTA solution at 37°C. Detachment of cells was examined under the microscope. Trypsin was inactivated by adding fresh medium. After pelleting the cells at 500 x g for 5 min, supernatant was sucked off and cells were washed with PBS. Finally, cells were suspended in fresh medium and an appropriate aliquot was transferred to a cultivation flask and then placed back into the incubator.

Confluent RAW264.7 cells were splitted by scratching the cells with a cell “scraper”. After aspirating the medium, cells were washed with PBS and 1 ml fresh medium was added. The cells were scratched off and part of the suspension was transferred to a new flask for further cultivation.

3.2.2.5 Primary cells: Mouse peritoneal macrophages

Mouse peritoneal macrophages (MPM) were obtained from mice of different strains after injecting the mice intraperitoneally with 3 ml of sterile 3 % thioglycollate medium. After 3 days mice were killed by cervical dislocation and MPM were washed from the peritoneal cavity with 10 ml of sterile PBS. Cells were centrifuged at 500 x g for 5 min and the pellet was washed once with PBS. MPM were resuspended in DMEM and seeded out in 6-well plates, 12-well plates or on chamberslides. After 2 h cells were washed with PBS and non-adherent cells were removed. MPM were used immediately for experiments or cultured overnight in DMEM containing 10 % LPDS.

For incubation of MPM with LPS, MPM were seeded in 6-well plates in DMEM/ 10 % LPDS and different concentrations of LPS (1 ng/ml, 10 ng/ml, 10 µg/ml in PBS) for 6 h, 24 h, 48 h, and 72 h. MPM with the same amount of PBS were used as controls.

3.2.3 Molecular biological methods

3.2.3.1 RNA isolation from cell lines with Qiagen RNeasy Kit

In order to isolate RNA from cells, medium was aspirated and cells were washed once with PBS. Thereafter, the cells were incubated for 1 min with RLT buffer supplemented with β-mercaptoethanol (10 µl β-mercaptoethanol/ml RLT buffer). Then the cells were scraped off and the cell lysate was applied in 700 µl portions to a QIA shredder. The shredders were centrifuged for 20 s at maximum speed. One volume of RNase-free EtOH per shredder was added, mixed and transferred in 700 µl portions to a RNeasy Mini Spin column. After centrifugation at maximum speed for 20 s, the flow-through was thrown away and 700 µl RW1-buffer were added to the column. The flow-through was discarded and the column was washed two times with 500 µl RPE buffer. Thereafter, the column was dried by centrifugation at maximum speed for 1 min. To elute the RNA, the columns were put into a 1.5 ml RNase-free tube and RNase-free water was applied (the amount of water depended on the expected RNA concentration, usually about 20 µl). After 5 min incubation RNA was eluted by centrifugation at maximum speed for 1 min.

3.2.3.2 RNA isolation from murine tissues with TRI-reagent

Mice were killed by cervical dislocation and tissues were removed surgically as fast as possible. All tissues were frozen immediately in liquid nitrogen and stored at -70°C.

For RNA isolation frozen tissues were weighed and put into homogenization tubes. One ml TRI-reagent/100 mg tissue was added. The tissues were homogenized with a Precellys 24 homogenizer (Peqlab, Austria) at 5000 rpm for 25 s. After the addition of 0.2 ml chloroform/ml TRI-reagent, the mixture was vortexed vigorously and incubated for 10 min at RT. Then the samples were centrifuged at 8500 rpm in an Eppendorf centrifuge for 15 min at 4°C. The aqueous phase containing the RNA was transferred into a new centrifugation tube. For RNA precipitation 0.5 ml isopropanol/ml TRI-reagent was added and the samples were incubated for 10 min at RT. After another centrifugation step (8500 rpm, 10 min, 4°C) the supernatant was carefully discarded and the RNA pellet was washed with 1 ml 75 % EtOH/ml

TRI-reagent. The samples were centrifuged again for 5 min at 8500 rpm and 4°C. Finally, the supernatant was decanted carefully and the pellet was air-dried. RNA was dissolved in 20-200 µl DEPC water (depending on the size of the pellet) and stored at -70°C.

3.2.3.3 RNA quantification

Two µl of RNA were quantified on a spectrophotometer (NanoDrop) at a wavelength of 260 nm. To get information about the RNA quality the absorbancy ratio 260 nm/280 nm was determined. This ratio should be between 1.7 and 2. Higher ratios indicate impurities of EtOH or isopropanol, while lower ratios might come from protein impurities. RNA concentration was calculated according to the following equation:

$$C_{(ngRNA/\mu l)} = \lambda_{260nm} \times 40$$

3.2.3.4 RNA gel electrophoresis

The integrity of RNA was proven by RNA gel electrophoresis. RNA gel (15 x 7 cm) was prepared as follows: 1.1 g Agarose, 11 ml 10 x MOPS, 81.9 ml DEPC-water was boiled in a microwave. After cooling down to approximately 60°C, 17.1 ml formaldehyd was added. 1 x MOPS buffer was used as running buffer. Two µg of RNA were mixed with 4 µl RNA sample buffer (5 x) in a total volume of 20 µl. The gel was run at 150 V for 45 min.

3.2.3.5 Reverse transcription

During reverse transcription reverse transcriptase M-MLV-RT converts RNA to cDNA. This cDNA was used as template for real-time PCR.

Two µg RNA (in 10 µl ddH_2O) were reverse transcribed by using the High-Capacity cDNA Reverse Transcription Kit (Applied Biosystems, Austria) according to manufactor's instructions. The composition of the mastermix is shown in table 4, the program of the thermal cycling conditions in table 5.

Table 4: Composition of the Master Mix for reverse transcription using the High-Capacity cDNA Reverse Transcription Kit.

Component	**Volume (µl)/Reaction Kit**
10 x RT Buffer	2
25 x dNTP Mix (100 mM)	0.8
10 x RT Random Primers	2
Multiscribe Reverse Transcriptase	1

RNase Inhibitor	0.7
Nuclease-free H_2O	3.5
1 µg RNA/10 µl ddH_2O	10
Total volume per reaction	**20**

Table 5: Thermal cycling conditions for reverse transcription using the High-Capacity cDNA Reverse Transcription Kit.

	Step 1	**Step 2**	**Step 3**	**Step 4**
Temperature	25 °C	37 °C	85 °C	4 °C
Time	10 min	120 min	5 s	∞

3.2.3.6 Real time PCR using SYBR green

Quantitative real time PCR is a very sensitive method and allows quantification of rare transcripts and small changes in gene expression. Newly synthesized PCR products are detected by SYBR Green I fluorescence dye that binds specifically to the minor groove of double stranded DNA.

Table 6: PCR program used for real time PCR.

	temperature	**time**	**cycles**
Denaturation	95°C	5 min	1
Amplification	95°C 60°C	10 s 30 s	40
Melting curve	95°C 60°C 95°C	10 s 20 s continous	1 1
Cool down	40°C	20 s	1

The PCR program used for real time PCR is described in table 6. Successful PCR depends upon the design of optimal primer pairs. Primer sequences for real time PCR (table 7) were taken from the Harvard Primer Bank (http://pga.mgh.harvard.edu/primerbank/index.html), all having an annealing temperature of 60°C. All primers were obtained from Invitrogen.

First, the primer efficiency of each primer pair had to be determined. A pool of cDNAs, containing 200 ng of each used cDNA, was mixed and diluted 1:5, 1:25, 1:125, 1:625 with

ddH_2O. Then a mastermix was prepared with 5 µl QuantiFast™ SYBR® Green PCR Kit and 1 µl forward (10 pmol/µl) and 1 µl revers primer (10 pmol/µl) per sample. Seven µl of this mastermix and 3 µl of cDNA pool were transferred to a Light Cycler 480 Multiwell Plate 96 and measured in triplicates. Afterwards, this plate was centrifuged for 1 min at 800 rpm and analyzed on a ROCHE Light Cycler 480. After the primer efficiency had been checked (between 1.8 and 2), the single cDNAs were used to determine the relative gene expression. Cyclophilin A was used as internal normalization standard. For analyzing the expression profiles and associated statistical parameters the public domain program Relative Expression Software Tool - REST (http://www.gene-quantification.com/download.html) was used.

Table 7: Primer sequences and product sizes for real time PCR primers from the Harvard Primer Bank.

Gene	Forward primer (5`-3`)	Reverse primer (5`-3`)	Product size
Cyclophilin A	TTCCAGGATTCATGTGCCAG	CCATCCAGCCATTCAGTCTT	202 bp
HSL	GCTGGTGACACTCGCAGAAG	TGGCTGGTGTCTCTGTGTCC	182 bp
KIAA1363	TCGCAGCGGCTCTTCTGGTT	GATGCTGCTGGACGCCACTT	220 bp
iNOS	GTTCTCAGCCCAACAATACAAGA	GTGGACGGGTCGATGTCAC	127 bp

3.2.3.7 DNA agarose gel electrophoresis

DNA size and purity were analyzed by agarose gel electrophoresis. The concentration of agarose used for analysis is inversely proportional to the size of interest.

Table 8: Agarose concentrations used for different DNA sizes.

Agarose concentration (%)	DNA size (kb)
0.7	20-1
0.9	7-0.5
1.2	6-0.4
1.5	4-0.2
2	3-0.1

Agarose was weighed and dissolved in 1 x TAE buffer by boiling in a microwave. The solution was allowed to cool down to 60°C or lower before ethidium bromide was added to yield a final concentration of 0.5 µg/ml. The gel solution was poured into a gel rack and was allowed to polymerize completely. Afterwards the gel was put into a gel chamber with 0.5 x TAE buffer, the sample DNA was mixed with loading buffer and loaded into the slot. Gel electrophoresis was carried out at 90 V.

3.2.3.8 DNA quantification

Similar to RNA quantification (3.2.3.3), 2 µl DNA were quantified on a spectrophotometer (NanoDrop) at a wavelength of 260 nm. DNA concentration was calculated with the following formula:

$$C_{(ngDNA/\mu l)} = \lambda_{260nm} \times 50$$

3.2.3.9 Maxi preparation of plasmid DNA with EndoFree plasmid Maxi-Kit (Qiagen)

Five ml culture medium containing the appropriate selective antibiotic were inoculated with a single colony and incubated at 37°C under vigorous shaking. After 8 h 200 ml culture medium were inoculated with 2 ml starter culture and incubated overnight at 37°C under vigorous shaking. Cells were harvested by centrifugation at 6000 x g for 15 min at 4°C. The bacteria were completely suspended in 10 ml buffer P1 by vortexing. Thereafter, 10 ml buffer P2 were added, the solution was mixed gently by inverting the tube 4-6 times and then incubated at RT for 5 min. During this time the QIAfilter cartridge was prepared as described in the manufacturer's instruction. After the incubation 10 ml chilled buffer P3 were added to the lysate and mixed immediately but gently by inverting 4-6 times. The lysate was poured into the barrel of the QIAfilter cartridge and incubated at RT for 10 min. Afterwards, the cap from the QIAfilter cartridge outlet nozzle was removed, the plunger was gently inserted into the QIAfilter maxi cartridge and the cell lysate was filtered into a 50 ml tube. ER buffer (2.5 ml) was added to the lysate, mixed by inverting the tube approximately for 10 min and incubated for 30 min on ice. Then a QIAGEN-tip 500 was equilibrated by applying 10 ml buffer QBT. Next the lysate was applied to the QIAGEN-tip and allowed to enter the resin by gravity flow. After washing the QIAGEN-tip twice with 30 ml buffer QC, the DNA was eluted with 15 ml buffer QN. DNA was precipitated with 10.5 ml isopropanol. After mixing and centrifugation at 15000 x g for 30 min at 4°C, the supernatant was decanted carefully and the pellet was washed with 5 ml of endotoxin-free, 70 % EtOH and centrifuged at 15000 x g

for 10 min. After decanting the supernatant, the pellet was air-dried for 5-10 min and finally dissolved in a suitable volume of endotoxin-free TE buffer. DNA concentration was determined by UV spectrophotometrically (3.2.3.8).

3.2.4 Biochemical methods

3.2.4.1 Transfection of COS-7 cells

Before transfection, COS-7 cells were collected in the logarithmic growth phase. Cells (150000 cells/well) were plated in 6-well dishes and cultured overnight. Transient transfection of COS-7 cells with pcDNA4/HisMax encoding His-tagged KIAA1363, HSL, or ß-galactosidase (LacZ) was performed using Metafectene™. For that purpose, 2.5 µg of purified DNA per well were incubated with 10 µl Metafectene™ for 20 min at RT in serum-free DMEM in a total volume of 100 µl. Subsequently, cells were incubated with the DNA/ Metafectene™ complex for 4 h in serum-free medium. Afterwards the medium was replaced by DMEM containing 10 % FCS. Fourty eight h after transfection cells were washed twice with PBS, scraped in lysis buffer and used for lysate preparations. As transfection control a LacZ staining was performed (126). After washing two times with PBS cells were fixed for 10 min at RT with 1 ml 0.5 % glutaraldehyd. Then cells were washed again with PBS containing 1 mM $MgCl_2$ and covered with 500 µl staining solution. The cells were incubated at 37°C ON and on the next day the transfection rate was determined by counting blue cells. A normal transfection rate for COS-7 cells was achieved between 60-80 %.

3.2.4.2 Preparation of cell lysates and sub fractions

For lysate preparation, confluent cells (COS-7 or MPM) were washed two times with PBS and sonicated twice for 10 s in 100 mM potassium phosphate lysis buffer. Nuclei and cell debris were removed by centrifugation at 4°C and 1000 x g for 5 min. Cytosolic and membrane fractions were prepared by centrifugation at 100000 x g for 1 h (4°C). For western blot analysis cells were lysed in RIPA-buffer, scraped off the plates and sonicated two times for 10 s. Protein of all cell lysates was quantitated by the method of Bradford (3.2.4.6).

3.2.4.3 Lipid droplet (LD) isolation from RAW264.7 macrophages

RAW264.7 cells were cultured to 100 % confluency in 150 mm plates containing 25 ml DMEM + 10 % FCS and 50 µg/ml acLDL for 72 h. Foam cells were washed with ice-cold PBS, scraped off, pooled and placed in a 50 ml tube. The cell suspension from 9 plates was centrifuged at 500 x g for 5 min at 4°C. The supernatant was discarded and the cells were resuspended in 8 ml lysis buffer, vortexed and incubated on ice for 20 min. Cells were homogenized by sonification for 20 s with 1 min of ice in between for three times. After centrifugation at 1000 x g for 10 min the supernatant was transferred to a SW41 tube and the pelleted cell nuclei were discarded. 3.5 ml LD buffer were transferred on 7 ml supernatant fraction and centrifuged at 40000 rpm for 3 h at 4°C. LD concentrated in a white band on the top of the gradient. LD were collected with a 1 ml pipette tip and transferred to a 1.5 ml tube. Afterwards the lipids were determined enzymatically (3.2.4.9).

3.2.4.4 Cholesterol efflux from MPM

Per well, 100 µg of freshly prepared acLDL was incubated with 1µCi [1, 2- ^{3}H]cholesterol for 3 h at 37°C in a water bath. Next, the complex was loaded onto a PD-10 column to remove the unincorporated radioactivity. MPM were seeded in 12-well plates (three wells per condition) and incubated with 50 µg ^{3}H-cholesterol- enriched acLDL for 24 h. Afterwards, cells were equilibrated ON in medium containing 0.2 % FA-free BSA and 0.3 mM dibutyryl cAMP. After two washing steps with PBS and 0.2 % BSA, cells were incubated with 100 µg/ml human HDL_3 or 15 µg/ml purified human apoA-I in 1 ml DMEM/0.2 % BSA supplemented with 2 µg/ml ACAT-inhibitor 58-035. After 1, 3, 6, and 9 h an aliquot of medium was taken, cell debris and cholesterol crystals were precipitated at 6000 x g for 10 min and radioactivity in the supernatant was determined by liquid scintillation counting. Cells were washed with PBS, lysed in 1 ml of 300 mM NaOH and radioactivity and protein content were determined. In all experiments, fractional efflux was corrected for the radioactivity released to DMEM in the absence of an acceptor. Cholesterol efflux was expressed as the percentage of the radioactivity released from cells into the medium relative to the total radioactivity in cells and medium.

3.2.4.5 FFA and cholesterol uptake of MPM

The FFA-BSA complex was prepared as follows. Seventy µCi of ^{3}H-oleate were evaporated, resuspended in 5 µl 5 M NaOH, vortexed and incubated at 37°C for 5 min in a water bath. 700 mg FA- free BSA was dissolved in 70 ml DMEM and 4.26 mg Na-oleate in EtOH was

added. The radiolabelled complex was mixed with the medium and incubated at 37°C in a water bath for 1 h. Afterwards, the medium was sterile filtrated and stored at -20°C.

MPM were seeded in 12 –well plates (three wells per condition) with medium + 0.2 % FA-free BSA ON. After 2 washing steps with PBS, cells were incubated for 24 h with the radiolabelled FFA complex or the [^{3}H]cholesterol complex (3.2.4.4). On the next day, cells were washed three times with PBS in the 4°C room and the neutral lipids were extracted by incubation with 1 ml hexane:isopropanol (3:2, v/v) for 1 h at 4°C. Afterwards, the cells were lysed with 1 ml 300 mM NaOH and protein was determined by the method of Bradford (3.2.4.6).

Ten µl of the lipid extracts were directly transferred to 4 ml Ultima Gold Cocktail (Perkin Elmer) and counted by liquid scintillation counting on a β-counter. The remaining part was dried under nitrogen, dissolved in 100 µl human serum and 50 µl were separated by thin layer chromatography (3.2.4.15). Bands were cut out and radioactivity was measured by scintillation counting. Percent of FFA or cholesterol in the different lipid fractions were calculated to 100 % of the lipid extract and normalized to mg cell protein.

3.2.4.6 Protein quantification according to the method of Bradford

The Bradford assay is a common method to determine total protein concentrations of a sample. This method is based on the observation that the absorbance maximum of Coomassie Brilliant Blue (Biorad Reagent) shifts from 465 nm to 595 nm after protein binding. Protein concentrations determined with this method were used for normalization of all cell culture experiments. After lipid extraction, cells were lysed with 2 ml of 0.3 M NaOH for 30 min. For an optimal cell disruption cells were frozen at -20°C. Thereafter, cells were scraped off and the cell lysate was transferred into a 1.5 ml tube. For the assay 200 µl ddH_2O and 60 µl Biorad-Reagent were pipetted into a microtiter plate. Fifteen µl of the samples were added and the content was mixed accurately. After 5 min of incubation, samples were measured spectroscopically at 595 nm. Each time, an appropriate standard curve with BSA was prepared to calculate the protein concentrations in the samples.

3.2.4.7 Neutral lipid extraction from cells and tissues

MPM were seeded in 6- well plates and lipids were extracted with 2 ml hexane:isopropanol (3:2, v/v) for 1 h at 4°C. Lipid extracts were dried under nitrogen, redissolved in 100 µl 1 % Triton X-100 in chloroform, dried under nitrogen and resuspended in 100 µl ddH_2O for 15 min at 37°C. Aliquots were used for enzymatic determinations of TG (50 µl), TC (15 µl) and

FC (15 µl) concentrations (3.2.4.9). Proteins of extracted cells were dissolved in 2 ml of 0.3 M NaOH for 1 h at RT and protein content was quantitated using a Bradford assay (3.2.4.6).
Neutral lipids from tissues were extracted by the method of Folch (127). Tissues were surgically removed, washed in PBS containing 1 mM EDTA, weighed and transferred into homogenization vials. These vials can be stored at -20°C. Before homogenization of the tissues with the Precellys 24 homogenizer, 1 ml chloroform:methanol (2:1, v/v)/ 100mg tissue were added to the vials. After homogenization two times at 6500 rpm for 20 s, the content was transferred to polypropylene tubes. Another 2 ml chloroform:methanol (2:1, v/v)/ 100mg tissue were added. The lipids were extracted for 20 min on a spinning wheel at RT and afterwards the tubes were centrifuged at 4000 rpm for 10 min to precipitate the homogenized tissues. The supernatant was transferred into a new tube and 200 µl 0.9 % NaCl /ml extraction phase were added. The tubes were centrifuged again at 4000 rpm for 2 min to separate the phases. The phase below was pipetted into a glas tube, evaporated with nitrogen and dissolved in 1 ml chloroform:methanol (2:1, v/v). Lipid extracts can be stored at -20°C. For the determination of lipid parameters, 300 µl were transferred into a new glas tube, 100 µl 1 % Triton X-100 in chloroform were added and dried under nitrogen. The lipids were suspended in 100 µl ddH_2O for 15 min at 37°C in a water bath. Aliquots (5-10 µl) were used for enzymatic determinations of TG, TC and FC concentrations (3.2.4.9) and normalized to the tissue weight.

3.2.4.8 Fatty acid composition of MPM

To analyze the FA composition of the cellular lipid fraction from MPM, lipids were extracted twice with hexane:isopropanol (3:2, v/v; 1ml/dish), dried under nitrogen, and redissolved in 1 ml of chloroform. Aliquots of 100 µl were separated by TLC under argon using hexane:diethylether:acetic acid (70:29:1; v/v/v) as mobile phase. Plates were dried, stained with iodine vapor, and PL, DG, FFA, TG, and CE bands were scraped off the plates. After addition of the internal standard (pentadecanoic acid; 10 µg), lipids were transesterified (1 ml toluene and 1 ml boron trifluoride-methanol (20 %) directly on the silica gel at 110°C for 1h. GC analysis of the corresponding FA methyl esters was performed as described (128). Quantification was performed by peak area comparison with the internal standard.

3.2.4.9 Lipid parameter determination in lipid extracts and plasma

Lipid parameters were quantitated with standard kits according to the manufacturer's instructions. The kits for FC and TG determination were obtained from DiaSys (Holzheim,

Germany), for TC measurements from Greiner Diagnostics (Langenthal, Switzerland) and for FFA detection from WAKO Chemicals GmbH (Neuss, Germany).
For the lipid parameter determination in plasma, blood was taken from fed and fasted age-matched mice by retro-orbital bleeding. One µl 0.5 M EDTA/ 100 µl plasma were added and immediately centrifuged at 4°C, 8000 rpm for 5 min. Five µl of plasma were used for the enzymatic measurements. CE was calculated from TC content minus FC content, multiplied with the factor 1.7253 for esters.

3.2.4.10 DG determination of MPM by liquid chromatography and mass spectrometry

MPM from each mouse were seeded in two 6-wells for DG estimation and one 12-well for protein normalization. After adherence of MPM, cells in the 6-wells were washed twice with PBS and scraped off the plate in 2.5 ml methanol. An internal standard (12:0/12:0 diacylglycerol, 16 nmol/sample) was added in 1.25 ml chloroform. The samples were vortexed for 30 s. For the lipid extraction another 1.25 ml chloroform was pipetted to the samples and after vortexing, 1.25 ml dH_2O was transferred to the sample tubes, which were again vortexed. The samples were incubated at RT for 10 min and centrifuged at 4000 rpm for 5 min to separate the phases. The organic phase was transferred into a new glas vial, dried under nitrogen, resuspended in 1 ml chloroform:methanol (2:1, v/v) and stored at -20°C. For the measurements lipid extracts were diluted 1:100 in acetonitrile/isopropanol (5:2, v/v) containing 1 % ammonium acetate and 0.1 % formic acid (solvent B). The chromatography was performed on a Thermo Hypersil Gold C18 column (Thermo Fisher scientific, Vienna Austria) with a flow rate of 250 µl/min. Data acquisition was done by FT-ICR-MS full scan at a resolution of 100 k and < 2 ppm mass accuracy with external calibration. MS/MS data were taken from the most abundant species in each spectrum. For data analysis peak areas were calculated by QuanBrowser for all lipid species, identified previously by exact mass (< 2 ppm) and retention time. The calculated peak areas for each species were expressed as % of 12:0/12:0 diacylglycerol internal standard. MS/MS data were used to confirm the identity of molecular species.

3.2.4.11 Lipoprotein profile

Plasma samples of overnight fasted mice were pooled and lipoproteins were isolated by fast protein liquid chromatography (FPLC) on a Pharmacia FPLC system (Karlsruhe, Germany) equipped with a Superose 6 column (Amersham Biosciences, Piscataway, NJ). For each run

200 µl pooled plasma samples were diluted, subjected to FPLC analysis and lipoproteins were eluted with 10 mM Tris-HCl, 1 mM EDTA, 0.9 % NaCl, and 0.02 % NaN_3 (pH 7.4). Sixty fractions of 0.5 ml each were collected and TG and TC concentrations were assayed enzymatically using above mentioned kits (3.2.4.9). To enhance sensitivity, reaction buffers were supplemented by the addition of sodium 3.5-dichloro-2-hydroxy-benzenesulfonate.

3.2.4.12 SDS-polyacrylamid gel electrophoresis (SDS-PAGE)

SDS-PAGE is used to separate proteins according to their molecular weights. The gel mixture contains SDS to denaturate proteins and also provides a negative charge to the proteins. Due to their linear form and negative charge, the proteins move through the gel with large proteins moving slower than smaller ones. The SDS gel is discontinuous and consists of a separating and a stacking gel on top.

Table 9: Components of the separating gel.

reagent	**8 % SDS-gel**	**12.5 % SDS-gel**
acrylamid	2293 µl	3583 µl
buffer 1	2170 µl	2170 µl
ddH_2O	4137 µl	2847 µl
10 % SDS	100 µl	100 µl
TEMED	4.4 µl	4.4 µl
10 % APS	76 µl	76 µl
final volume	**87804.4 µl**	**87804.4 µl**

Table 10: Components of the stacking gel.

reagent	**volume**
acrylamid	326 µl
buffer 2	500 µl
50 % glycerin	1650 µl
10 % SDS	21.5 µl
TEMED	1.25 µl
10 % APS	19 µl
final volume	**2517.75 µl**

Cells were lysed as previously described (3.2.4.2). After protein quantitation using the Bradford assay (3.2.4.6), 50-100 µg protein were diluted 1:1 (v/v) with sample buffer and boiled for 10 min at 95°C. After a 1 min centrifugation at 12000 rpm, the denaturated protein samples were loaded into the gel slot and the gel was run at 150 V for 1.5 h. On each SDS gel a protein standard (Fermentas, Austria) was loaded to reveal the molecular protein weight.

3.2.4.13 Western blot analysis

Proteins separated by SDS-PAGE were transferred onto a nitrocellulose membrane for Western blotting experiments. Two sheets of whatman paper and one piece of nitrocellulose membrane were cut according to the size of the gel. A special sponge and one sheet of paper were immersed in the blot buffer and placed in the chamber. Then the gel and the moistened membrane were placed onto the paper. Another sheet of whatman paper and a sponge were dipped into the buffer and placed on top. Finally, the proteins were transferred onto the membrane by applying a current of 150 mA for 40 min in the 4°C room. After the transfer the membrane was washed shortly with blot-washing buffer and then incubated with 15 ml 5 % BSA for 30 min at RT. After blocking the non-specific interaction sites, the membrane was shaken with the primary antibody in 5 % BSA solution ON or over the weekend at 4°C. Table 11 shows the used antibody dilutions.

Table 11: Dilutions of primary and secondary antibodies and the detectable protein size.

Prim. Antibody	Dilution	Second. antibody	Dilution	Protein size
anti-HSL (Cell Signaling Technology, Danvers, MA, USA)	1:800	Polyclonal-Goat-Anti-Rabbit IgG-HRP	1:2000	84 kDa
anti-KIAA1363 (120)	1:1000	Polyclonal-Goat-Anti-Rabbit IgG-HRP	1:2000	45 and 50 kDa
Selfmade anti-HSL (129)	1:10000	Polyclonal-Goat-Anti-Rabbit IgG-HRP	1:2000	84 kDa
β-Actin (Santa Cruz Biotechnology Inc., Heidelberg, Germany)	1:2000	Polyclonal-Rabbit-Anti-Mouse IgG-HRP	1:1000	46 kDa

After incubation with the primary antibody, the membrane was washed twice for 10 min with 20 ml blot-washing buffer. Then the membrane was incubated with the secondary antibody for 2 h at RT. Afterwards, the membrane was washed with blot-washing buffer for four times for 15 min each. The proteins were detected by chemiluminescence. The membrane was incubated with a mixture of detection reagent 1 and 2 (1:1 ratio) (ECL plus, Amersham Bioscience, Piscataway, NJ) for 1 min and then wrapped into a cling film. The wrapped blot was placed in a film cassette and a sheet of AGFA Curix Ultra X Ray film (Siemens, Graz, Austria) was applied on top of the membrane. Exposure times varied from 1 min to 45 min, depending on the protein.

3.2.4.14 Binding of the specific fluorescent activity recognition probes NBD-sn1-TGP, NBD-sn3-TGP, and NBD-CP to enzymes

Due to the binding of the specific fluorescent activity recognition probes to the active site of enzymes it is possible to selectively screen for lipolytic enzymes and make them “visible”. Thus, they can be detected and quantified on the basis of their fluorescent signal.

Cytoplasmic extracts of COS-7 were prepared as described above (3.2.4.2). Fifty µg of cellular protein were incubated with 1 nmol of the specific fluorescently labeled probes 7-nitrobenz-2-oxa-1,3-diazole (NBD) cholesteryl phosphonate (CP) and enantiomeric TG analogs (NBD-sn1-TGP and NBD-sn3-TGP) (130), as well as 1 mM Triton X-100 at 37°C for 2 h under shaking as described (131). Total protein was precipitated with 10 % trichloro acetic acid for 1 h on ice, washed with acetone and subjected to 10 % SDS-PAGE (3.2.4.12). Gels were treated with 10 % EtOH and 7 % acetic acid and fluorescent signals were detected on a BioRad FX Pro laser scanner (excitation 488 nm, emission 530 nm).

3.2.4.15 Thin layer chromatography (TLC)

TLC is used for the separation of various lipid classes. To separate lipids, silica gel plates are used as stationary phase and organic solvents as mobile phase. Lipid extracts were spiked with 5 µg 1,2- diolein and 1,3- diolein (3.2.4.5), evaporated an suspended in 100 µl human serum extract. Fifty µl sample were spotted on silicagel-plates (Merck, Darmstadt, Germany). The plates were run in a chamber filled with 50 ml of hexane:diethyl ether:acetic acid (65:35:1, v/v/v) for 30 min. Lipids were visualized by iodine evaporation for 5 min. The bands corresponding to PL, FFA, TG, FC, and CE were labelled, cut out on the next day and radioactivity was measured by liquid scintillation counting.

3.2.4.16 *p*-Nitrophenyl valerate esterase assay

This assay was performed to determine esterase activity of HSL and KIAA1363. *p*-Nitrophenyl valerate hydrolysis was determined in a microtiter plate using 5 µg of whole cell lysate (3.2.9.2) and 100 µl of 3 mM *p*-nitrophenyl valerate in 100 mM potassium phosphate buffer pH 8, containing 0.2 mM EDTA and 0.03 % Triton X-100. The absorbance of released p-nitrophenol was measured at 405 nm at RT after 15 and 30 min. The molar extinction coefficient of *p*-nitrophenol ($\varepsilon_{405\ nm}$) used for the calculation of enzymatic activity was 18,300 $M^{-1}\ cm^{-1}$.

3.2.4.17 Assays for neutral CE, TG, DG and RE hydrolase activitites

For determination of CE, TG, DG, and RE hydrolase activities, substrates were always freshly prepared (Table 12).

Table 12: Substrate components per sample.

Substrate	Tracer	Non-radioactive component	PC/PI (3:1, w/w)
Cholesteryl oleate (CO)	cholesteryl [1-^{14}C]-oleate (50000 cpm/nmol)	20 nmol CO	35.5 µg
Triolein (TO)	[9,10-^{3}H(N)]-triolein (40000 cpm/nmol)	25 nmol TO	15 µg
1,2 Diolein (DO)	dioleyl-rac-glycerol [oleoyl-1-^{14}C] (120000 cpm/nmol)	40 nmol DO	15 µg
Retinyl palmitate (RP)	retinyl palmitate and [9,10(n)-^{3}H] palmitate (50000 cpm/nmol)	20 nmol RP	7.5 µg

Table 13: Alternative mixed micelles for the CE hydrolase assay.

Substrate	Alternative mixed micelles
Cholesteryl oleate (CO)	35.5 µg PC/PI (3:1, w/w) without sodium taurocholate
Cholesteryl oleate (CO)	35.5 µg PC + 2 µM sodium taurocholate

All lipid substrates (Table 12 + 13) were prepared by sonification and the amount of substrate and chemicals is described per sample. After evaporation, substrates were sonicated for 30 s (Virsonic 475) (132) on ice in 50 µl 100 mM potassium phosphate buffer, pH 7.0, containing 4 µM Na- taurocholate. Next, 25 µl 5 % FA-free BSA (pH 7.0) was added and the substrate was sonicated again for 1 min on ice. After addition of 25 µl 20 % FA-free BSA (pH 7.0), 100 µl substrate were incubated with 100 µg of cell extracts (lysates or subfractions 3.2.4.2) in a water bath at 37°C for 1 h. To reveal the spontaneous hydrolysis of the substrates, 100 µl lysis buffer were incubated with 100 µl substrate. The reaction was terminated by the addition of 3.25 ml of methanol:chloroform:heptane (10:9:7, v/v/v), 1 ml of 100 mM potassium carbonate and 100 mM boric acid, pH 10.5. After centrifugation (800 x g, 20 min) the radioactivity in 1 ml of the upper phase was determined by liquid scintillation counting. Hydrolase activities in MPM and foam cells were determined in cell lysates, cytosolic and membrane fractions by liquid scintillation counting.

Tissue preparation:

For determination of CE and AcMAGE hydrolase activities in murine tissues, tissues were surgically removed and washed in PBS containing 1 mM EDTA. Homogenization was performed in lysis buffer on ice using a Precellys24 homogenizer. Lysates were centrifuged for 30 min at 20,000 x *g* (4°C). Radioactivity in 100 µg of the lipid-free infranatant was determined by liquid scintillation counting. Protein concentrations were determined using a Bradford assay (3.2.4.6). The enzyme activity was calculated as follows:

Factor A =

$$\frac{\text{[total volume of upper phase x nmol total FFA/sample x correction protein to 1 mg]}}{\text{Extraction coefficient (0.76)}}$$

Lipase activity [nmol/h/mg] =

$$\frac{\text{[cpm (sample)- cpm (spontaneous hydrolysis of substrate)] x Factor A}}{\text{cpm (100 µl substrate)}}$$

3.2.4.18 Assays for acid CE and TG hydrolase activitites

Assays were performed as described in 3.2.4.17, only the pH of the solutions was different. The pH of the 100 mM potassium phosphate buffer as well as the BSA solutions for the

substrate was set to 3.0. Afterwards, 100 µl substrate (pH 3.0) were mixed with 100 µl cell extracts (pH 7.0) and a pH of 4.2 was reached.

3.2.4.19 AcMAGE hydrolase activity assay

This assay was performed as described previously (125). First, the substrate [^{3}H-acetyl]AcMAGE was prepared for approximately 50 samples by incubation of 10 mM unlabeled PAF with 10 µCi [^{3}H-acetyl] PAF and 20 units phospholipase C from *Bacillus cereus* in 500 µl 100 mM phosphate buffer pH 7.4 for 30 min at 25°C. For the enzyme reaction 5 µl [^{3}H-acetyl]AcMAGE was added to 2 µg of cell lysates, sub fractions or tissues (3.2.4.17) and were incubated for 2 h at 37°C in a water bath. Reactions were terminated by addition of 2.5 ml of chloroform:methanol:hexane (1.25:1.4:1, v/v/v) and 0.83 ml of 100 mM potassium carbonate, 100 mM boric acid, pH 10.5. After extraction, the upper aqueous layer containing potassium [^{3}H]acetate was removed for scintillation counting. The enzyme activity was expressed as % acetate release.

3.2.4.20 LPL activity assay

MPM were incubated in 12-wells with 1 ml medium + 2 % BSA containing 2 units/ml heparin for 1 h at 37°C. WAT (used as positive control) was surgically removed, washed in PBS, weighed, minced with scissors and transferred to ice-cold tubes containing 1 ml medium + 2 % BSA containing 2 units/ml heparin for 1 h at 37°C. For the substrate preparation per sample, 0.6 µCi of radioactive triolein, 920 ng of non-radioactive glycerol trioleate and 0.1 % Triton X-100 in chloroform were evaporated under a stream of nitrogen. Fourty µl Tris/HCl (pH 8.6, 1 M) and 80 µl ddH_2O were added and the mixture was sonicated six times (1 min on, 1 min off) on ice. Then 40 µl of heat-inactivated human serum containing apoCII as activator (obtained from a pool of donors, then heated at 50°C for 1 h and stored at -20°C) and 40 µl 10 % BSA were added to the substrate. For the analysis, 200 µl of substrate were incubated with 100 µl of sample for 1 h at 37°C. The reaction was stopped by the addition of 3.25 ml of a mixture of methanol:chloroform:heptane (1.41:1.25:1, v/v/v) and 1 ml of 100 mM potassium carbonate, 100 mM boric acid, pH 10.5. NEFA were extracted by vortex-mixing for 10 s and phases were separated by centrifugation at 3200 rpm for 10 min. One ml of the upper phase was pipetted into 4 ml Ultima Gold scintillation Cocktail and counted in a β-counter (133). MPM were lysed and protein was quantitated by the method of Bradford (3.2.4.6). The enzyme activity was calculated as described in 3.2.4.17.

3.2.5 Microscopy

3.2.5.1 Nile red and filipin staining of MPM

MPM were seeded on chamber slides and loaded with 100 µg/ml acLDL for 48 h and 72 h. Cells were fixed with 4 % paraformaldehyde for 30 min and lipid droplets were visualized after nile red staining (2.5 µg/ml) by confocal laser scanning microscopy using an LSM 510 META microscope system (Carl Zeiss GmbH, Vienna, Austria). Pictures (60 x) were taken at excitation 543 nm and signals recorded using a 560 nm long pass filter.

For filipin staining MPM were fixed with 4 % paraformaldehyde for 30 min and then incubated with 10 µl filipin [5mg/ml stock] in 1 ml PBS for 2 h on the shaker. Afterwards cells were washed 3 times with PBS and FC was visualized by confocal laser scanning microscopy using an LSM 510 META microscope system. Pictures (60 x) were taken at excitation 335 nm and signals recorded using a 365 nm long pass filter.

3.2.5.2 Cell preparation and transmission electron microscopy

Standard chemical fixation

MPM grown on a Melinex Film (Gröpl, Tulln, Austria) were transferred into vials containing 2.5 glutardialdehyde in 0.06 M phosphate buffer at pH 7.2 for 90 min at RT. Subsequently, the MPM were rinsed two times in 0.06 M phosphate buffer for 10 min. Postfixation was performed in 1 % osmium tetroxide in 0.06 M phosphate buffer pH 7.2 for 60 min. Then the specimens were rinsed four times for 10 min in 0.06 M phosphate buffer (pH 7.2) and dehydrated in 50 %, 70 %, 90 %, and 100 % cold acetone for 20 min each.

Thereafter, samples were infiltrated in 2:1, 1:1, 1:2 mixtures of 100 % aceton and agar 100 epoxy resin (Gröpl, Tulln, Austria) and pure agar 100 epoxy resin for at least 3 h. Then the samples were placed in fresh agar 100 epoxy resin at RT for at least 3 h, transferred in embedding molds and polymerized at 60°C for 48 h.

Ultrathin sections (75 nm) were cut with a Reichert Ultracut S ultramicrotome and post stained for 5 min with lead citrate and for 15 min with uranyl acetate before they were observed in the Philips CM 10 transmission electron microscope (TEM) (134).

Chemical fixation for immunogold labeling

Cells were fixed in 2.5 % paraformaldehyde/0.5 % glutardialdehyde in 0.06 M phosphate buffer (pH 7.2) for 60 min at RT. After the samples had been washed two times in 0.06 M

phosphate buffer (pH 7.2), they were gradually dehydrated in increasing concentrations of EtOH (50 % to 90 %). Infiltration was accomplished with 2:1, 1:1, 1:2 mixtures of 90 % EtOH and LR White and pure LR White for 3 h each step at RT. Then the samples were placed in fresh LR White at RT for at least 3 h, transferred in embedding molds and polymerized at 50 °C for 48 h.

Immunogold labeling

Ultrathin sections of 75 nm cut with a Reichert Ultracut S ultramicrotome were mounted on nickel grids and blocked with 2 % BSA in PBS (pH 7.2) for 20 min at RT. Next the samples were treated with the primary antibody (HSL antibody Rabbit polyclonal IgG,(129) diluted 1:5 in 1 % BSA for 2 h at RT. After a short rinse the samples were incubated with a 10 (20) nm gold- conjugated secondary antibody (goat anti rabbit IgG– British BioCell International) diluted 1:5 in 1 % BSA for 90 min at RT. Then the samples were washed for 15 min in PBS and finally in ddH_2O. The labeled grids were either immediately observed in the TEM or were post stained with uranyl acetate (30 s) before the observation. Post staining was applied to facilitate the distinction of different cell structures enabling a clear identification of the investigated organelles.

3.2.5.3 Antibody staining and fluorescence microscopy

Macrophages were seeded on coverslips in 6-wells. To achieve foam cell formation they were loaded for 48 h with acLDL. For the antibody labelling cells were washed 3 times with PBS and fixed with 4 % paraformaldehyde/0.02 % glutardialdehyde for 20 min. After 1 h blocking with blocking solution on the shaker, cells were incubated with the first HSL-AB (129) at a dilution of 1: 50 in blocking solution for 30 min at RT. After one washing step with washing buffer, foam cells were incubated with the second fluorescently labelled antibody (Alexa Fluor red, 595 nm, Molecular probes® by Invitrogen, Austria) for 45 min, 1: 250 diluted in blocking solution. Cells were washed afterwards three times with washing buffer. Before visualizing, cells were stained for 3 min with 0.5 mM Bodipy green (488 nm, Molecular probes® by Invitrogen, Austria) and coverslips were transferred to a Leica SP2 AOBS confocal microscope (Leica Microsystems, Mannheim, Germany) with spectral detection to take pictures at an amplification of 60. Pictures were edited using the LCS Lite 2611537 software.

3.2.6 Statistics

Statistical analyses were performed with GraphPad Prism 5.0 using the Student's t-test. Significance levels were set at $p < 0.05$ (*), $p \leq 0.01$ (**), and $p \leq 0.001$ (***).

4. Results

4.1 Characterization of macrophages and foam cells

4.1.1 Nile red and filipin staining of C57BL/6 MPM and foam cells

In first experiments, a double staining with nile red (stains the neutral lipids) and filipin (stains FC) was performed to determine the difference in lipid content between MPM and foam cells of C57BL/6 mice. MPM were loaded with 100 µg acLDL for 48 h to achieve foam cell formation. The cells were grown on chamberslides, stained and the neutral lipids and FC were visualized by confocal laser scanning microscopy (in collaboration with Heimo Wolinski).

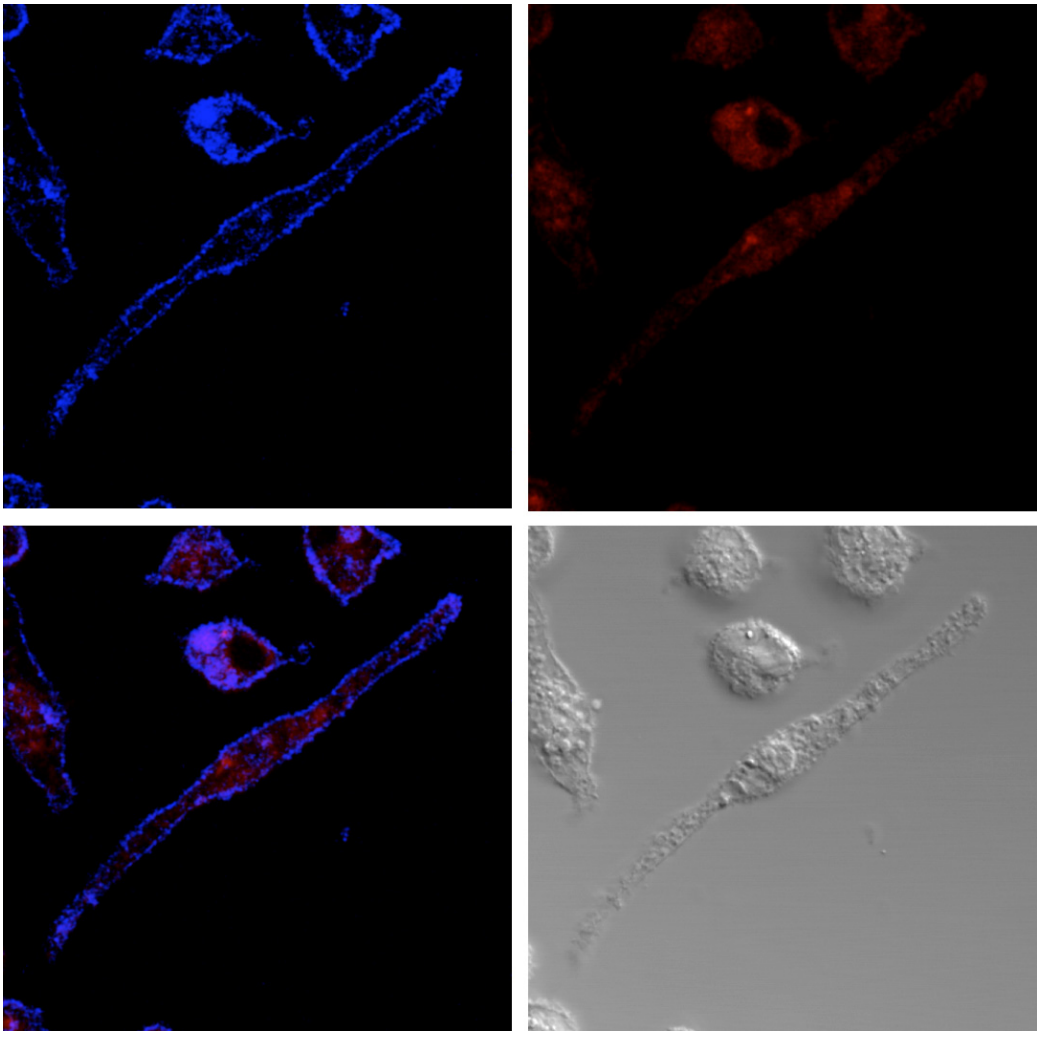

Figure 19: MPM double stained with filipin (blue) and nile red (red). Filipin stains FC, which is a component of the plasma membrane. Nile red labels neutral lipids in the lipid droplets (LD). Confocal laser scanning microscopy was performed to visualize the lipids. Under transmitted light the cell structure was obvious. MPM from C57BL/6 mice did not exhibit LD.

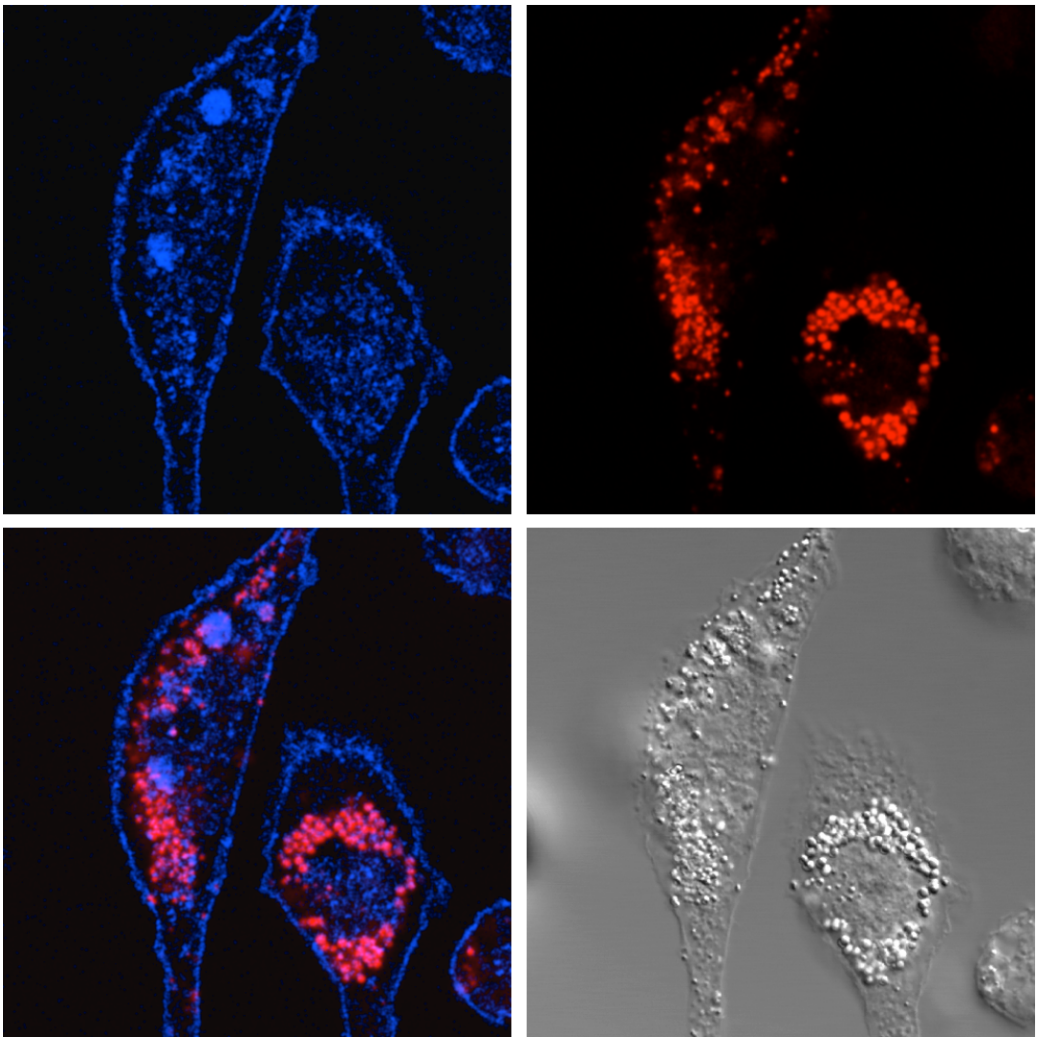

Figure 20: Foam cells double stained with filipin (blue) and nile red (red). Foam cell formation was achieved by loading MPM from C57BL/6 mice for 48 h with 100 µg acLDL. Filipin stains FC and nile red labels neutral lipids in the LD. Confocal laser scanning microscopy was performed to visualize the lipids. LD were also seen by an increase of transmitted light.

FC was visible under UV-light by filipin staining (blue). In foam cells (Figure 20), FC was apparent because of more metabolic activity in the lysosomes/endosomes compared to MPM. FC, a component of plasma membranes, was seen in both MPM and foam cells (Figure 19, 20). MPM from C57BL/6 mice did not contain LD (Figure 19). Quite contrary to foam cells: they exhibit a lot of LD (Figure 20).

4.1.2 Lipid content of male and female C57BL/6 MPM and foam cells

The lipid content of MPM and foam cells isolated from C57Bl/6 male and female mice were determined enzymatically to confirm the results from the lipid staining.

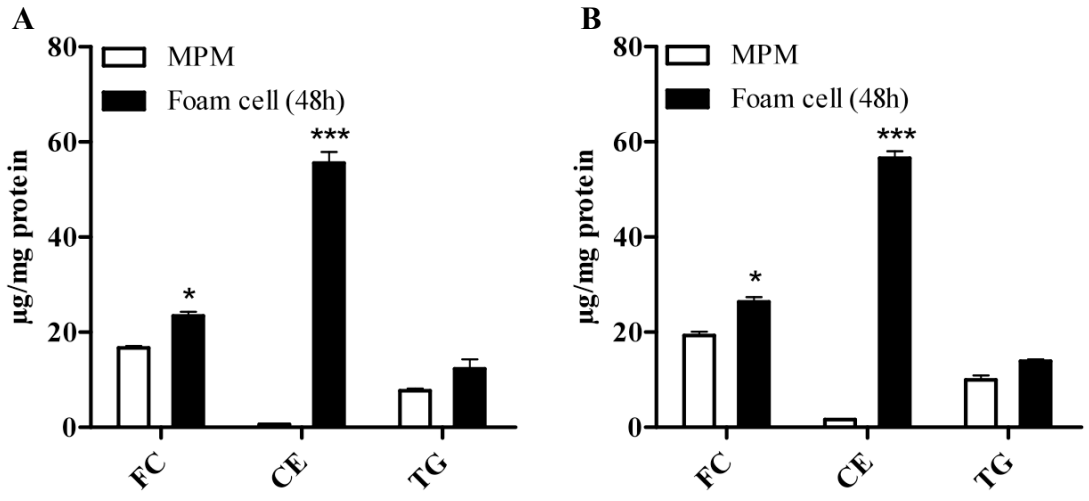

Figure 21: FC, CE and TG content of male and female C57BL/6 MPM and foam cells. Lipids from MPM and foam cells of C57BL/6 male (A) and female (B) mice were extracted with hexane:isopropanol (3:2, v/v) for 1 h at 4°C and FC, TC and TG were determined enzymatically. Afterwards cells were lysed with 1 ml 0.3 M NaOH and protein concentration was estimated with the method of Bradford.

The content of FC was increased by 40 % in male foam cells and 37 % in female foam cells compared to MPM (Figure 21 A, B). CE were almost absent in MPM of both sexes (Figure 21 A, B). In contrast, foam cells contained more CE than FC (54.2 µg/mg protein, 56.6 µg/mg protein). TG concentrations in foam cells were elevated (+ 40 % and + 35 %) compared to MPM (Figure 21 A, B).

4.1.3 Lipid content of LD from RAW264.7 cells

Next, I determined the lipid content of LD isolated from RAW264.7 macrophages. Nine confluent 150 mm dishes were needed to isolate enough LD. The cells were loaded with acLDL for 72 h before they were scraped off the plates. LD were isolated and TC, FC and TG levels were determined enzymatically.

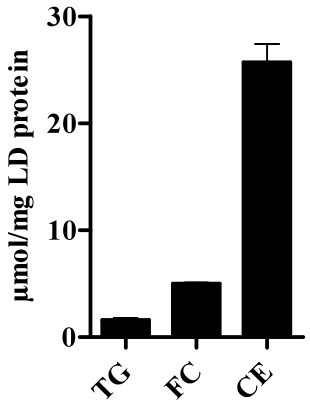

Figure 22: Lipid content of LD isolated from 72 h acLDL-loaded RAW264.7 cells.
Macrophages were scraped off the plates, lysed, homogenized by sonification and LD were isolated by ultracentrifugation for 3 h at 40000 rpm (4°C). TG, TC and FC levels were determined enzymatically and CE content was calculated. Protein was quantitated by the method of Bradford.

CE were highly abundant in LD from acLDL-loaded RAW264.7 cells (25.7 μmol/mg LD protein, Figure 22. LD contained less FC concentration (5.0 μmol/mg protein) and negligible amounts of TG (1.6 μmol/mg protein).

4.2 Role of HSL and KIAA1363 in murine cells and tissues

Macrophages are able to take up huge amounts of lipids and store CE and TG in lipid droplets, leading to foam cell formation, which is one of the earliest and important steps in the initiation and progression of atherosclerosis. Foam cells are able to counteract massive lipid accumulation by the action of a neutral CE hydrolase. Due to the importance of this enzyme activity in macrophages and conflicting publications over 40 years I compared the lipolytic activities as well as the tissue pattern of two suggested neutral CE hydrolases in MPM: hormone-sensitive lipase (HSL) and KIAA1363.

4.2.1 Murine tissue expression profiles of HSL and KIAA1363

First, I investigated the murine tissue pattern of HSL and KIAA1363 on the mRNA level. Murine tissues were isolated from C57BL/6 male and female mice. After reverse transcription of total RNA real time PCR was performed with specific primers for HSL and KIAA1363.

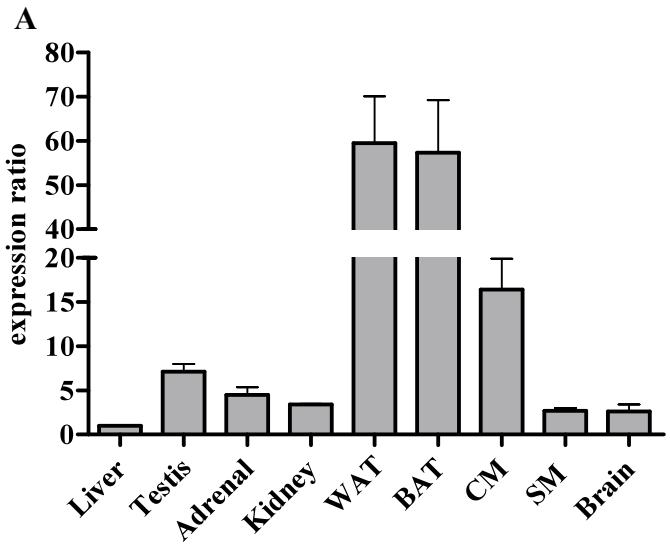

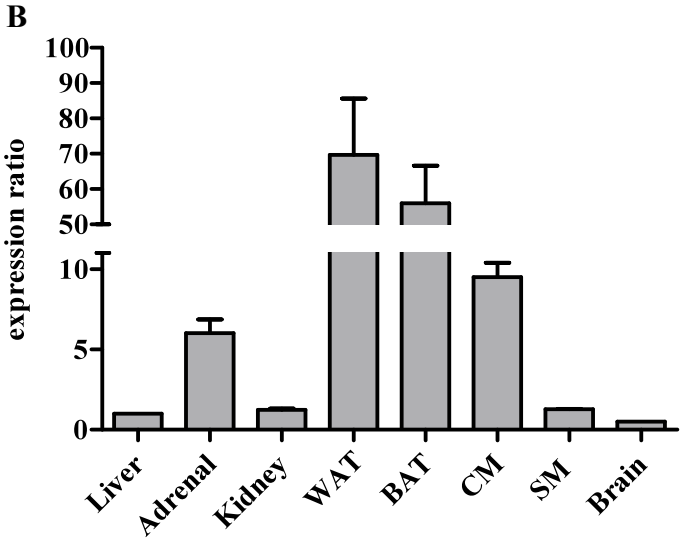

Figure 23: HSL mRNA expression in murine tissues isolated from male and female C57BL/6 mice. Total RNA was isolated from tissues of male (A) and female (B) C57BL/6 mice and HSL mRNA concentrations were determined by real time PCR. mRNA quantities were normalized to the house-keeping gene cyclophilin A. mRNA levels are presented in relation to the expression in liver (arbitrarily set to 1). WAT: white adipose tissue, BAT: brown adipose tissue, CM: cardiac muscle, SM: skeletal muscle. Bars represent the mean values ± SEM o two experiments performed in triplicates.

The highest mRNA expression of HSL was found in both sexes in WAT (male: 59.5-fold, female: 69.7-fold) and BAT (male: 57.3-fold, female: 56.0-fold) compared to the expression in liver, which was arbitrarily set to 1 (Figure 23 A, B). HSL is also expressed in cardiac muscle (CM) (male: 16.4-fold, female: 9.5-fold), testis (7.1-fold), adrenals (male: 4.5-fold, female: 6.0-fold), kidney (male: 3.4-fold, female: 1.3-fold), and skeletal muscle (SM) (male: 2.7-fold, female: 1.3-fold). In the brain, HSL mRNA expression was 40 % less in male mice and 2.6 fold increased in female mice compared to the liver.

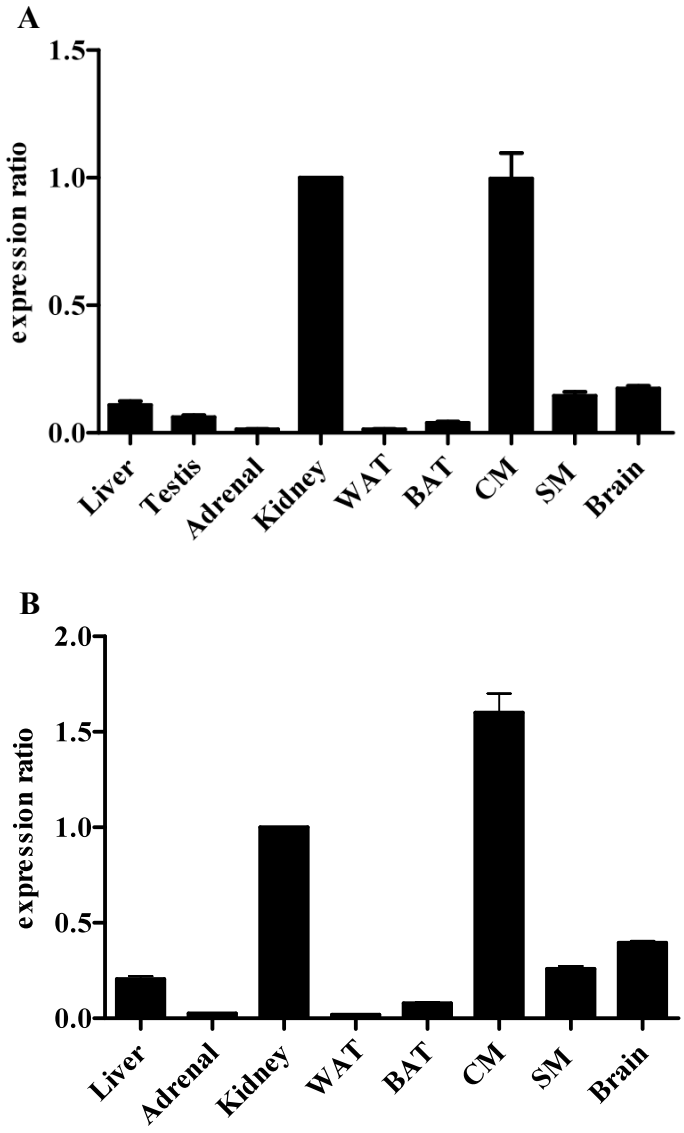

Figure 24: KIAA1363 mRNA expression in murine tissues isolated from male and female C57BL/6 mice. Total RNA was isolated from tissues of male (A) and female (B) C57BL/6 mice and KIAA1363 mRNA concentrations were determined by real time PCR. mRNA quantities were normalized to the house-keeping gene cyclophilin A. mRNA levels are presented in relation to the expression in kidney (arbitrarily set to 1). WAT: white adipose tissue, BAT: brown adipose tissue, CM: cardiac muscle, SM: skeletal muscle. Bars represent the mean values ± SEM o two experiments performed in triplicates.

Figure 24 shows the expression profile of KIAA1363 in male and female murine tissues relative to the expression level in kidney, which was arbitrarily set to 1. KIAA1363 mRNA expression was highest in kidney (1-fold) and CM (male: 0.9-fold, female: 1.6-fold). Furthermore KIAA1363 is expressed at low levels in brain (male: 0.17-fold, female: 0.4-fold) and in liver (male: 0.1-fold, female: 0.2-fold). Negligible mRNA expression was also observed testis, adrenals, WAT, SM and BAT of both sexes.

4.2.2 Gene expression of HSL and KIAA1363 in MPM and foam cells of both sexes

To check whether these two genes are differently expressed between the two sexes, the mRNA levels of HSL and KIAA1363 were determined in cDNAs of male and female C57BL/6 MPM and foam cells.

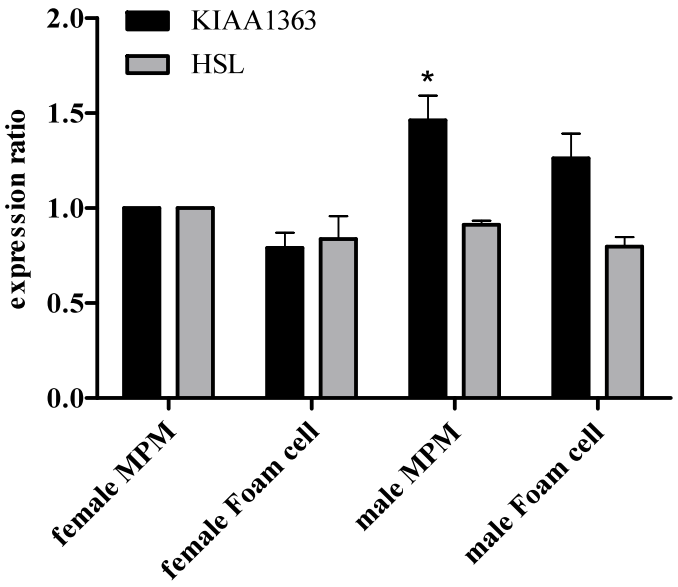

Figure 25: HSL and KIAA1363 mRNA expressions in MPM and foam cells of female and male C57Bl/6 mice. Total RNA was isolated from cells and HSL and KIAA1363 mRNA concentrations were determined by real time PCR. mRNA quantities were normalized to the house-keeping gene cyclophilin A. mRNA levels are presented in relation to the expression in female MPM (arbitrarily set to 1). Bars represent the mean values ± SEM of two experiments performed in triplicates. *, $p < 0.05$.

No sex-specific differences on the mRNA level of MPM and foam cells of C57BL/6 mice were observed regarding HSL and KIAA1363. However, the mRNA expression of KIAA1363 was only slightly increased by 1.4-fold in male MPM and 1.3-fold in male foam cells compared to female cells (Figure 25).

4.3 Hydrolase activities in COS-7 cells overexpressing HSL and KIAA1363

4.3.1 Western blot analysis of overexpressed HSL and KIAA1363 in COS-7 cells

To determine the lipolytic avtivities of recombinant HSL and KIAA1363, I overexpressed both enzymes in COS-7 cells and used cell lysates for activity assays. Overexpression of proteins was verified by western blot analysis using anti-HSL (84 kDa) and anti-KIAA1363 (45 and 50 kDa) antibodies. COS-7 cells were transfected with Metafectene™ and 2.5 µg of HSL, KIAA1363 or LacZ (negative control) plasmid-DNA. After 48 h cells were scraped off the plates with RIPA buffer and 75 µg of protein were separated by SDS-PAGEs.

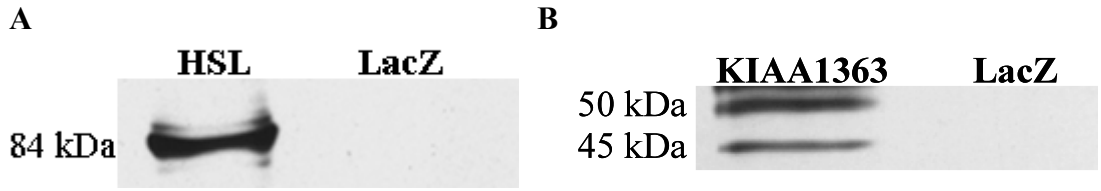

Figure 26: Western blots of recombinant HSL and KIAA1363 overexpressed in COS-7 cells. COS-7 cells were transfected with Metafectene™ and 2.5 µg of HSL (A) or KIAA1363 (B) plasmid-DNA. As negative control LacZ transfected cell protein was used. After 48 h cells were scraped off in RIPA buffer and protein was determined by the method of Bradford. Seventy-five µg cell protein was loaded on SDS gels. Western blot analyses were performed using specific anti-HSL (A) or anti-KIAA1363 (B) antibodies.

HSL protein (84 kDa) was successfully overexpressed in COS-7 cells in contrast to LacZ transfected cells, where no HSL protein was detectable (Figure 26 A). Both glycated forms of KIAA1363 protein (50 and 45 kDa) were detectable in COS-7 cells (Figure 26 B). In LacZ transfected cells no KIAA1363 was found.

4.3.2 Esterase activity of recombinant HSL and KIAA1363

Next, the esterase activities of COS-7 cells overexpressing HSL and KIAA1363 were determined using *p*-nitrophenylvalerate (PNPV) as substrate.

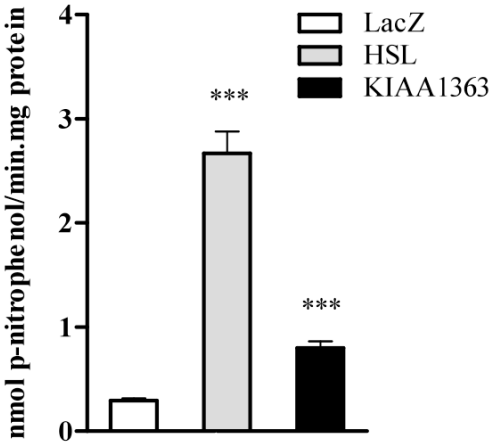

Figure 27: Esterase activities of HSL and KIAA1363. COS-7 cell lysates transiently overexpressing HSL and KIAA1363 were assayed for *p*-nitrophenylvalerate (PNPV) activity. LacZ was used as negative control. Data are presented as mean values ± SEM of 3 independent experiments performed in triplicate. ***, $p \leq 0.001$.

Both enzymes, HSL and KIAA1363, exhibited a significant 9.3-fold and 2.7-fold increase in esterase activity, respectively, compared to LacZ-transfected cells (Figure 27).

4.3.3 Binding of specific fluorescent activity recognition probes NBD-sn1-TGP, NBD-sn3-TGP, and NBD-CP to HSL and KIAA1363

Extracts of transiently transfected COS-7 cells were preincubated with fluorescent TG (NBD-sn1-TGP, NBD-sn3-TGP) or CE (NBD-CP) hydrolase activity recognition probes and subsequently subjected to SDS-PAGE analysis and fluorography (in collaboration with Ruth Birner-Gruenberger). These fluorescent probes have been shown to recognize and react with enzymatically active TG or CE hydrolases (130). In HSL-transfected cells, fluorescent signals were observed with NBD-sn1-TGP and NBD-CP in the position corresponding to the expected molecular mass of HSL (84 kDa), whereas no signals were detectable in KIAA1363-transfected cells (45 and 50 kDa) (Figure 28). In LacZ-transfected cells, intrinsic lipolytic and esterolytic activities of the host COS-7 cells were recognized by the inhibitors which resulted in multiple faint bands as described previously (130).

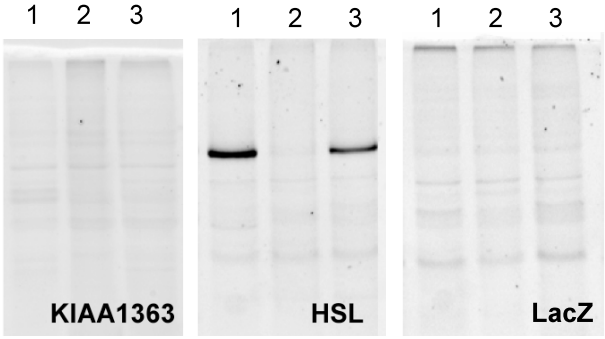

Figure 28: COS-7 cell lysates transiently overexpressing HSL and KIAA1363 were incubated with fluorescent activity recognition probes NBD-sn1-TGP (lanes 1), NBD-sn3-TGP (lanes 2), and NBD-CP (lanes 3). LacZ was used as negative control. After separation by SDS-PAGE, visualization was performed by laser scanning on aBioRad FY Pro laser scanner (in collaboration with Ruth Birner-Gruenberger).

4.3.4 CE hydrolase activities of HSL and KIAA1363

Next, CE hydrolase activities of COS-7 cell lysates overexpressing HSL and KIAA1363 were measured using different mixed micelles as substrates.

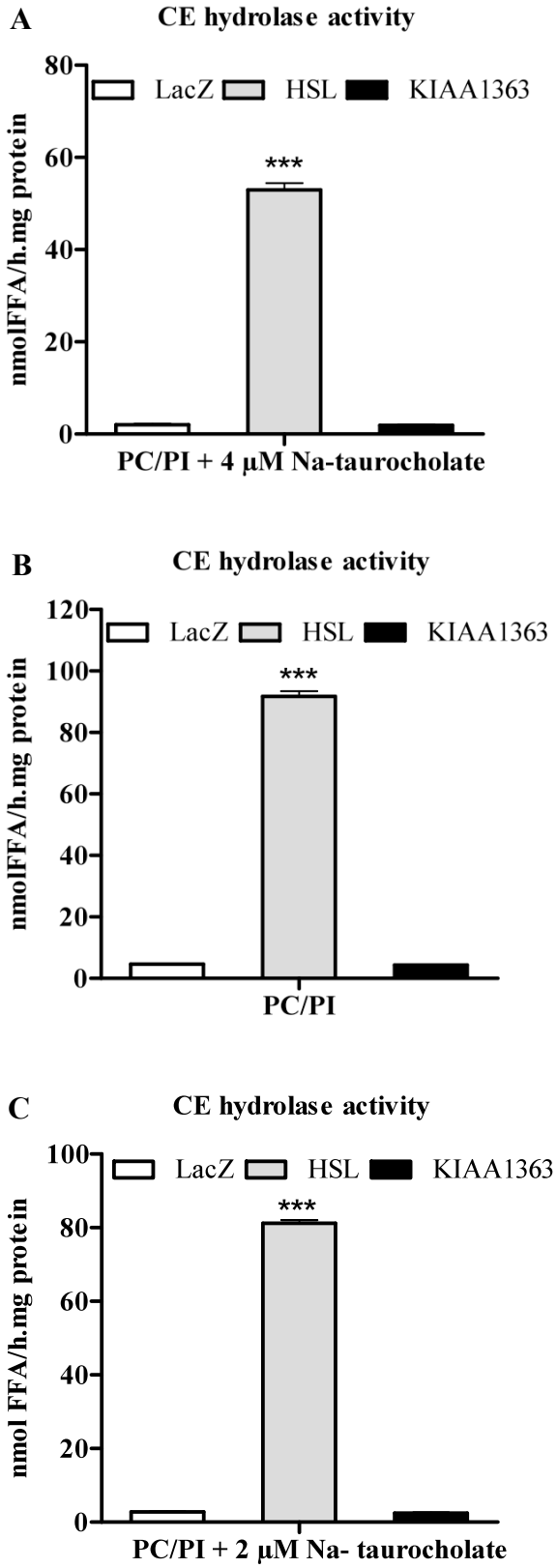

Figure 29: Neutral CE hydrolase activities of HSL and KIAA1363 using different mixed micelles. COS-7 cells were transiently transfected with HSL, KIAA1363 or LacZ (negative control). CE hydrolase activities were determined in cell lysates of transfected COS-7 cells adding 35.5 µg mixed micelles of PC and PI (3:1, w/w) (B) or 35.5 µg PC and 2 µM Na-taurocholate (C) to the substrate. Data are presented as mean values ± SEM of 3 independent experiments. ***, $p \leq 0.001$.

With the standard micelles used in our lab for measuring hydrolase activities, (35.5 µg of mixed micelles of phosphatidylcholine (PC) and phosphatidylinositol (PI) (3:1, w/w) and 4 µM Na- taurocholate), a 26-fold increase in CE hydrolase activity of HSL overexpressing lysate in comparison to LacZ- transfected cells was observed. Unlike to KIAA1363 overexpressing cell lysate, where CE hydrolase activity was similar as in LacZ-transfected cells (Figure 29 A). Moreover I compared neutral CE hydrolase activities in HSL- and KIAA1363-transfected COS-7 cells using alternative mixed micelles as substrates. I prepared the same mixed micelles as Okazaki (35.5 µg PC/PI and 2 µM Na-taurocholate) (124) and Holm (35.5 µg PC/PI) (135). With both PC/PI and PC/Na-taurocholate, neutral CE hydrolase activity was significantly increased in cell lysates overexpressing HSL compared to LacZ-transfected controls, whereas no differences were found in cells overexpressing KIAA1363 (Figure 29 B, C).

4.3.5 DG and TG hydrolase activities of HSL and KIAA1363

DG and TG hydrolase activities in cell lysates overexpressing HSL and KIAA1363 were then investigated. HSL cleaved both substrates (Figure 30 A, B); the enzyme activity towards DG (13-fold) and TG (22-fold) were significantly elevated compared to LacZ or KIAA1363 transfected cells. KIAA1363 was not able to hydrolyze DG or TG (Figure 30 A, B).

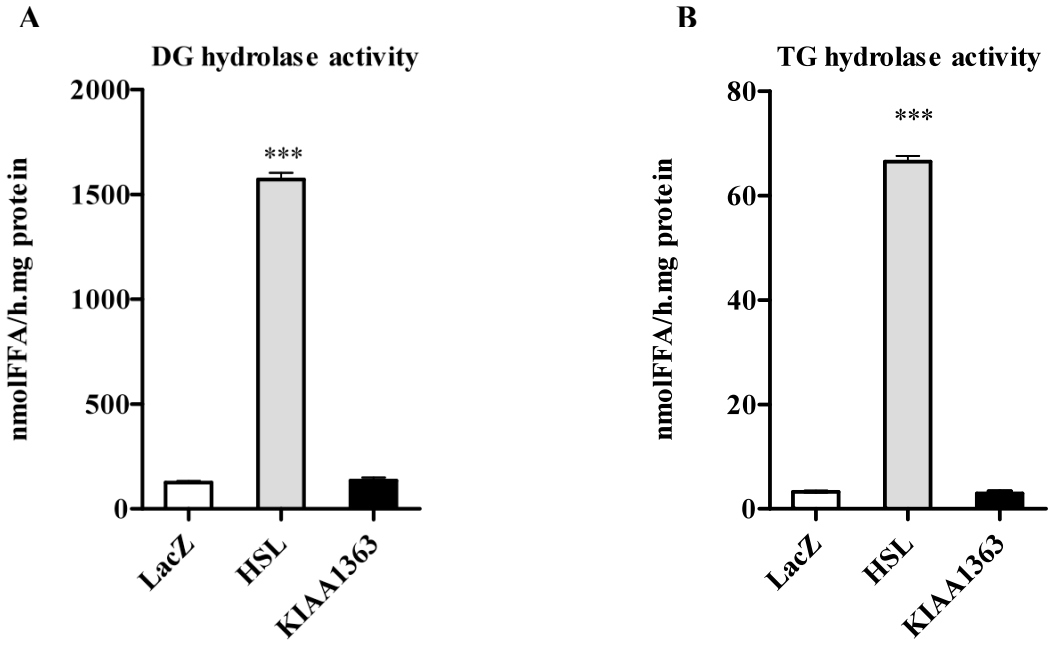

Figure 30: DG and TG hydrolase activities of HSL and KIAA1363. COS-7 cells were transiently transfected with HSL, KIAA1363, or LacZ (negative control). DG (A) and TG (B) hydrolase activities were determined in cell lysates of transfected cells adding 15 µg mixed micelles of PC and PI (3:1, w/w) and 4 µM Na-taurocholate to the respective substrates. Data are presented as mean values ± SEM of 3 independent experiments. ***, $p \leq 0.001$.

4.3.6 AcMAGE hydrolase activity of HSL and KIAA1363

KIAA1363 has been shown to hydrolize AcMAGE in murine brain to form the hydrolysis product MAGE (125). Thus, I measured AcMAGE hydrolase activity in whole lysates, cytosolic and membrane fractions from HSL and KIAA1363-transfected COS-7 cells. Both, HSL and KIAA1363 exhibited increased AcMAGE hydrolase activity compared to LacZ-transfected cells (1.6- and 2.0-fold, respectively) (Figure 31). The cytosolic fraction of HSL-transfected cells exhibited a 4-fold increase in hydrolase activity compared to the controls, whereas no difference was found in the membrane fraction. This is likely due to the localization of HSL in the cytosol. Regarding KIAA1363, AcMAGE hydrolase activity was increased (2-fold) in the membrane fraction, because KIAA1363 is a membrane standing protein (Figure 31).

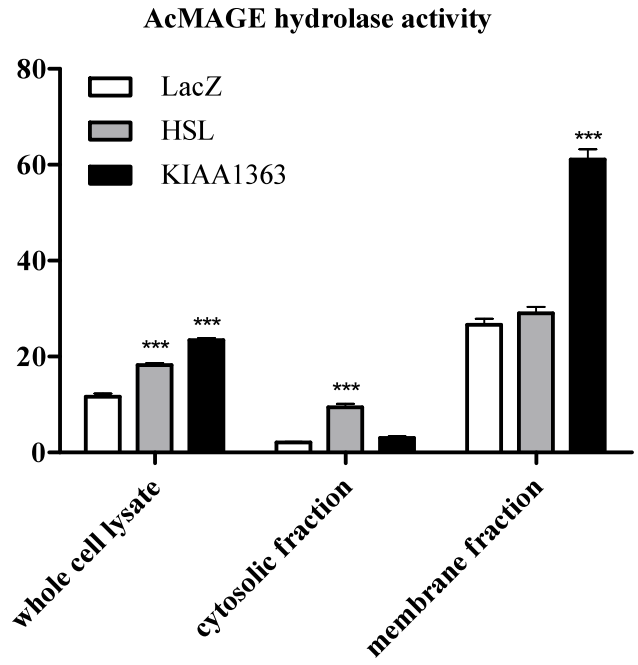

Figure 31: AcMAGE hydrolase activities of HSL and KIAA1363. COS-7 cells were transiently transfected with HSL, KIAA1363, or LacZ (negative control). The cytosolic and membrane fractions were separated by centrifugation at 100000 g for 1 h (4°C). AcMAGE hydrolase activities were determined in whole cell lysates, cytosolic and membrane fractions of transfected cells. Data are presented as mean values ± SEM of 2 independent experiments. ***, $p \leq 0.001$.

4.3.6 RE hydrolase activity of HSL and KIAA1363

Moreover the RE hydrolase activity of COS-7 cells overexpressing HSL and KIAA1363 were determined in collaboration with Renate Schreiber. HSL and KIAA1363 were able to hydrolize RE (1.7- fold and 1.3- fold) (Figure 32).

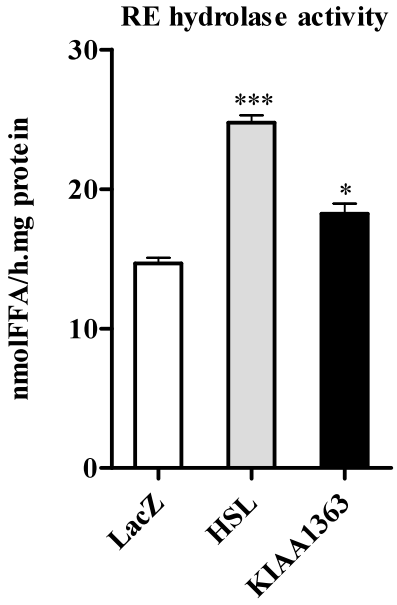

Figure 32: RE hydrolase activities of HSL and KIAA1363. COS-7 cells were transiently transfected with HSL, KIAA1363, or LacZ (negative control). RE hydrolase activities were determined in cell lysates of transfected cells adding 15 µg mixed micelles of PC and PI (3:1, w/w) to the respective substrates. Data are presented as mean values ± SEM measured in triplicates. *, $p < 0.05$; ***, $p \leq 0.001$.

4.4 Experiments with HSL(-/-) and KIAA1363(-/-) mice and their littermates

HSL(-/-) mice were obtained from Guenter Haemmerle (103, 105) and KIAA1363(-/-) (122, 125) mice were a gift from Benjamin Cravatt. Mice used for the experiments were bred in-house in our animal facility.

4.4.1 Western blot analysis to confirm the absence of HSL and KIAA1363

To check whether our animal strains really lack HSL and KIAA1363 proteins, western blot analyses were performed with MPM and foam cells of these mouse lines. HSL(-/-) mice lacked HSL (Figure 33 A) and no KIAA1363 protein was detectable in KIAA1363(-/-) MPM and foam cells (Figure 33 B).

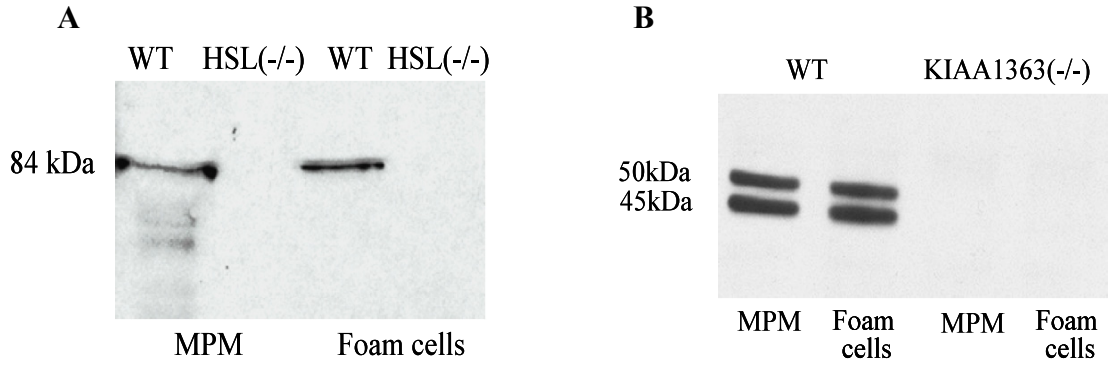

Figure 33: Western blots of macrophages from HSL(-/-), KIAA1363(-/-) and control mice (WT). using anti-KIAA1363 antibody. MPM were loaded for 48 h with acLDL to achieve foam cell formation. MPM and foam cells from HSL(-/-) (A), KIAA1363 (-/-) (B) and their littermates were scraped off with RIPA buffer and after protein estimation, 75 µg protein were loaded on SDS gels. Western blot analyses were performed using specific anti-HSL (A) or anti-KIAA1363 (B) antibodies.

4.4.2 Gene expression of HSL and KIAA1363 in MPM and foam cells of HSL(-/-) and KIAA1363(-/-) mice

Next, I wanted to find out, whether HSL or KIAA1363 compensate for the lack of the other gene. In this experiment the mRNA level of HSL in MPM and foam cells of KIAA1363(-/-) mice as well as their littermates (WT) and the gene expression of KIAA1363 in HSL(-/-) MPM and foam cells and their littermates (WT) were investigated.

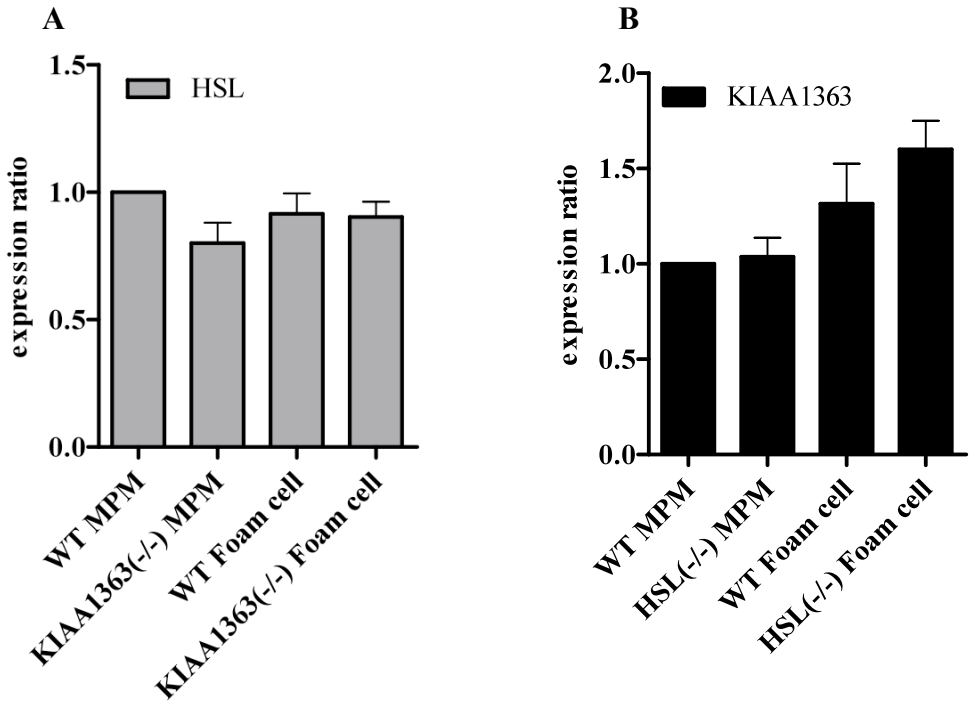

Figure 34: HSL and KIAA1363 mRNA expression in MPM and foam cells of KIAA1363(-/-), HSL(-/-) and WT mice. HSL (A) mRNA concentrations were determined in KIAA1363(-/-) animals and KIAA1363 (B) mRNA concentrations were determined in HSL(-/-) mice by real time PCR. mRNA quantities were normalized to the house-keeping gene cyclophilin A. mRNA levels are presented in relation to the expression in WT MPM (arbitrarily set to 1). Bars represent the mean values ± SEM of two experiments performed in triplicates.

No differences in the mRNA level of HSL in MPM and foam cells of KIAA1363(-/-) mice and their littermates (Figure 34 A) were found. KIAA1363 mRNA expression was the same in MPM of WT and HSL(-/-) mice, as well as in WT and HSL(-/-) foam cells (Figure 34 B).

4.4.3 Plasma lipid parameters from HSL(-/-) and KIAA1363(-/-) mice

The consequences of HSL and KIAA1363 deficiency with regard to plasma lipid levels were investigated in fed and ON fasted male and female mice (Table 14). Consistent with previous studies (103), plasma TG levels of fasted HSL(-/-) mice were decreased by 31 % in female animals and by 57 % in male individuals. Non esterified fatty acid (FFA) concentrations were significantly reduced in both sexes by 39 % and 56 %. Independent of the dietary status, plasma TC levels were increased. Absence of KIAA1363 did not affect plasma lipid parameters in either the fed or the fasted state (Table 14).

Table 14: Plasma lipid parameters of HSL(-/-), KIAA1363(-/-), and control (WT) female and male mice. Blood was drawn from 8-10 week old mice in the fed and fasted state. TG, TC and FC concentrations were determined enzymatically. Data are presented as mean values (n=9) ± SEM. *, $p < 0.05$; **, $p \leq 0.01$.

fed	**female n**	**mg/dl TG**	**TC**	**FC**	**FFA [mM]**
WT	9	67.9 ± 3.5	76.9 ± 2.9	19.1 ± 1.6	n.d.
KIAA1363(-/-)	9	66.8 ± 4.2	71.9 ± 2.3	17.4 ± 2.3	
HSL(-/-)	9	70.1 ± 9.6	90.3 ± 3.2*	21.9 ± 2.4	
fasted					
WT	9	53.5 ± 4.6	62.0 ±2.4	16.1 ± 0.9	1,8 ± 0,3
KIAA1363(-/-)	9	59.6 ± 3.3	60.4 ± 4.9	14.9 ± 1.4	2,0 ± 0,4
HSL(-/-)	9	36.9 ± 5.7*	76.5 ± 3.2**	19.0 ± 1.6	1,1 ± 0,2 *
fed	**male n**	**mg/dl TG**	**TC**	**FC**	**FFA [mM]**
WT	6	74.0 ± 8.2	80.2 ± 5.0	22.6 ± 3.2	n.d.
KIAA1363(-/-)	6	67.5 ± 14.2	73.5 ± 3.1	18.6 ± 2.9	
HSL(-/-)	6	66.2 ± 13.1	86.1 ± 2.6	20.7 ± 2.4	
fasted					
WT	6	50.9 ± 7.6	64.0 ± 6.7	14.0 ± 1.9	1.6 ± 0,6
KIAA1363(-/-)	6	56.9 ± 5.6	68.7 ± 6.8	14.5 ± 2.2	1.4 ± 0.8
HSL(-/-)	6	24.9 ± 3.3**	73.8 ± 2.6*	16.9 ± 1.8	0.7 ± 0,3 *

4.4.4 Lipoprotein profile from HSL(-/-) and KIAA1363(-/-) mice

To investigate the lipid distribution among lipoprotein subclasses, plasma samples of ON fasted HSL(-/-), KIAA1363(-/-) and their littermates were subjected to FPLC analysis. The TG content in the VLDL-TG fraction was reduced by 15 % in HSL(-/-) animals (Figure 35 A), whereas HDL cholesterol was increased by 50 % in these mice compared to controls (Figure 35 B). In the LDL fraction, elevated TC (66 %) was found as well as reduced TG (29 %) (Figure 35 A, B).

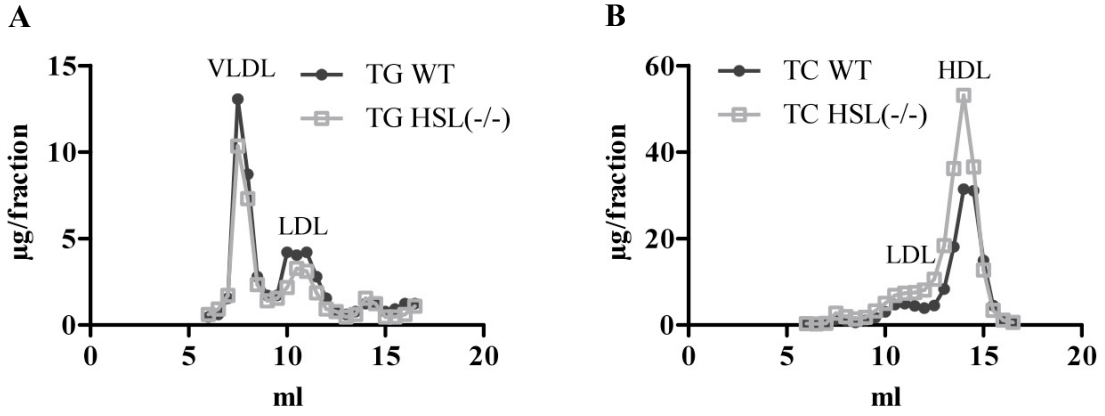

Figure 35: Lipoprotein profile of HSL(-/-)- and control mice. Plasma pools from 5 ON fasted HSL(-/-) males and 4 controls at the age of 10 weeks were used. Plasma lipoproteins were separated using a Pharmacia FPLC system with a Superose 6 column. FPLC fractions were collected, and TG, TC and FC concentrations in each fraction were measured enzymatically.

In contrast, lipoprotein profiles were unchanged in KIAA1363(-/-) mice compared to their littermates (Figure 36). VLDL-TG (117 %) (Figure 36 A), HDL-cholesterol (91 %) (Figure 36 B) and LDL-cholesterol were the same among the two groups.

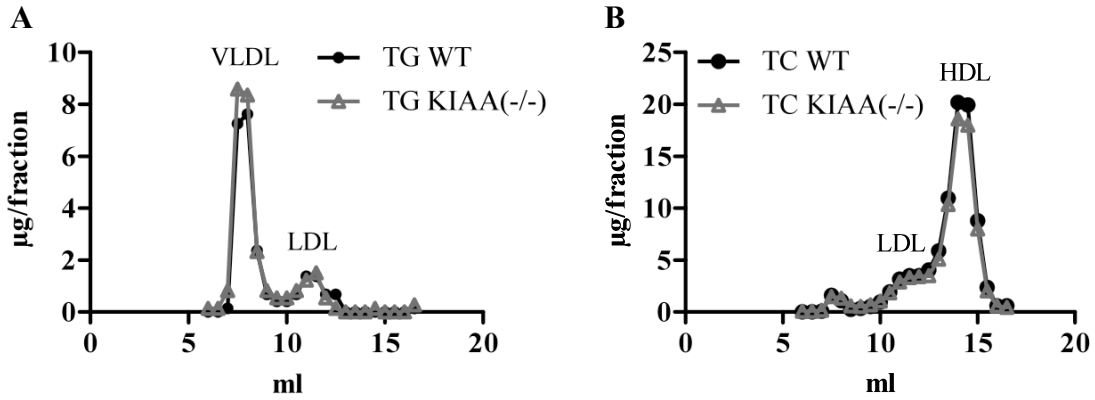

Figure 36: Lipoprotein profile of KIAA1363(-/-)- and control mice. Plasma pools from 4 ON fasted KIAA1363(-/-) males and 4 controls at the age of 10 weeks. Plasma lipoproteins were separated using a Pharmacia FPLC system with a Superose 6 column. FPLC fractions were collected, and TG, TC, and FC concentrations in each fraction were measured enzymatically.

4.4.5 Effect of HSL and KIAA1363 deficiency on hydrolase activitites in mouse tissues

CE and AcMAGE hydrolase activities in tissues of HSL(-/-) and KIAA1363(-/-) mice were then determined. Neutral CE hydrolase activities were significantly reduced in BAT and WAT, CM, SM, liver, kidney, testis, and brain of HSL(-/-) mice compared to WT littermates

(Figure 37 A). I could not find any differences in CE hydrolase activity in the corresponding tissues of KIAA1363(-/-) mice (Figure 37 B).

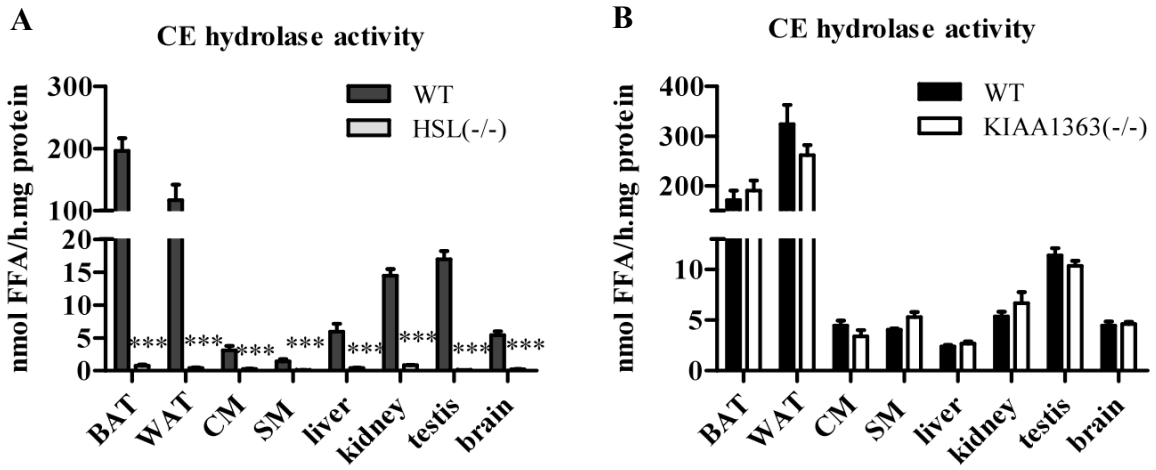

Figure 37: CE hydrolase activities in HSL(-/-)- and KIAA1363(-/-) tissues. Neutral CE hydrolase activities were determined in tissues isolated from HSL(-/-) (A) and KIAA1363(-/-) (B) mice and their respective littermates. Data are presented as mean values ± SEM of 2 independent experiments (using 3 mice in each experiment). ***, $p \leq 0.001$.

Conversely, absence of HSL did not change AcMAGE hydrolase activity in murine tissues (Figure 38 A), whereas deficiency of KIAA1363 resulted in reduced AcMAGE hydrolase activity in brain (-76 %), CM (-76 %), kidney (-25 %), and testis (-50 %) (Figure 38 B). No differences were found in liver, SM, BAT, and WAT of KIAA1363(-/-) mice.

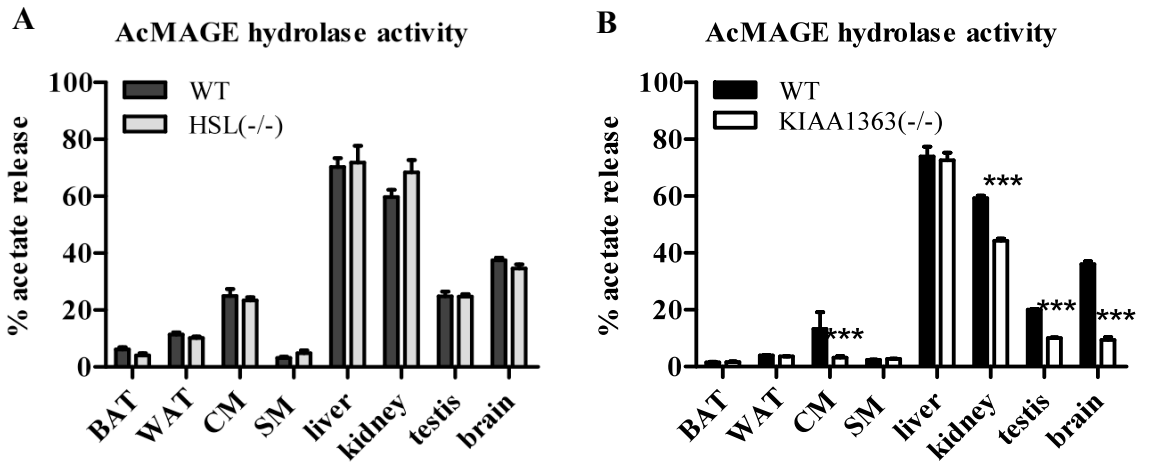

Figure 38: AcMAGE hydrolase activities in HSL(-/-)- and KIAA1363(-/-) tissues. AcMAGE hydrolase activities were determined in tissues isolated from HSL(-/-) (A) and KIAA1363(-/-) (B) mice and their respective littermates. Data are presented as mean values ± SEM of 2 independent experiments (using 3 mice in each experiment). ***, $p \leq 0.001$.

It was already published by Sekiya et al. (108), that the TG hydrolase activity was unchanged between HSL(-/-) and WT liver. Grober et al. (110) showed in the year 2003, that HSL is responsible for a part of the DG hydrolase activity in murine jejunum and ileum.

KIAA1363 was also shown to exhibit retinylester (RE) hydrolase activity (Achim Lass, unpublished data). Thus, we compared the RE hydrolase activity of WT tissues with tissues from KIAA1363(-/-) mice (in collaboration with Renate Schreiber). It seems that KIAA1363 plays no role as RE hydrolase in any investigated tissue *in vivo*, because the RE hydrolase activity was the same in KIAA1363(-/-)- and WT tissues (Figure 39). It was recently published from Strom et al (107), that WAT and BAT from HSL(-/-) mice exhibited only negligible RE hydrolase activities compared to WT tissues.

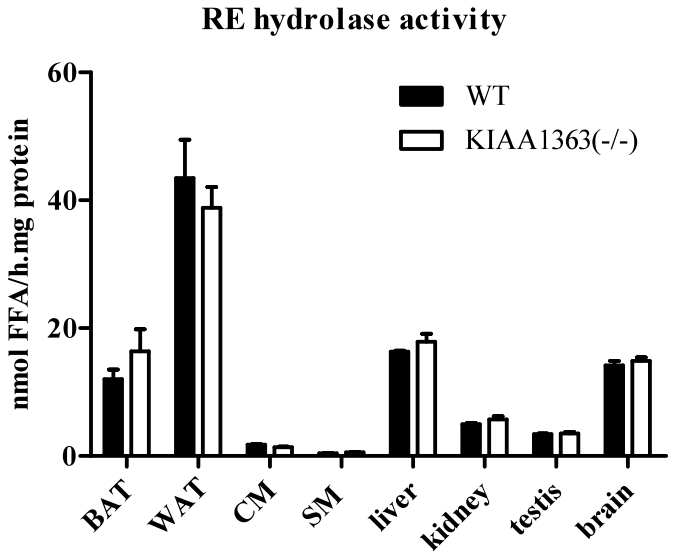

Figure 39: RE hydrolase activities in KIAA1363(-/-) tissues. RE hydrolase activities were determined in tissues isolated from KIAA1363(-/-) mice and their respective littermates. Data are presented as mean values ± SEM of 1 independent experiment (using 3 mice).

4.4.6 FC and CE concentrations in tissues of HSL(-/-) and KIAA1363(-/-) mice

Since I found almost abolished neutral CE hydrolase activities in tissues of HSL(-/-) mice, I determined the FC and CE content in the respective tissues (Table 15). FC concentrations were similar in all tissues of both HSL(-/-) and KIAA1363(-/-) mice compared to WT. CE concentrations were significantly increased in BAT (2.2-fold), kidney (3.1-fold), and testis (3.3-fold) of HSL(-/-) mice. No differences in CE content were observed in CM, SM, liver, and brain of HSL(-/-) mice as well as in all tissues of KIAA1363(-/-) mice.

Table 15: Free cholesterol (FC) and cholesteryl ester (CE) concentrations in tissues from HSL(-/-), KIAA1363(-/-) and WT mice. Tissue lipids were extracted by the method of Folch (127). FC and TC concentrations were determined enzymatically, and CE concentrations were calculated. Data are presented as mean values (n=4) ± S.E.M. *, $p < 0.05$.

			Tissue lipids, mg/g tissue	
Tissue	**Genotype**	**n**	**FC**	**CE**
BAT	WT	4	1,10 ± 0,25	0,26 ± 0,14
	HSL(-/-)	4	0,97 ± 0,36	0,57 ± 0,12*
	KIAA1363(-/-)	4	0,96 ± 0,18	0,31 ± 0,15
WAT	WT	4	0,31 ± 0,11	0,14 ± 0,05
	HSL(-/-)	4	0,46 ± 0,13	0,15 ± 0,07
	KIAA1363(-/-)	4	0,38 ± 0,07	0,13 ± 0,1
CM	WT	4	0,69 ± 0,06	0,06 ± 0,03
	HSL(-/-)	4	0,70 ± 0,06	0,05 ± 0,02
	KIAA1363(-/-)	4	0,74 ± 0,05	0,07 ± 0,03
SM	WT	4	0,29 ± 0,04	0,04 ± 0,03
	HSL(-/-)	4	0,32 ± 0,03	0,03 ± 0,02
	KIAA1363(-/-)	4	0,21 ± 0,06	0,05 ± 0,04
Liver	WT	4	2,11 ± 0,16	0,31 ± 0,11
	HSL(-/-)	4	2,20 ± 0,31	0,50 ± 0,14
	KIAA1363(-/-)	4	2,24 ± 0,23	0,28 ± 0,23
Kidney	WT	4	1,12 ± 0,17	0,18 ± 0,04
	HSL(-/-)	4	1,08 ± 0,11	0,55 ± 0,19*
	KIAA1363(-/-)	4	1,11 ± 0,48	0,11 ± 0,03
Testis	WT	4	4,05 ± 0,33	0,88 ± 0,05
	HSL(-/-)	4	4,51 ± 0,21	2,89 ± 0,73*
	KIAA1363(-/-)	4	3,92 ± 0,25	1,07 ± 0,34
Brain	WT	4	0,94 ± 0,09	0,13 ± 0,03
	HSL(-/-)	4	0,86 ± 0,12	0,11 ± 0,02
	KIAA1363(-/-)	4	1,06 ± 0,22	0,12 ± 0,01

4.4.7 Effect of HSL and KIAA1363 deficiency on neutral CE hydrolase activity in MPM and foam cells

Furthermore, the neutral CE hydrolase activity in MPM of HSL(-/-) and KIAA1363(-/-) mice was analyzed. With our standard micelles, 35.5 µg of mixed micelles of phosphatidylcholine (PC) and phosphatidylinositol (PI) (3:1, w/w) and 4 µM Na-taurocholate, the neutral CE hydrolase activity was nearly abolished in cell lysates (-96 %), cytosolic (-96 %), and membrane fractions (-87 %) of HSL deficient MPM (Figure 40 A). In contrast, no differences were found KIAA1363(-/-) MPM compared to their littermates (Figure 40 B).

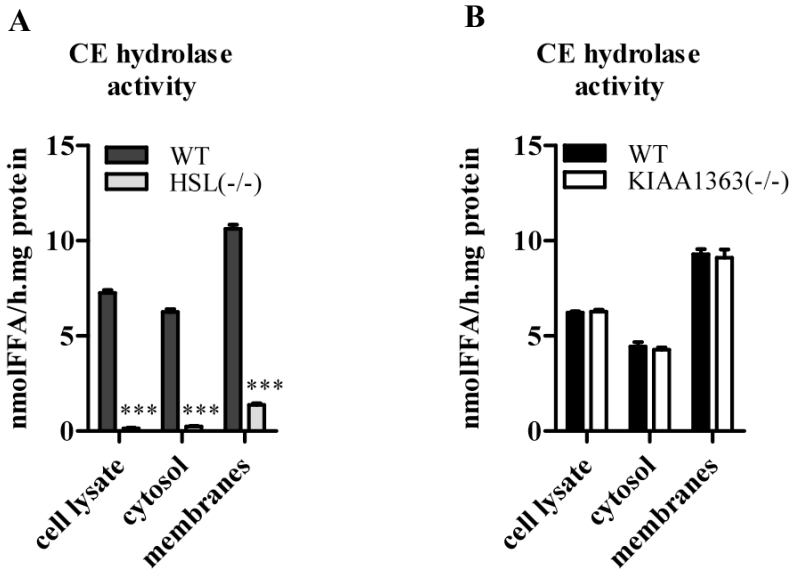

Figure 40: Neutral CE hydrolase activities in HSL(-/-)- and KIAA1363(-/-) macrophages. Neutral CE hydrolase activities were determined in cell lysates, cytosolic and membrane fractions of HSL(-/-) (A), KIAA1363(-/-) (B) and WT macrophages from littermates adding 35.5 µg mixed micelles of PC and PI (3:1, w/w) and 4 µM Na-taurocholate to the respective substrates. Data are presented as mean values of 3 independent experiments ± SEM (using 3 mice in each experiment). ***, $p \leq 0.001$.

Since a previous study has shown unchanged neutral CE hydrolase activity in HSL(-/-) MPM (99), I reinforced my data using alternative substrate conditions. Under all assay conditions used, HSL(-/-) macrophages showed a significantly decreased neutral CE hydrolase activity (-83 % and -95 %, respectively) compared to macrophages from WT littermates (Figure 41 A) and KIAA1363(-/-) mice (Figure 41 B).

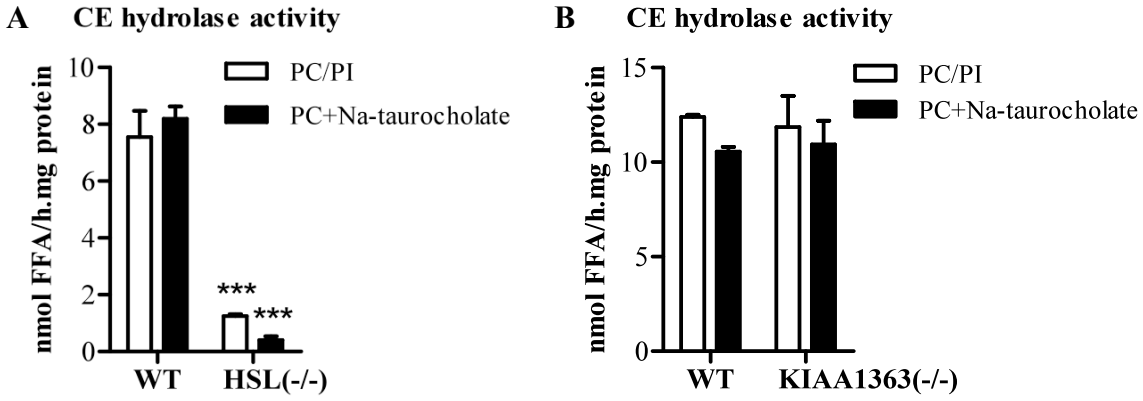

Figure 41: CE hydrolase activities in HSL(-/-)- and KIAA1363(-/-) macrophages using alternative mixed micelles. CE hydrolase activities were determined adding 35.5 µg mixed micelles of PC and PI (3:1, w/w) or 35.5 µg PC and 2 µM Na-taurocholate to the substrate. Neutral CE hydrolase activities were determined in cell lysates from (A) HSL(-/-) and (B) KIAA1363(-/-) macrophages and compared to their WT littermates (3.2.4.17). Data are presented as mean values (n=3) ± SEM. ***, $p \leq 0.001$.

Moreover, the neutral CE hydrolase activity of 24 h aggLDL- loaded MPM from different genotypes was investigated. Whereas foam cells from HSL(-/-) mice exhibited nearly no neutral CE hydrolase activity anymore (Figure 42 A), the neutral CE hydrolase activity in KIAA1363(-/-) foam cells was unchanged in comparison to their littermates (Figure 42 B).

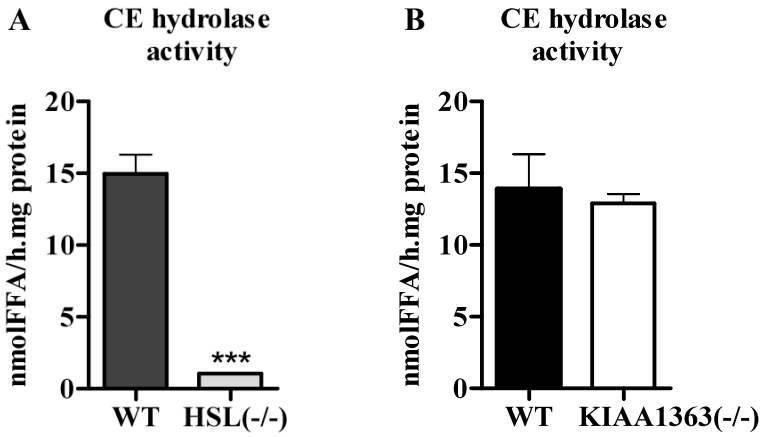

Figure 42: Neutral CE hydrolase activities in HSL(-/-)- and KIAA1363(-/-) foam cells. Neutral CE hydrolase activities were determined in cell lysates of 24 h- aggLDL loaded MPM of HSL(-/-) (A), KIAA1363(-/-) (B) and WT mice adding 35.5 µg mixed micelles of PC and PI (3:1, w/w) and 4 µM Na-taurocholate to the respective substrates. Data are presented as mean values of 2 independent experiments ± SEM (using 3 mice in each experiment). ***, $p \leq 0.001$.

4.4.8 Effect of HSL and KIAA1363 deficiency on DG and TG hydrolase activities in MPM

In subsequent experiments the DG and TG hydrolase activities of HSL(-/-) and KIAA1363(-/-) MPM were investigated. HSL deficiency in MPM resulted in decreased DG hydrolase activities in cell lysates (-42 %), cytosolic (-80 %), and membrane fractions (-47 %) (Figure 43 A). In addition, TG hydrolase activities were reduced in cell lysates (-49 %), cytosolic (-78 %), and membrane fractions (-57 %) (Figure 43 B).

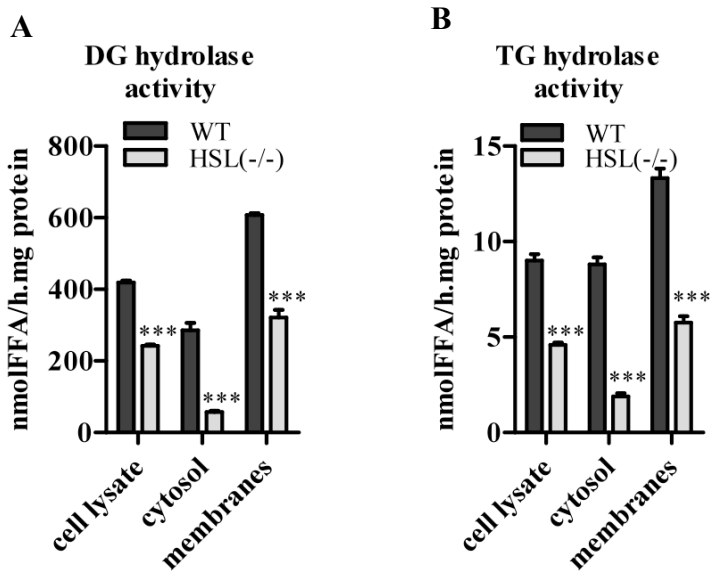

Figure 43: **DG and TG hydrolase activities in HSL deficient macrophages**. DG (A) and TG (B) hydrolase activities were determined in cell lysates, cytosolic and membrane fractions of HSL(-/-) and WT macrophages from littermates adding 15 µg mixed micelles of PC and PI (3:1, w/w) and 4 µM Na-taurocholate to the respective substrates. Data are presented as mean values of 3 independent experiments ± SEM (using 3 mice in each experiment). ***, $p \leq 0.001$.

MPM lacking KIAA1363 showed similar DG- (Figure 44 A) and TG hydrolase activities (Figure 44 B) in cell lysates, cytosolic, and membrane fractions as control MPM.

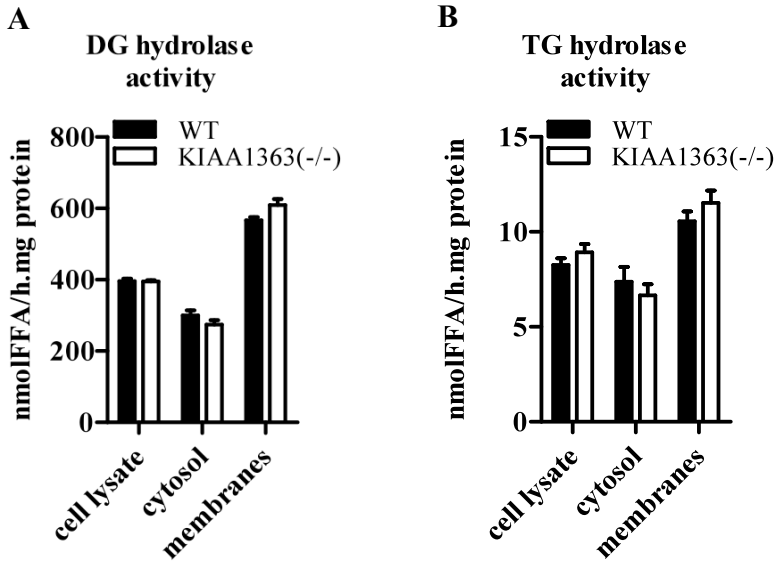

Figure 44: DG and TG hydrolase activities in KIAA1363 deficient macrophages. DG (A) and TG (B) hydrolase activities were determined in cell lysates, cytosolic and membrane fractions of KIAA1363(-/-) and WT macrophages from littermates adding 15 µg mixed micelles of PC and PI (3:1, w/w) and 4 µM Na-taurocholate to the respective substrates. Data are presented as mean values of 3 independent experiments ± SEM (using 3 mice in each experiment).

4.4.9 Effect of HSL and KIAA1363 deficiency on AcMAGE hydrolase activities in MPM

Next, I analyzed AcMAGE hydrolase activities in HSL(-/-) and KIAA1363(-/-) MPM. HSL deficiency resulted in unchanged hydrolysis of AcMAGE in macrophage cell lysates, cytosolic, and membrane fractions (Figure 45 A). In contrast, KIAA1363(-/-) MPM exhibited a marked reduction in AcMAGE hydrolase activity in cell lysates (-59 %) and membrane fractions (-79 %) compared to control cells. AcMAGE hydrolase activities in cytosolic fractions were unchanged (Figure 45 B).

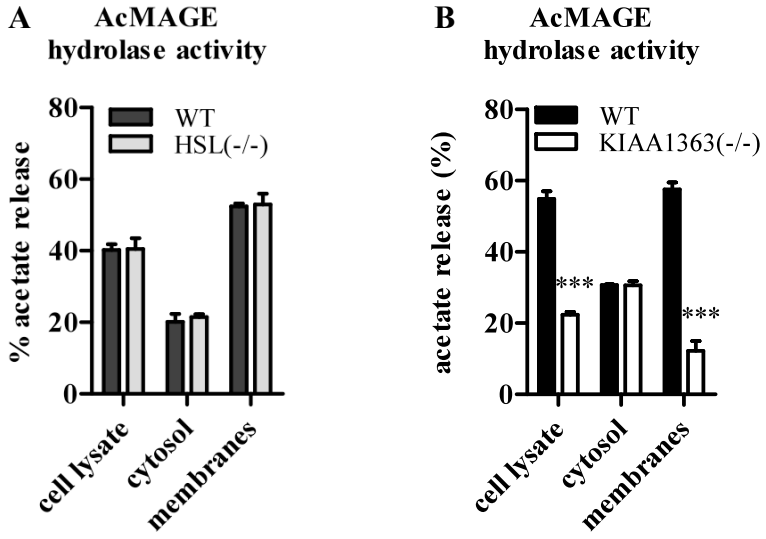

Figure 45: AcMAGE hydrolase activities in HSL(-/-)- and KIAA1363(-/-) macrophages. AcMAGE hydrolase activities were determined in cell lysates, cytosolic and membrane fractions of HSL(-/-) (A), KIAA1363(-/-) (B) and WT macrophages from littermates. Data are presented as mean values of 3 independent experiments ± SEM (using 3 mice in each experiment). ***, $p \leq 0.001$.

4.4.10 Effect of KIAA1363 deficiency on RE hydrolase activity in MPM

To check whether KIAA1363 plays a role as RE hydrolase in MPM, a RE hydrolase assay was performed with liver as positive control (in collaboration with Renate Schreiber). RE hydrolase activity in MPM of WT and KIAA1363(-/-) mice was almost absent compared to RE hydrolase activity in the liver (Figure 46).

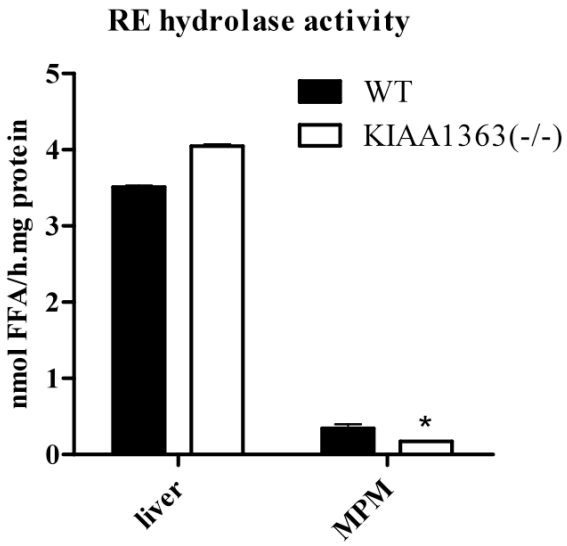

Figure 46: RE hydrolase activities in KIAA1363(-/-) MPM and liver. RE hydrolase activities were determined in MPM lysates and livers of KIAA1363(-/-) and WT mice. Data are presented as mean values of 1 experiment performed in duplicate ± SEM (using 3 mice).

4.4.11 Effect of HSL and KIAA1363 deficiency on macrophage lipid content

To investigate the effects of HSL or KIAA1363 deficiency on the lipid droplet morphology in macrophages, cells were analyzed using nile red staining and fluorescence microscopy.

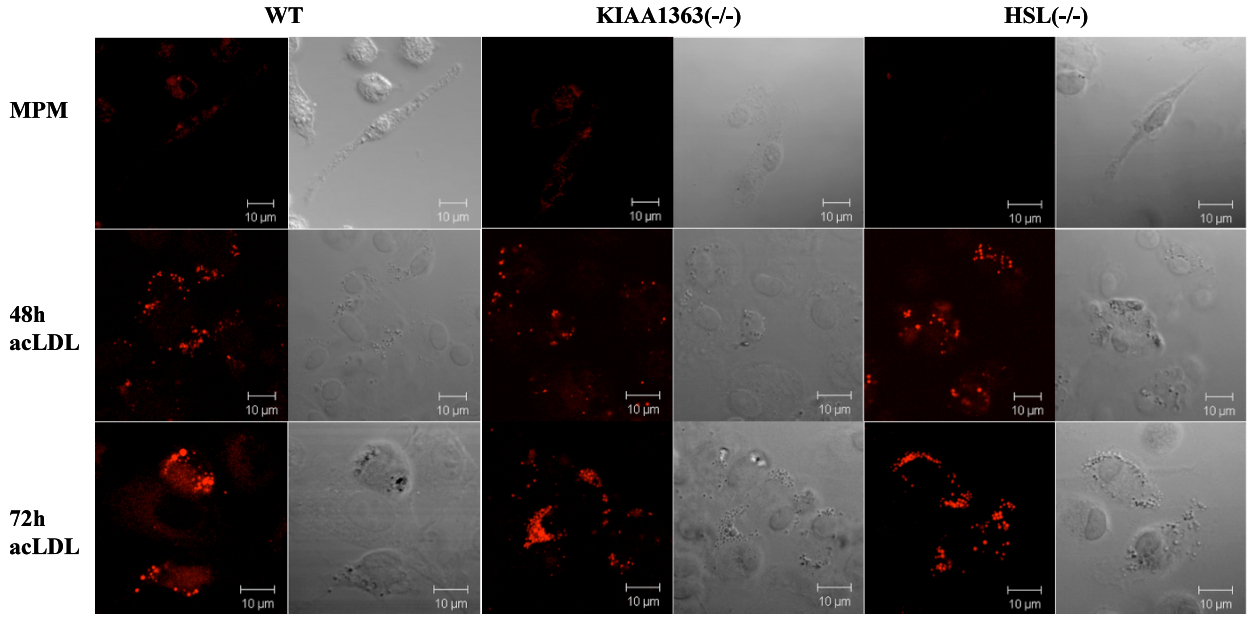

Figure 47: Foam cell formation of HSL(-/-) and KIAA1363(-/-) macrophages. Representative fluorescent microscopy after nile red staining of HSL(-/-), KIAA1363(-/-), and control (WT) macrophages and foam cells. Foam cell formation was achieved by loading macrophages with 100 µg acLDL for 48 h and 72 h. Images were taken on a Zeiss LSM 510 Meta microscope.

Unexpectedly, HSL(-/-) and KIAA1363(-/-) macrophages as well as macrophages incubated with acLDL for 48 h and 72 h showed unaltered lipid droplet staining compared to cells from WT littermates (Figure 47).

To determine the lipid content biochemically, I measured TG, FC and CE concentrations in macrophages and acLDL-loaded foam cells of HSL(-/-), KIAA1363(-/-) and control mice. In accordance with morphological analysis, both MPM and foam cells of HSL(-/-)- and KIAA1363(-/-) mice showed similar concentrations of TG, FC and CE levels compared to cells from control mice (Table 16). Thus, neither HSL nor KIAA1363 deficiency in macrophages led to noticeable alterations in lipid content compared to control cells.

Table 16: Lipid composition of macrophages and acLDL-loaded foam cells of HSL(-/-), KIAA1363(-/-) and wild-type (WT) mice. TG, FC and TC concentrations were determined enzymatically, and CE concentrations were calculated. Data are presented as mean values (n=4) ± S.E.M.

		µg/mg protein		
	n	TG	FC	CE
macrophages				
WT	4	15.5 ± 1.3	24.6 ± 1.4	0.24 ± 0.07
HSL(-/-)	4	17.1 ± 1.8	24.8 ± 1.9	0.33 ± 0.09
KIAA1363(-/-)	4	17.8 ± 1.1	26.9 ± 2.5	0.40 ± 0.07
foam cells				
WT	4	19.2 ± 1.6	27.8 ± 1.7	34.0 ± 2.4
HSL(-/-)	4	19.1 ± 1.2	30.5 ± 1.1	38.2 ± 3.2
KIAA1363(-/-)	4	18.4 ± 1.2	26.6 ± 3.8	33.1 ± 6.5

Furthermore, the DG content of HSL(-/-), KIAA1363(-/-) and WT MPM was determined by liquid chromatography (LC) and mass spectrometry (MS) (in collaboration with Harald Koefeler). The chromatography was performed on a Thermo Hypersil Gold C18 column and the data acquisition was done by FT-ICR-MS full scan. As internal standard 12:0/12:0 diacylglycerol was used. As shown in Figure 48 A and B, MPM from HSL(-/-) and KIAA1363(-/-) mice as well as their littermates possessed the same DG content.

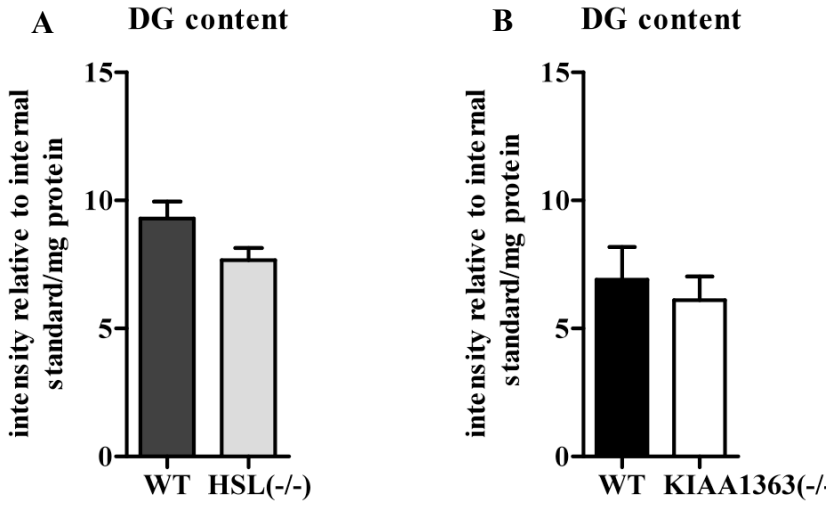

Figure 48: DG content of macrophages from HSL(-/-), KIAA1363(-/-) and WT mice. DG concentrations in HSL(-/-) (A), KIAA1363(-/-) (B) and WT MPM were determined by liquid chromatography on a Thermo Hypersil Gold C18 column and the data acquisition was performed by FT-ICR-MS full scan. As internal standard 12:0/12:0 diacylglycerol was used. Data are presented as mean values (n=4) ± S.E.M.

In the following experiments the FA composition of the cellular lipid fractions from HSL(-/-)-, KIAA1363(-/-)- and WT MPM were investigated by gas chromatography (GC) analysis (in collaboration with Wolfgang Sattler). The DG fraction of HSL(-/-) MPM exhibited slightly more (40 %) FA in comparison to the WT fraction, whereas the FA in the TG fraction of HSL(-/-) MPM were decreased (-65 %) (Figure 49). The FA composition in KIAA1363(-/-) MPM was similar to WT (Figure 49).

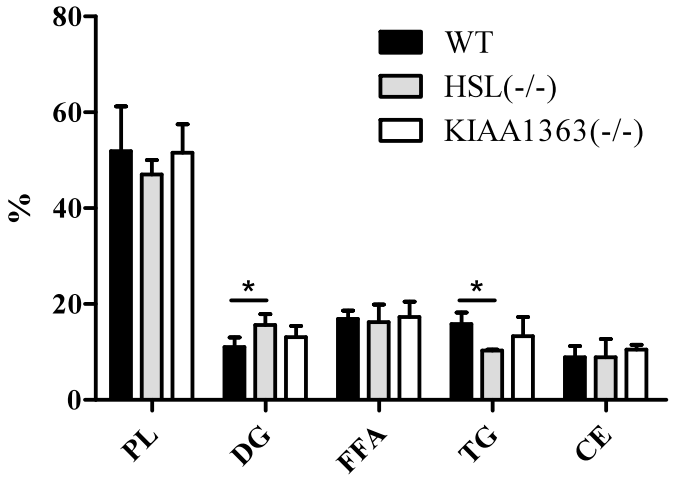

Figure 49: FA composition in the subcellular lipid fractions from HSL(-/-)-, KIAA1363(-/-) and WT MPM. Lipids were extracted twice with hexane:isopropanol (3:2, v/v), separated on TLC and analyzed by GC. As internal standard 10 µg pentadecanoic acid was used. Data are presented as mean values ± SEM of 3 mice per genotype performed in triplicate. *, $p < 0.05$.

4.4.12 Effect of HSL and KIAA1363 deficiency on cholesterol efflux

To analyze if HSL or KIAA1363 deficiency affects reverse cholesterol transport *in vivo*, MPM of HSL(-/-) and KIAA1363(-/-) mice were loaded with ^{3}H-cholesterol labeled acLDL, equilibrated for 16 h, and subsequently various pathways of cholesterol efflux were analyzed. Absence of HSL expression markedly reduced ATP-binding cassette transporter (ABC)G1-mediated cholesterol efflux to HDL_3 between 29 % and 42 % (Figure 50 A). ABCA1-mediated efflux to lipid-free apoA-I was also decreased by 34 % and 44 % after 6 h and 9 h, respectively, compared to WT MPM (Figure 50 B).

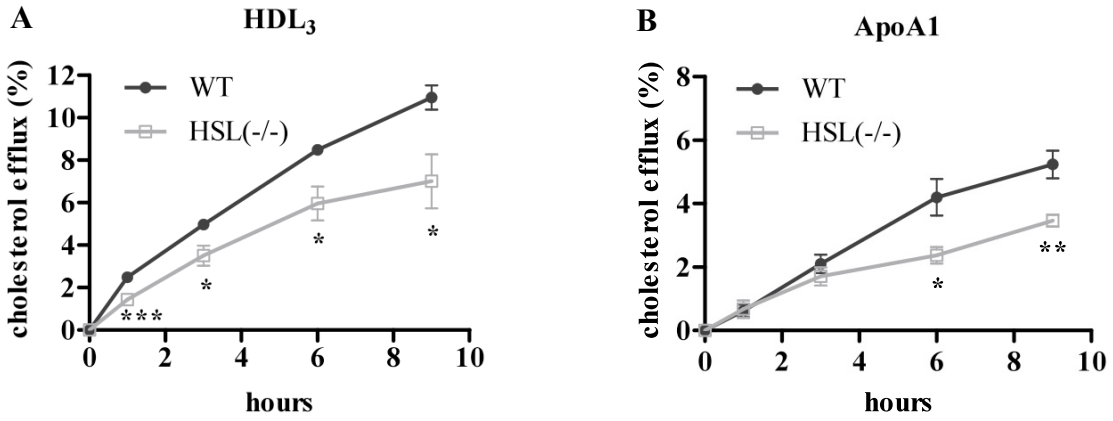

Figure 50: Cholesterol efflux from HSL(-/-) macrophages to HDL_3 and ApoA1. Macrophages from HSL(-/-) mice and control littermates (WT) were labeled with [^{3}H]-cholesterol and cholesterol efflux to 100 µg HDL_3 (A) and 15 µg apoA1 (B) was assessed in the presence of 300 µM dibutyryl-cAMP. Cholesterol efflux was expressed as the percentage (%) of [^{3}H]-cholesterol transferred from cells to medium. Data are presented as mean values ± SEM of 2 independent experiments for 6-10 mice per genotype performed in triplicate. *, $p < 0.05$; **, $p \leq 0.01$; ***, $p \leq 0.001$.

To investigate whether these differences depend on the activation of HSL by cAMP in WT macrophages, I repeated cholesterol efflux in the absence of dibutyryl-cAMP in the incubation medium. No significant differences between HSL(-/-) and control MPM were obtained when media lacked dibutyryl-cAMP (Figure 51 A, B).

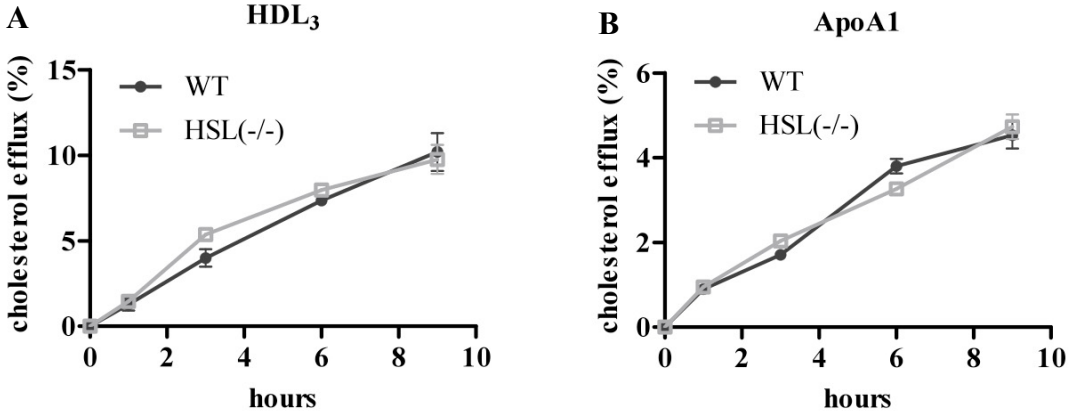

Figure 51: Cholesterol efflux from HSL(-/-) macrophages to HDL_3 and ApoA1. Macrophages from HSL(-/-) mice and control littermates (WT) were labeled with [^{3}H]-cholesterol and cholesterol efflux to (A) 100 µg HDL_3 and (B) 15 µg apoA1 was assessed without dibutyryl-cAMP. Cholesterol efflux was expressed as the percentage (%) of [^{3}H]-cholesterol transferred from cells to medium. Data are presented as mean values ± SEM of 2 independent experiments for 6-10 mice per genotype performed in triplicate.

KIAA1363 deficiency did not alter cholesterol efflux to HDL_3 (Figure 52 A) or apoA-I (Figure 52 B) confirming that the absence of KIAA1363 does not affect cholesterol mobilization from murine macrophages *ex vivo*.

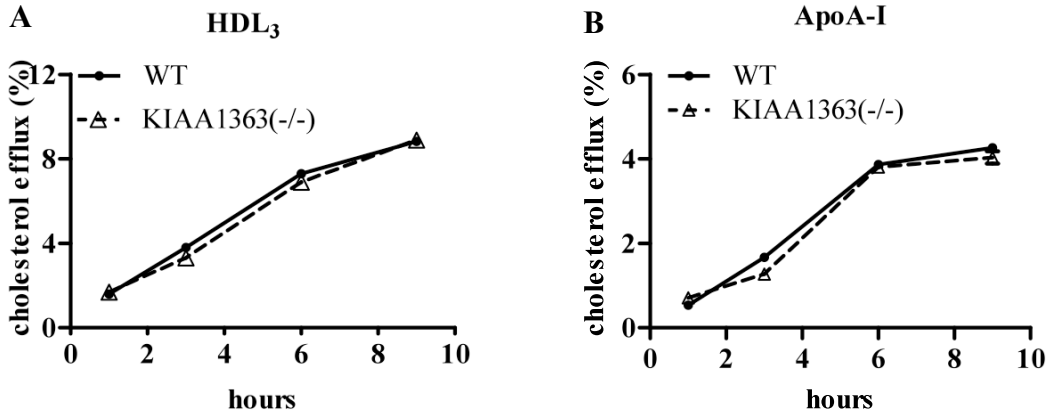

Figure 52: Cholesterol efflux from HSL(-/-) macrophages to HDL_3 and ApoA1. Macrophages from KIAA1363(-/-) mice and control littermates (WT) were labeled with [^{3}H]-cholesterol and cholesterol efflux to (A) 100 µg HDL_3 and (B) 15 µg apoA1 was assessed in the presence of 300 µM dibutyryl-cAMP. Cholesterol efflux was expressed as the percentage (%) of [^{3}H]-cholesterol transferred from cells to medium. Data are presented as mean values ± SEM of 2 independent experiments for 6-10 mice per genotype performed in triplicate.

4.4.13 Effect of HSL deficiency on macrophage FFA uptake

To determine if the FFA uptake in the lipid fractions of HSL(-/-) MPM is different to WT cells, macrophages were loaded for 24 h with a [^{3}H]oleic acid/BSA complex. Then the lipids were extracted and directly counted or separated on TLC. Radioactivity in the different fractions were normalized to total cell protein. After 24 h loading with [^{3}H]oleic acid, similar amounts of total FFA were taken up by WT and HSL(-/-) MPM (Figure 53 A). Evenmore,

also the different lipid fractions of WT and HSL(-/-) MPM contained the same amount of radiolabelled FFA (Figure 53 B).

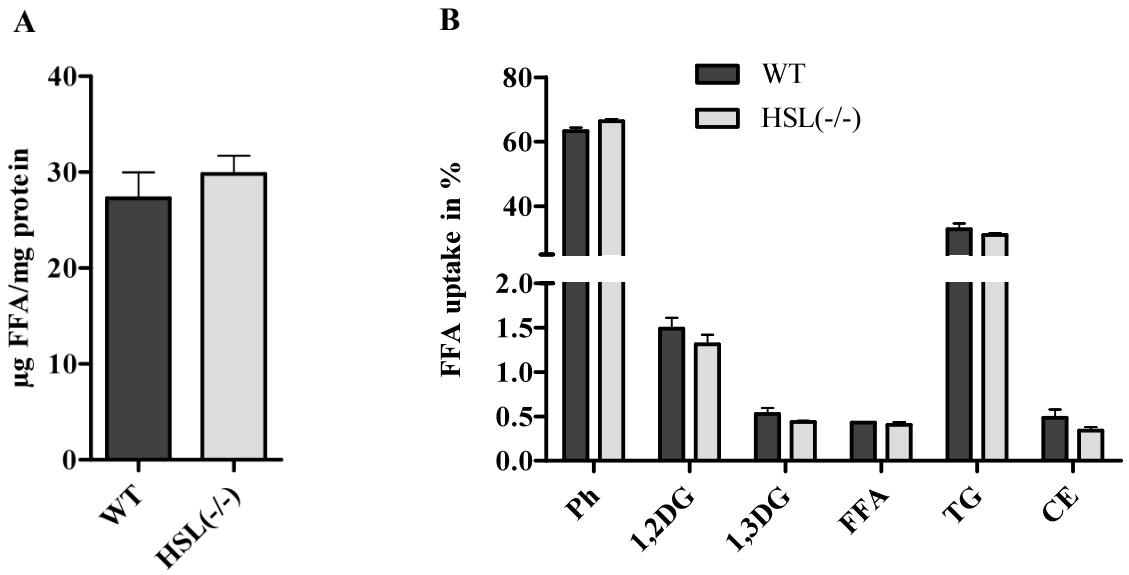

Figure 52: FFA uptake in lipid fractions of MPM from WT and HSL(-/-) mice. MPM were loaded for 24 h with a [^{3}H]oleic acid/BSA complex. Afterwards, lipids were extracted with hexane:isopropanol (3:2, v/v) and directly measured (A) or separated by TLC (B). Lipid fractions were cut out, radioactivity was measured and normalized to total cell protein. Data are presented as mean values ± SEM of 4 female mice per genotype performed in triplicate.

4.4.14 Effect of HSL deficiency on macrophage VLDL uptake

Moreover the VLDL uptake of HSL(-/-) and WT MPM was measured. After 2 h, 8 h, 24 h and 72 h lipids were extracted and TG, FC and CE levels were determined enzymatically. No differences in the TG, FC and CE content between WT and HSL(-/-) MPM were observed (Figure 54).

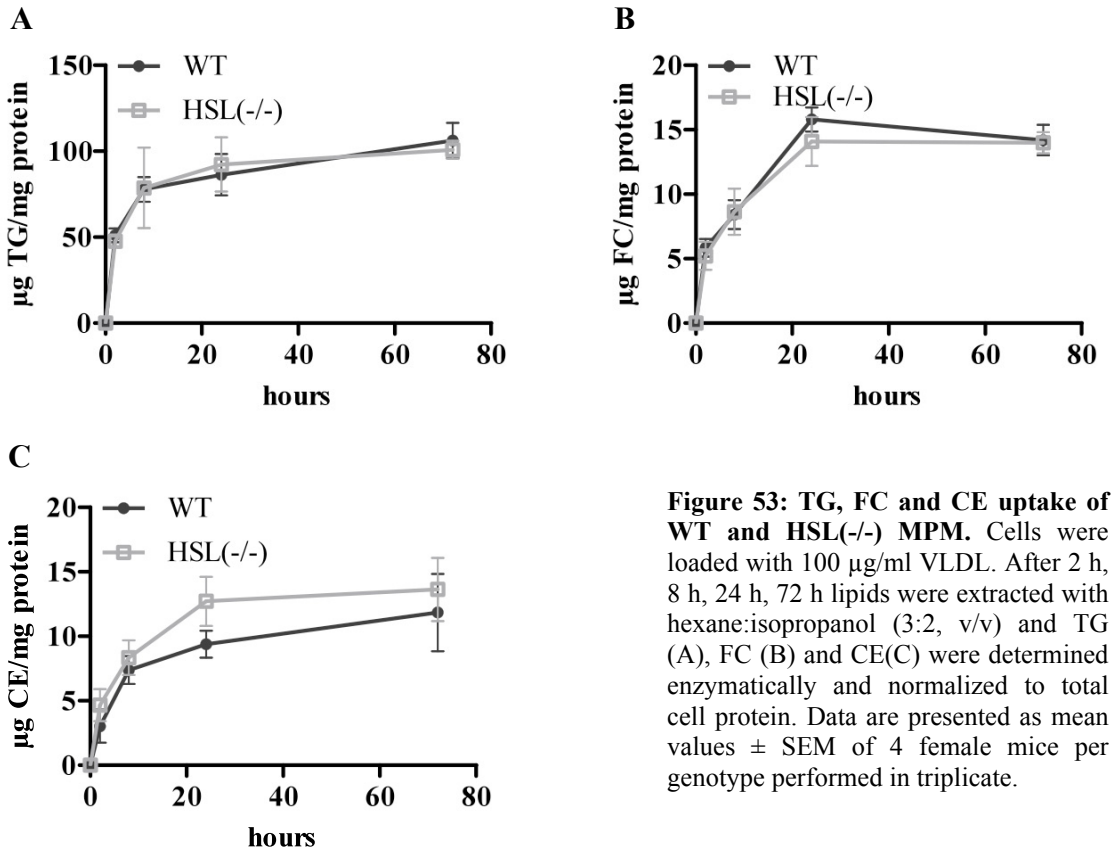

Figure 53: TG, FC and CE uptake of WT and HSL(-/-) MPM. Cells were loaded with 100 µg/ml VLDL. After 2 h, 8 h, 24 h, 72 h lipids were extracted with hexane:isopropanol (3:2, v/v) and TG (A), FC (B) and CE(C) were determined enzymatically and normalized to total cell protein. Data are presented as mean values ± SEM of 4 female mice per genotype performed in triplicate.

4.4.15 Effect of HSL on macrophage cholesterol uptake

Since HSL(-/-) MPM exhibited only a negligible CE hydrolase activity but an equal amount of FC, CE and TG, the uptake behavior of these cells in comparison to WT MPM was determined. Therefore, a short term cholesterol uptake experiment of WT and HSL(-/-) MPM was set up. Cells were loaded for 1 h, 3 h, 6 h and 12 h with 100 µg [^{3}H]cholesterol/acLDL. Afterwards, lipids were extracted, directly counted or separated by TLC and FC and CE fractions were measured by scintillation counting. MPM of both genotypes showed the same cholesterol uptake behavior (Figure 55A) after the different time points, as well as the same amount of FC (Figure 55 B) and CE (Figure 55 C).

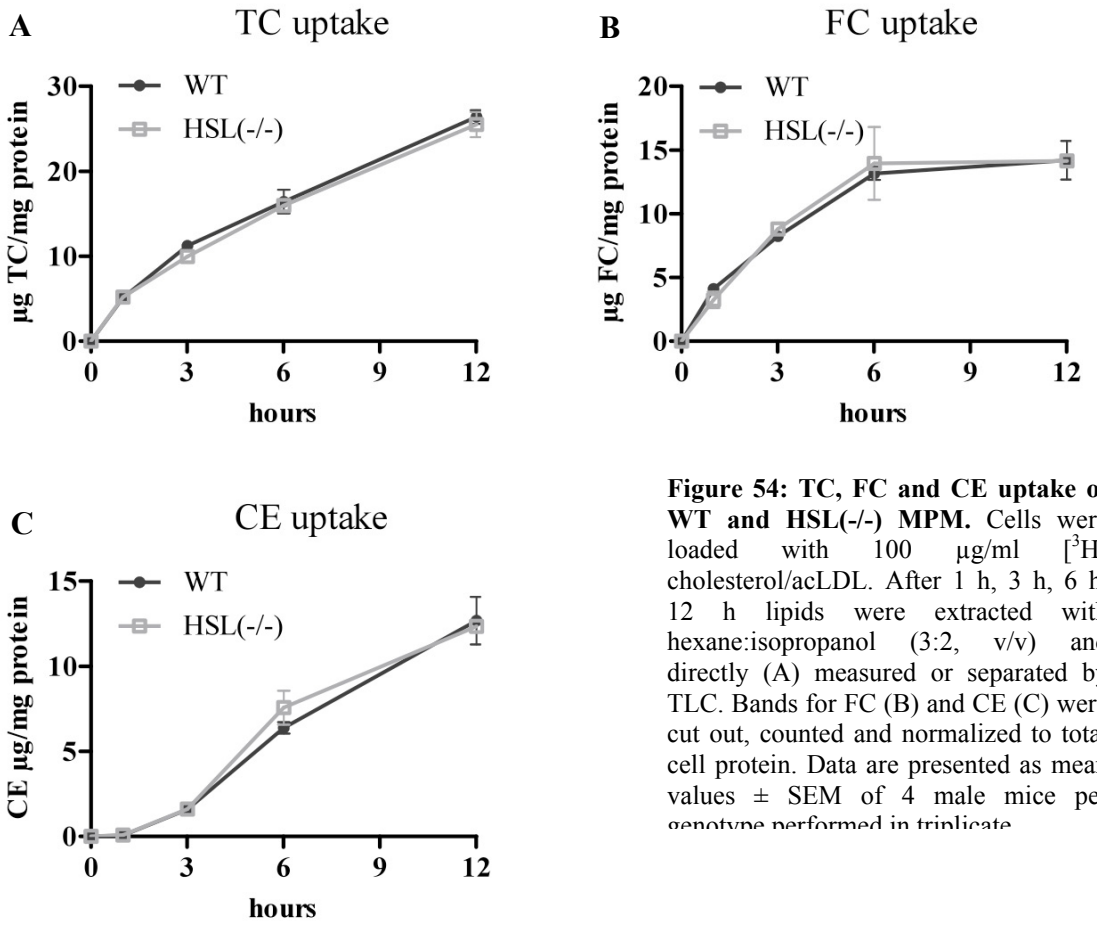

Figure 54: TC, FC and CE uptake of WT and HSL(-/-) MPM. Cells were loaded with 100 µg/ml [^{3}H] cholesterol/acLDL. After 1 h, 3 h, 6 h, 12 h lipids were extracted with hexane:isopropanol (3:2, v/v) and directly (A) measured or separated by TLC. Bands for FC (B) and CE (C) were cut out, counted and normalized to total cell protein. Data are presented as mean values ± SEM of 4 male mice per genotype performed in triplicate.

Thereafter, the uptake of cholesterol from acLDL was determined after loading of WT and HSL(-/-) MPM for a longer timepoint (24 h). As shown in Figure 56, no differences in TC, FC and CE fractions were measured between WT and HSL(-/-) MPM.

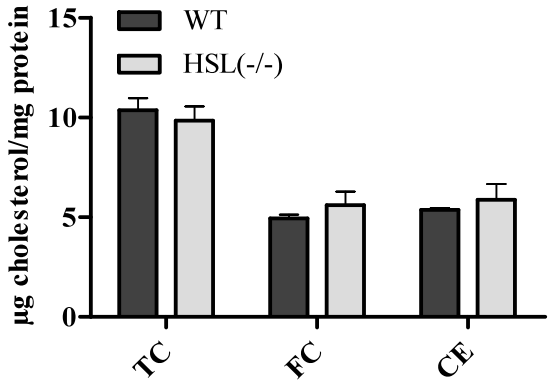

Figure 55: TC, FC and CE uptake of WT and HSL(-/-) female MPM after 24 h. Cells were loaded with 100 µg/ml [^{3}H] cholesterol/acLDL. After 24 h lipids were extracted with hexane:isopropanol (3:2, v/v) and directly measured or separated by TLC. Bands for FC and CE were cut out, counted and normalized to total cell protein. Data are presented as mean values ± SEM of 4 female mice per genotype performed in triplicate.

To compare the uptake of acLDL with aggLDL uptake, MPM of HSL(-/-) and WT mice were loaded for 24 h with 100 µg/ml [^{3}H]cholesterol-loaded aggLDL. Again, no differences were observed between WT and HSL(-/-) MPM (Figure 57). However, the cells loaded with agg LDL for 24 h contained 45 % less TC (Figure 57) in comparison to 24 h acLDL loaded cells (Figure 56).

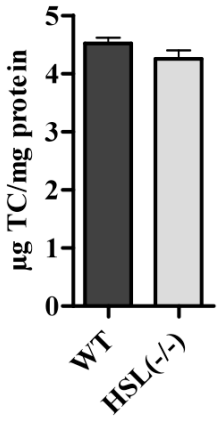

Figure 56: TC content of WT and HSL(-/-) female MPM after 24 h. Cells were loaded with 100 µg/ml [^{3}H]cholesterol-loaded aggLDL. After 24 h lipids were extracted with hexane:isopropanol (3:2, v/v). Radiolabelled cholesterol was directly measured and normalized to total cell protein. Data are presented as mean values ± SEM of 4 female mice per genotype performed in triplicate.

Due to the well known activation of HSL by cAMP, MPM of WT and HSL(-/-) mice were loaded for 24 h with 100 µg/ml [^{3}H]cholesterol-loaded acLDL and then equilibrated for 16 h with and without dibutyryl-cAMP. Addition of 300 µM dibutyryl-cAMP resulted in less TC (-23 %) and CE (-17 %) concentrations in comparison to MPM from HSL(-/-) (Figure 58 A). Without stimulation of HSL by cAMP, the difference between WT and HSL(-/-) MPM was abolished (Figure 58 B).

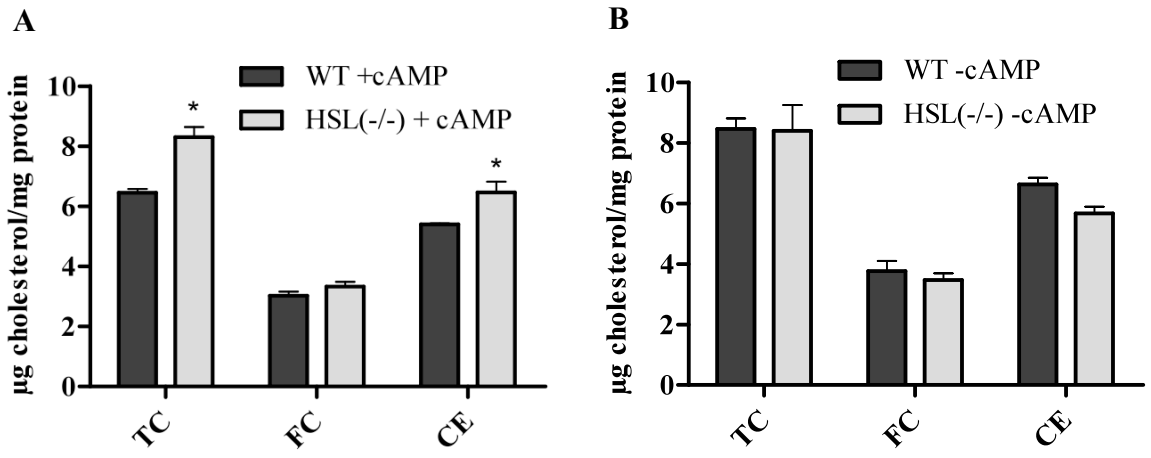

Figure 57: TC, FC and CE uptake of WT and HSL(-/-) female MPM after equilibration for 16 h with and without dibutyryl-cAMP. Cells were loaded for 24 h with 100 µg/ml [^{3}H]cholesterol-loaded acLDL. After 16 h equilibration without acLDL, lipids were extracted with hexane:isopropanol (3:2, v/v) and directly measured (TC) or separated by TLC. Bands for FC and CE were cut out and radioactivity was counted on a -counter. Data are presented as mean values ± SEM of 4 female mice per genotype performed in triplicate.*, $p < 0.05$.

Furthermore, a long term treatment with 100 µg/ml acLDL of MPM from the two different genotypes was performed. Cells were loaded for 48 h, 72 h and 96 h with 100 µg acLDL and after lipid extraction, TC, FC and TG were determined enzymatically. After 48 h, 72 h and 96 h HSL(-/-) MPM exhibited the same lipid content (FC, CE and TG Figure 59 A-C) as macrophages obtained from WT mice.

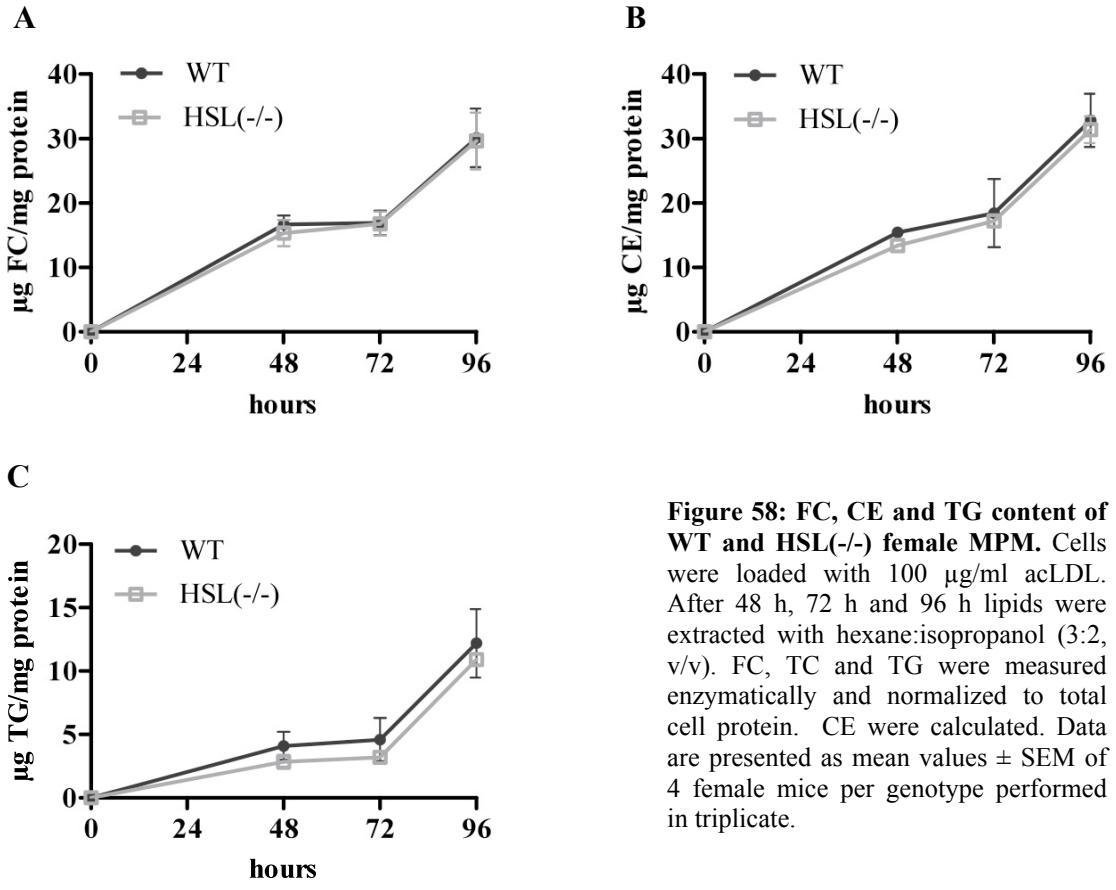

Figure 58: FC, CE and TG content of WT and HSL(-/-) female MPM. Cells were loaded with 100 µg/ml acLDL. After 48 h, 72 h and 96 h lipids were extracted with hexane:isopropanol (3:2, v/v). FC, TC and TG were measured enzymatically and normalized to total cell protein. CE were calculated. Data are presented as mean values ± SEM of 4 female mice per genotype performed in triplicate.

Next, MPM were loaded with 50 µg/ml [^{3}H]cholesterol-loaded ß-VLDL for 30 h. The ß-VLDL I used contained 1.8 µg CE/ mg protein. No changes in the TC, FC and CE fractions of both genotypes were found (Figure 60) after loading with the cholesterol rich ß-VLDL for 30 h.

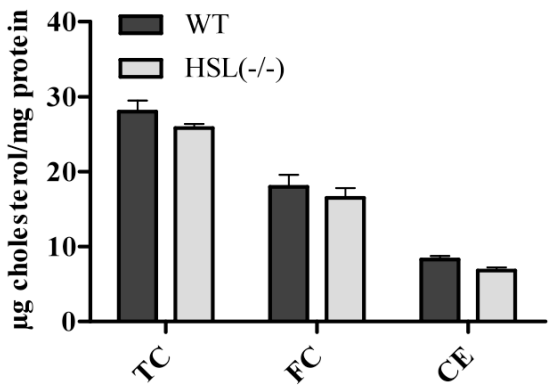

Figure 59: TC, FC and CE content of HSL(-/-) and WT MPM. Cells were loaded with 50 µg/ml [^{3}H]cholesterol-loaded ß-VLDL for 30 h. Then lipids were extracted with hexane:isopropanol (3:2, v/v) and radioactivity in an aliquot was directly measured with a ß-counter. Fourty µl were separated on TLC and bands for FC and CE were cut out and measured. Data are presented as mean values ± SEM of 4 female mice per genotype performed in triplicate.

4.4.16 Effect of KIAA1363 deficiency on macrophage cholesterol uptake

KIAA1363(-/-) and WT MPM were incubated with 50 µg/ml [^{3}H]cholesterol-loaded ß-VLDL for 30 h. The uptake behaviour of KIAA1363(-/-) and WT cells was the same (Figure 61).

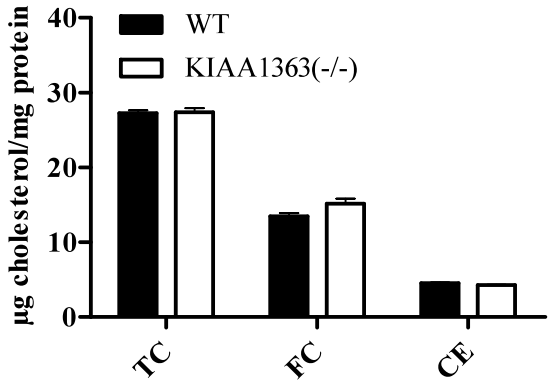

Figure 60: TC, FC and CE content of KIAA1363(-/-) and WT MPM. Cells were loaded with 50 µg/ml [^{3}H]cholesterol-loaded ß-VLDL for 30 h. Then lipids were extracted with hexane:isopropanol (3:2, v/v) and radioactivity in an aliquot was directly measured with a ß-counter. Fourty µl were separated on TLC and bands for FC and CE were cut out and measured. Data are presented as mean values ± SEM of 4 female mice per genotype performed in triplicate.

4.4.17 Effect of HSL and KIAA1363 deficiency on LPL activity of macrophages

Furthermore, the LPL activities from macrophages of HSL(-/-) and KIAA1363(-/-) mice as well as their littermates were determined to confirm the results from the uptake experiments of all genotypes. The LPL activity of WAT was 18333-fold increased in comparison to the spontaneous hydrolysis (Figure 62). However, no differences in LPL activity were observed in MPM of HSL(-/-), KIAA1363(-/-) and WT mice. Interestingly, WT MPM from the HSL strain showed a 2.3-fold higher LPL activity than littermates from the KIAA1363 strain (Figure 62).

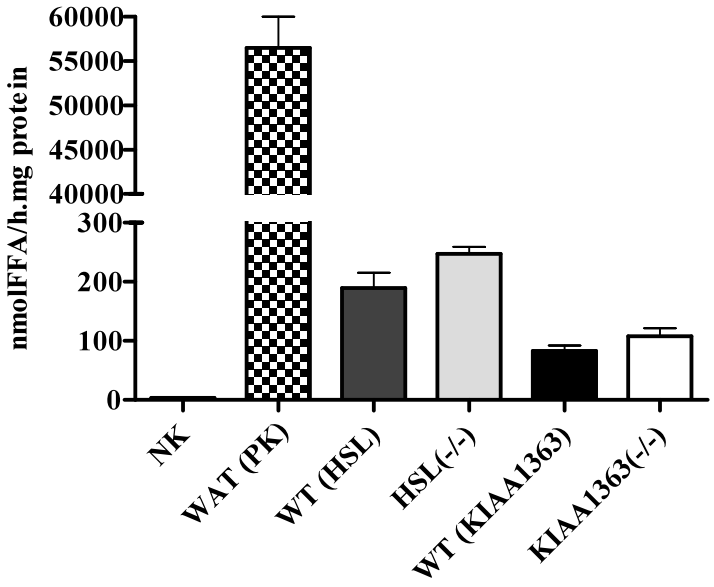

Figure 61: LPL activity of HSL(-/-), KIAA1363(-/-) and WT (littermate) MPM. LPL activity was measured in whole cell lysates of all genotypes. As positive control (PK) WAT and as negative control the spontaneous hydrolysis of the substrate was used. Data are presented as mean values of 3 mice ± SEM.

4.4.18 Acid CE and TG hydrolase activities in HSL(-/-) and KIAA1363(-/-) MPM

Due to the fact that HSL(-/-) MPM showed almost abolished neutral CE hydrolase activity and reduced levels of TG hydrolase activity, the acid lipase activities were measured. The acid CE hydrolase activity was nearly the same HSL(-/-) and WT MPM (Figure 63 A). In contrast, TG hydrolase activity was 1.4-fold increased in HSL(-/-) MPM compared to WT cells (Figure 63 B). Equal acid CE (Figure 45 C) and TG hydrolase (Figure 63 D) activities were observed in macrophages of KIAA1363(-/-) and WT mice.

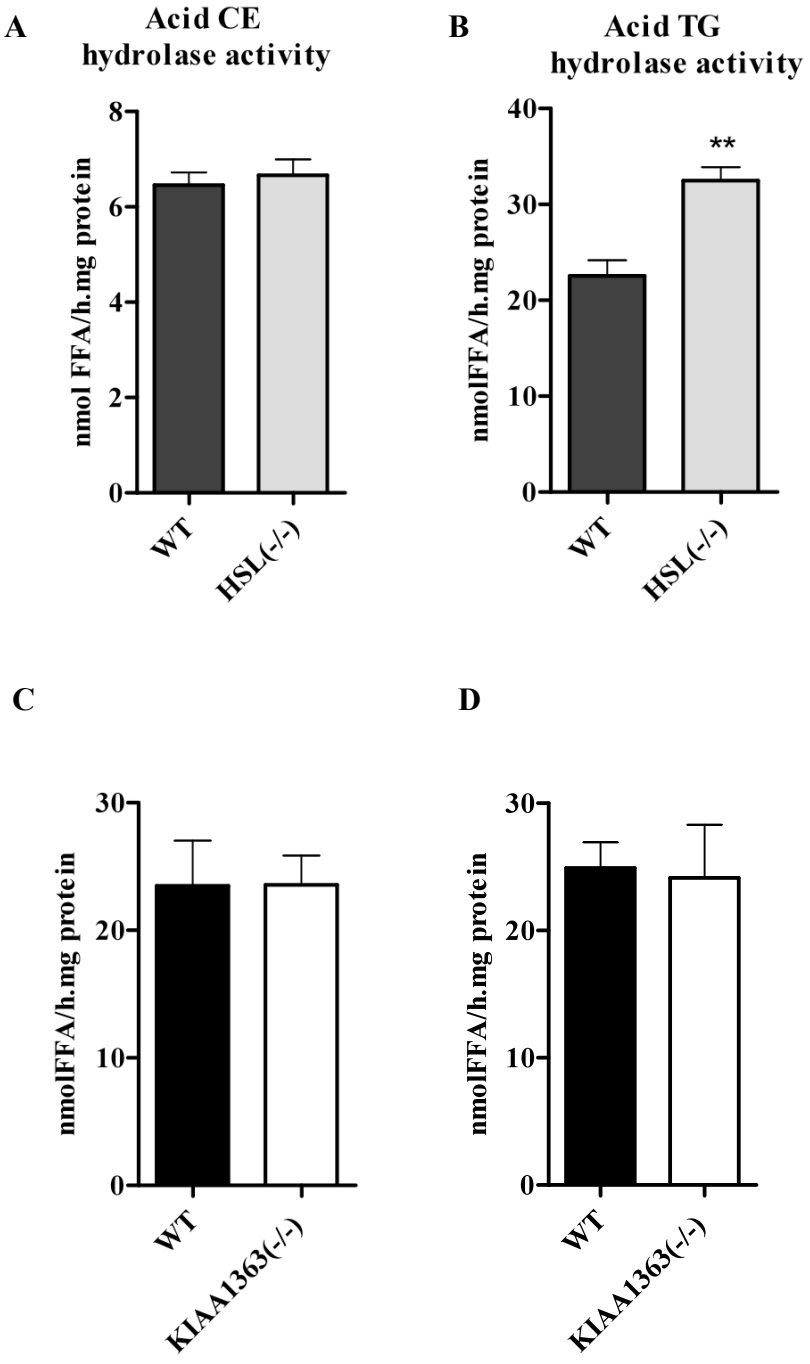

Figure 62: Acid CE and TG hydrolase activities of HSL(-/-), KIAA1363(-/-) and WT macrophages. Acid CE (A, C) and TG (B, D) hydrolase activities were determined in MPM of HSL(-/-) (A, B), KIAA1363(-/-) (C, D) and WT mice adding 35.5 µg mixed micelles of PC and PI (3:1, w/w) and 4 µM Na-taurocholate to the respective substrates. Data are presented as mean values of 2 independent experiments ± SEM.

4.4.19 Blocking of HSL activity with our selfmade HSL antibody

I received this polyclonal rabbit antibody from Thomas Pfeifer (129). He got this antibody by infecting a rabbit with an adenovirus containing the HSL gene. After 6 weeks blood was drawn, the IgG was isolated, lyophilized and resuspended in PBS [c = 7 µg/µl].

First, western blot analysis was performed to check the specificity of the HSL antibody. As positive controls HSL adenovirus or plasmid overexpressing COS-7 cell lysates were used and as negative control LacZ transfected COS-7 cells were taken. As shown in Figure 64 this HSL antibody was very specific. HSL (84 kDa) from the adenoviral construct was recognized as well as the HSL protein produced from the HSL gene on the plasmid construct. In the negative control no bands were detected.

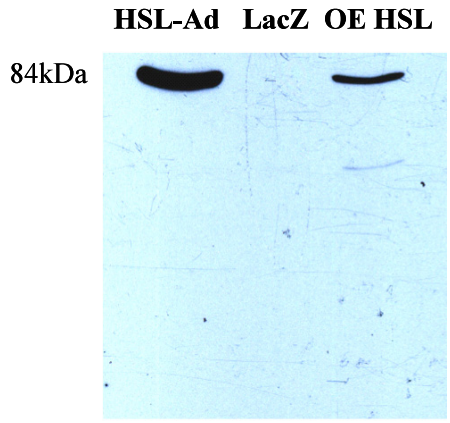

Figure 63: Western blot of HSL overexpressing COS-7 cells using the selfmade anti-HSL antibody. COS-7 cells were transfected with Metafectene™ and 2.5 µg of HSL or LacZ plasmid-DNA (OE HSL) or infected with 150 MOI HSL adenovirus (HSL-Ad). LacZ transfected cell protein was used as negative control. After 48 h, cells were scraped off in RIPA buffer and protein was determined by the method of Bradford. Seventy-five µg cell protein was separated on a SDS gel. Western blot analysis was performed with our selfmade anti-HSL antibody.

.

To investigate if this HSL antibody is able to inhibit CE, TG and AcMAGE hydrolase activities of HSL, activity assays were performed in MPM with different concentrations of HSL antibody. As negative control the same amount of non IgG was used (isolated from the same rabbit before adenoviral infection). HSL antibody inhibited the CE hydrolase activity of HSL in MPM (Figure 65), thus the antibody likely binds to the active site of the enzyme or in the surrounding area. The CE hydrolase activity in WT MPM was blocked in a concentration dependent manner. With 14 µg of the antibody the enzyme activity was blocked to the same level as in HSL(-/-) MPM, whereas no differences were observed between HSL(-/-) MPM incubated with or without 14 µg of the antibody. As expected, non immune IgG was not able to block the CE hydrolase activity in MPM (Figure 65).

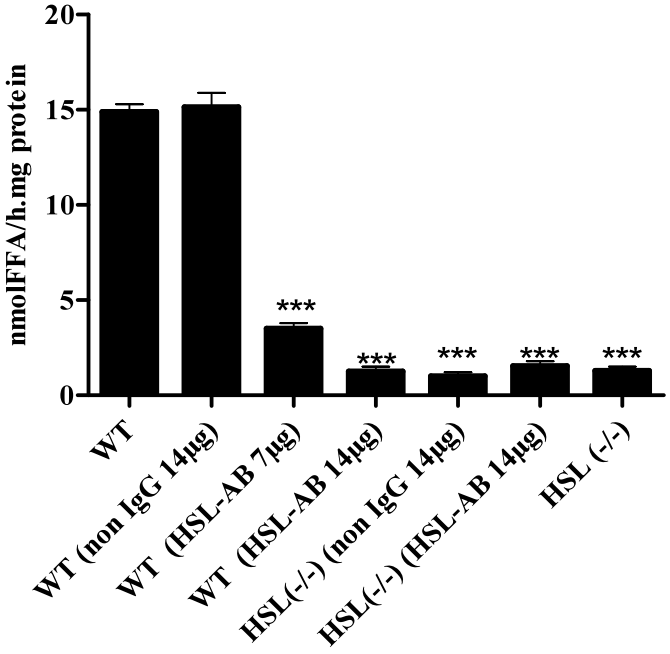

Figure 64: CE hydrolase activity of HSL(-/-) and WT MPM incubated with different concentrations of HSL antibody (HSL-AB) and non IgG. Neutral CE hydrolase activities were determined in cell lysates of HSL(-/-) and WT macrophages from littermates adding 35.5 µg mixed micelles of PC and PI (3:1, w/w) and 4 µM Na-taurocholate to the respective substrate. Data are presented as mean values of 4 mice in triplicate ± SEM. ***, $p \leq 0.001$.

Next, the antibody was tested in TG hydrolase activity assays. The TG hydrolase activity in MPM of WT mice was blocked to the same level as in HSL(-/-) MPM (Figure 66). The non IgG antibody did not result in reduction of TG hydrolase activity in MPM.

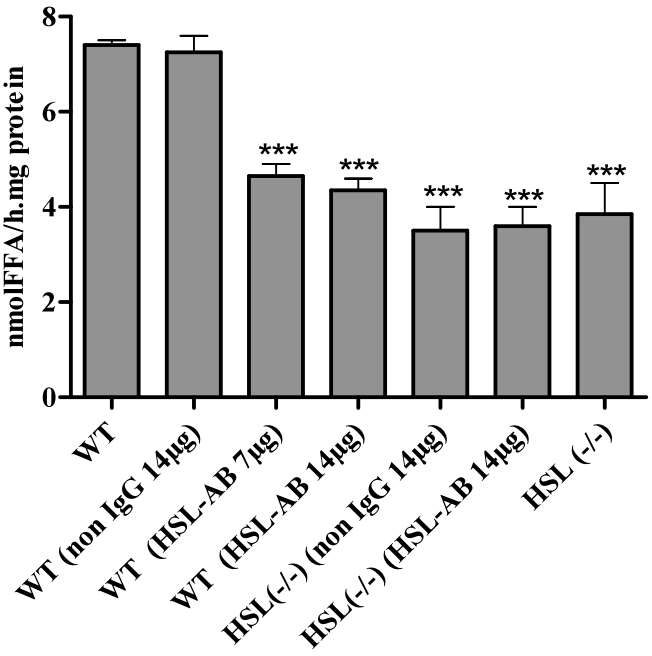

Figure 65: TG hydrolase activity of HSL(-/-) and WT MPM incubated with different concentrations of HSL antibody (HSL-AB) and non IgG. Neutral TG hydrolase activities were determined in cell lysates of HSL(-/-) and WT macrophages from littermates adding 15 µg mixed micelles of PC and PI (3:1, w/w) and 4 µM Na-taurocholate to the respective substrate. Data are presented as mean values of 4 mice in triplicate ± SEM. ***, $p \leq 0.001$.

AcMAGE hydrolase activity was not changed by our HSL-AB (Figure 67). These results were in line with my data of AcMAGE hydrolase activity in HSL(-/-) MPM, which were also unchanged compared to WT MPM (Figure 45 A).

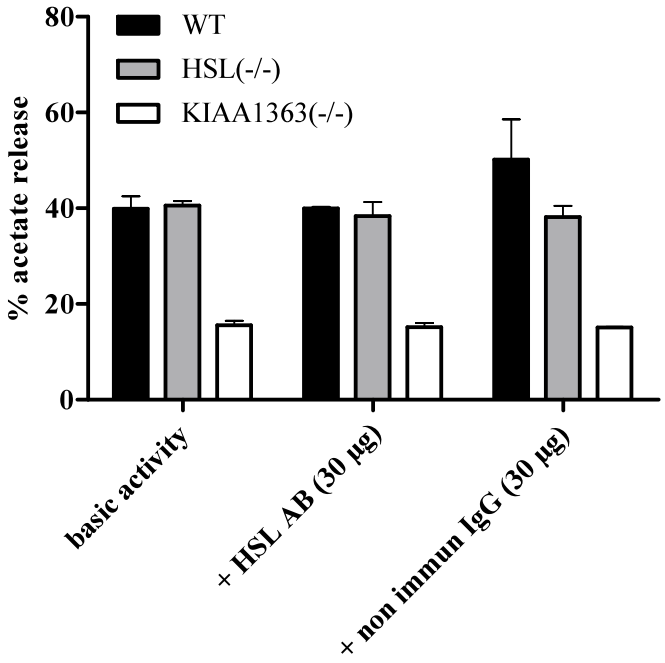

Figure 66: AcMAGE hydrolase activities in WT, HSL- and KIAA1363- deficient macrophages incubated with HSL-AB and non immune IgG. AcMAGE hydrolase activities were determined in cell lysates of HSL(-/-), KIAA1363(-/-), and WT macrophages with 30 µg HSL-AB, 30 µg non immune IgG and the basic activity was determined too. Data are presented as mean values of 1 experiment ± SEM (using 4 mice).

4.5 Does KIAA1363 play a role in inflammation in MPM?

KIAA1363 is not able to cleave CE, TG and DG *in vitro* and *in vivo*. Therefore this enzyme is not responsible for cholesterol mobilization in MPM and foam cells. But in this thesis I found out, that KIAA1363 is an AcMAGE hydrolase in MPM and might limit PAF levels by diverting AcMAGE to MAGE also in macrophages.

4.5.1 KIAA1363 mRNA expression in LPS- stimulated MPM

MPM from WT mice were stimulated with 1 and 10 ng LPS for 6 h. Afterwards, KIAA1363, HSL and iNOS mRNA expressions were determined by real time PCR. iNos, an inflammatory gene, was used as positive control, because it is known to be very strong induced by LPS. KIAA1363 was downregulated by 1 and 10 ng LPS in a concentration dependent manner (2.2- fold and 5.3- fold) respectively, which indicates that KIAA1363 plays a role as inflammatory regulated gene. In contrast HSL was only slightly 1.7-fold upregulated by 10 ng LPS (Figure 68).

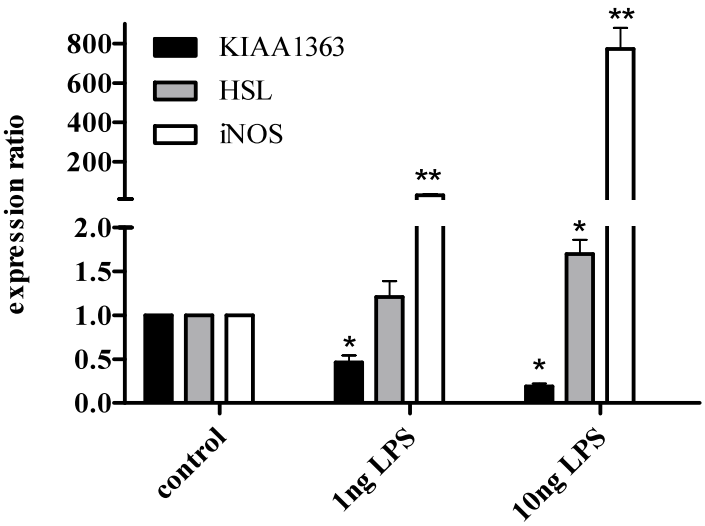

Figure 67: KIAA1363, HSL and iNOS mRNA expressions in MPM from WT mice. Total RNA was isolated from cells and mRNA levels were determined by real time PCR. mRNA quantities were normalized to the house-keeping gene cyclophilin A. mRNA levels are presented in relation to the expression in WT MPM (arbitrarily set to 1). Bars represent the mean values ± SEM of two experiments performed in triplicates. *, $p < 0.05$; **, $p \leq 0.01$.

4.5.2 KIAA1363 protein expression in LPS- stimulated MPM

Next, I checked for the protein expression of KIAA1363 in LPS- induced MPM. Cells were incubated for 6 h with different concentrations of LPS. Although KIAA1363 mRNA levels were downregulated by incubation with LPS after 6 h, no differences were observed on the protein level of KIAA1363 (Figure 69) in LPS- loaded MPM.

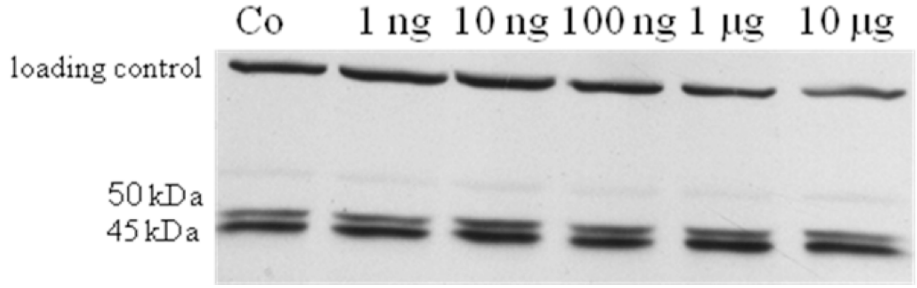

Figure 68: Western blot of WT MPM incubated for 6 h with different concentrations of LPS using anti-KIAA1363 antibody. MPM were scraped off with RIPA buffer and after protein estimation, 60 µg protein were loaded on SDS-PAGE. Western blot analysis was performed using a specific anti-KIAA1363 antibody.

Thus, I loaded MPM for 24 h, 48 h and 72 h with 10 ng and 10 µg of LPS and determined KIAA1363 protein level in these samples by Western blot. Incubation of MPM with LPS reduced KIAA1363 protein expression in a time and concentration dependent manner (Figure 70). The highest reduction was achieved after 72 h loading of 10 µg LPS.

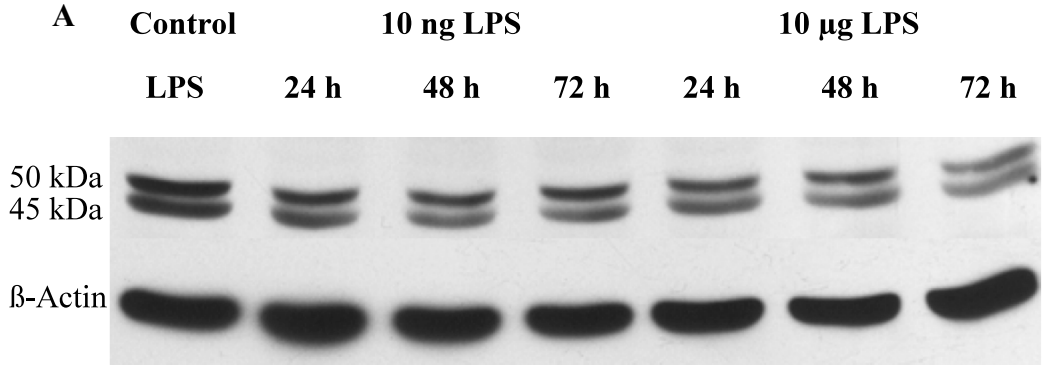

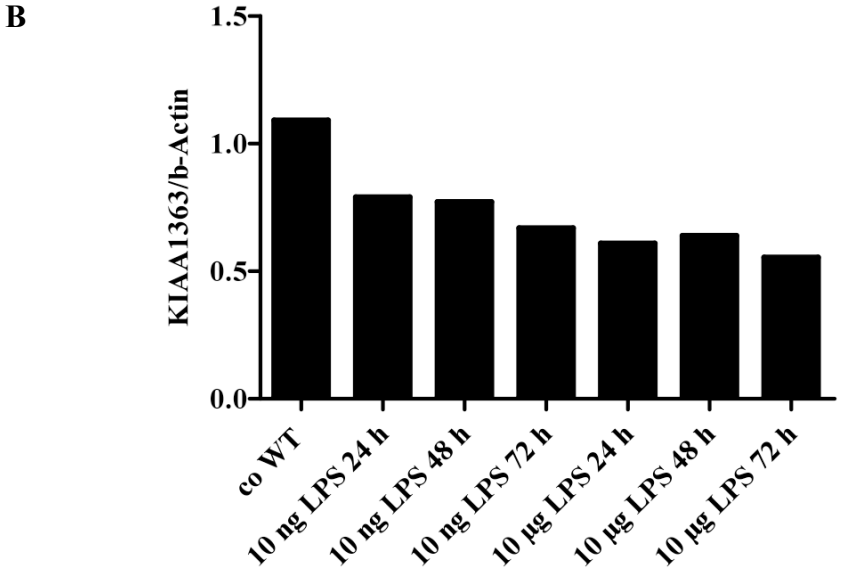

Figure 69: Western blot of WT MPM incubated for 24 h, 48 h and 72 h with 10 ng and 10 µg LPS and densidometric analysis. MPM were scraped off with RIPA buffer and after protein estimation, 60 µg protein were separated by SDS-PAGE. Western blot analysis (A) was performed using anti-KIAA1363 antibody and β-Actin antibody as loading control. KIAA1363 protein of each lane was normalized to β-Actin (B).

4.5.3 AcMAGE hydrolase activity assay of LPS- stimulated MPM

I determined the AcMAGE hydrolase activity in LPS- incubated MPM. A significantly decreased AcMAGE hydrolase activity was found after incubation of MPM with 10 ng (62 %) and 100 ng (31 %) LPS for 6 h compared to non incubated cells (Figure 71), although the protein level of KIAA1363 was not downregulated under these conditions.

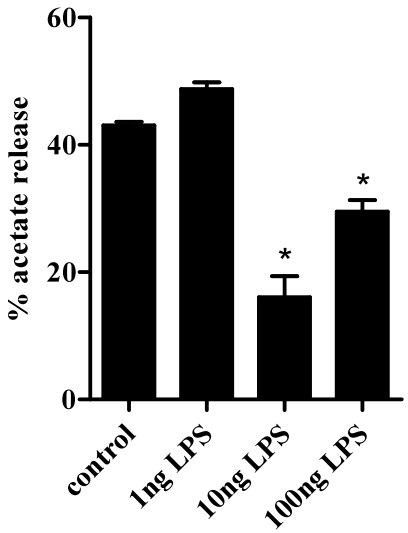

Figure 70: AcMAGE hydrolase activities of 6 h LPS induced MPM. MPM of WT mice were incubated for 6 h with 1 ng, 10 ng and 100 ng LPS. AcMAGE hydrolase activities were determined in whole lysates of MPM. Data are presented as mean values ± SEM of 1 experiment measured in triplicate. *, $p < 0.05$.

4.6 Localization of HSL in MPM and foam cells

To localize HSL in MPM and foam cells transmission electron microscopy (TEM) techniques and fluorescence microscopy were performed. As first antibody the HSL-AB was used to detect HSL, and as second antibodies an anti rabbit gold-conjugated antibody (TEM) or an anti- rabbit fluorescent labelled antibody (fluorescence microscopy) were chosen to make HSL "visible".

4.6.1 Macrophage structure determined by electron microscopy

All TEM pictures were taken in collaboration with Dagmar Kolb. MPM of WT mice were chemical fixed and conventional embedded to reveal the structure of these cells. As shown in Figure 72, MPM contain a large amount of ER revealing great metabolic activity in these cells. Also the nucleus (N) and a vacuole (V) can be seen in this picture.

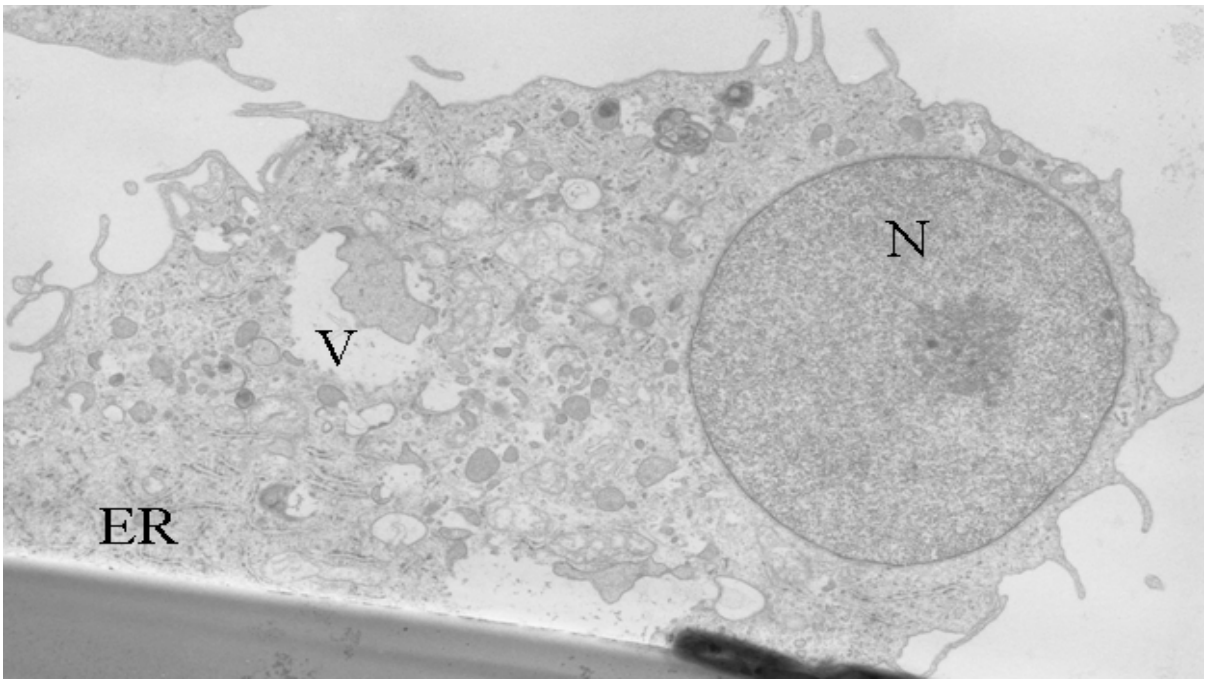

Figure 71: Transmission electron microscopy picture of WT MPM. MPM were seeded on a special foil, chemically fixed and conventionally embedded. Ultrathin sections (75 nm) were cut with a Reichert Ultracut S ultramicrotome and post stained for 5 min with lead citrate and for 15 min with uranyl acetate before they were observed in the Philips CM 10 transmission electron microscope (TEM). ER…endoplasmic reticulum, V… vacuole, N…nucleus

4.6.2 Localization of HSL in MPM-derived foam cells by electron microscopy

Next, 48 h acLDL- loaded MPM were chemically fixed and immunogold labelled with the HSL-AB and the second gold- conjugated antibody (10 nm gold particles) (Figure 73). MPM

from HSL(-/-) mice were incubated with the antibodies as negative control (picture not shown). The arrows in Figure 73 show HSL, which is localized in the cytosol as well as next to LD of foam cells, respectively.

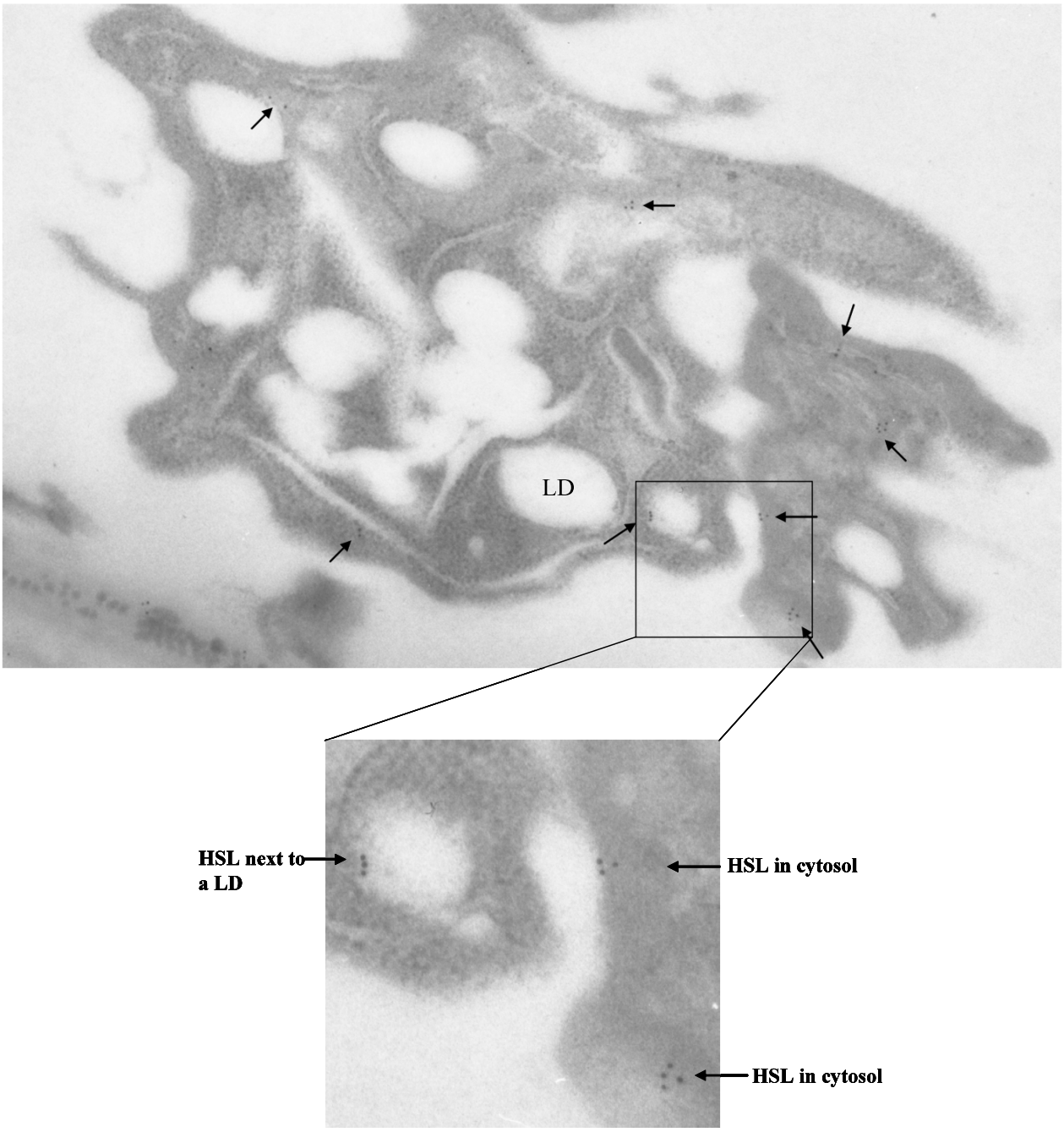

Figure 72: Transmission electron microscopy picture of immunogold labelled foam cells from WT mice. MPM, loaded for 48 h with acLDL, were seeded on a special foil, chemically fixed and immunogold labelled. Ultrathin sections (75 nm) were cut with a Reichert Ultracut S ultramicrotome and post stained for 5 min with lead citrate and for 15 min with uranyl acetate before they were observed in the Philips CM 10 transmission electron microscope (TEM). LD…lipid droplets, arrows show gold particles conjugated to HSL.

4.6.3 Localization of HSL in MPM-derived foam cells by fluorescence microscopy

MPM were seeded on coverslips and loaded for 48 h with acLDL to achieve foam cell formation. First, cells were incubated with HSL-AB and the fluorescently labelled Alexa Fluor red (595 nm) antibody. Coverslips were transferred to a Leica SP2 AOBS confocal microscope with spectral detection to take pictures at an amplification of 60 (in collaboration with Heimo Wolinski). Pictures were edited using the LCS Lite 2611537 software. Foam cells from HSL(-/-) deficient mice were used as negative control for the HSL-AB (Figure 74).

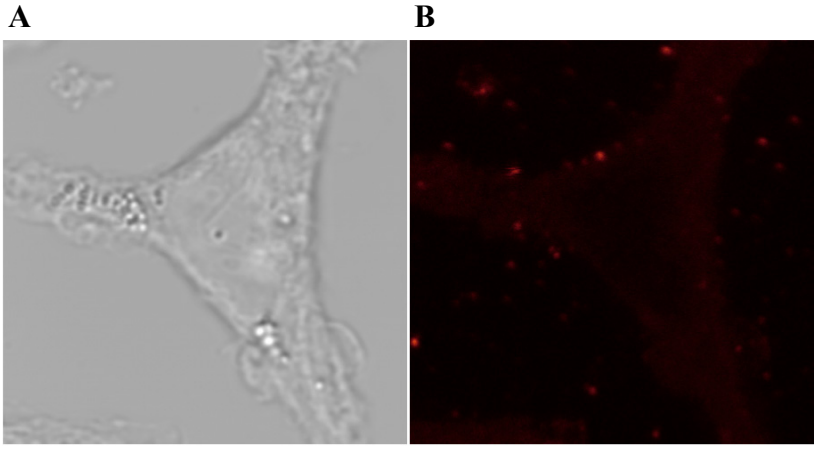

Figure 73: Microscopy picture of a HSL(-/-) foam cell labelled with HSL-AB. Foam cells were fixed with 4 % paraformaldehyde/0.02 % glutardialdehyde for 20 min. After 1 h blocking, cells were incubated with HSL-AB followed by incubation with the second fluorescently labelled Alexa fluor red antibody. Pictures were taken on a Leica SP2 AOBS confocal microscope.

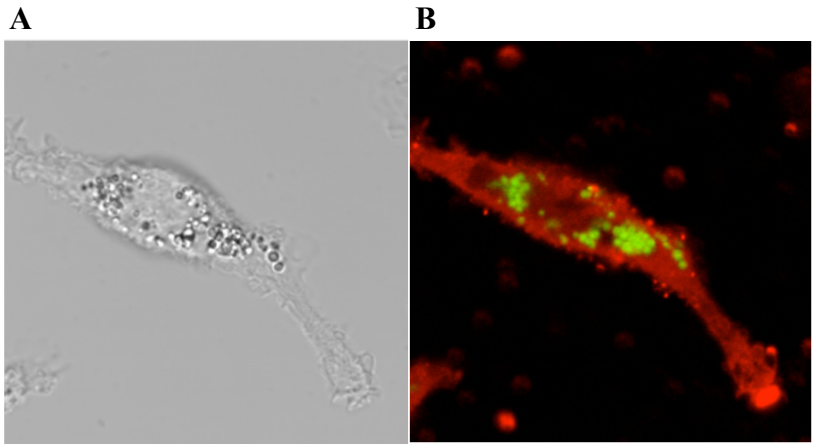

Figure 74: Microscopy picture of a WT foam cell labelled with HSL-AB and Bodipy green. Foam cells were fixed with 4 % paraformaldehyde/0.02 % glutardialdehyde for 20 min. After 1 h blocking, cells were incubated with HSL-AB followed by incubation with the second fluorescence labbeled Alexa fluor red antibody. Before pictures were taken on a Leica SP2 AOBS confocal microscope, coverslip was incubated with Bodipy green to stain the neutral lipids.

Next, foam cells were incubated ON with 300 μM dibutyryl- cAMP to activate PKA and Bodipy green (488 nm) was used to stain the LD. HSL was detectable in the whole cytosol of the cell (red), but not on LD (no overlay of green and red), suggesting that this antibody is not able to detect the protein kinase A phosphorylated form of HSL on the LD (Figure 75).

4.7 Experiments with KIAA1363(-/-)/HSL(-/-) mice (DKO) and their littermates

KIAA1363(-/-)/HSL(-/-) (DKO) mice were obtained from cross breeding of HSL(-/-) and KIAA1363(-/-) mice in our animal facility.

4.7.1 Plasma lipid parameters of DKO mice

First, the plasma lipid parameters of the DKO mice were investigated in the fed and ON fasted state (Table 17). Plasma lipid parameters were very similar to those of HSL(-/-) mice. Plasma TG levels of DKO mice were decreased by 46 % and FFA levels were decreased by 31 % after fasting. Independent of the dietary status, plasma TC levels were increased and also the FC level was slightly elevated in DKO mice in the fasted state.

Table 17: Plasma lipid parameters of DKO and control (WT) mice. Blood was drawn from 8-10 week old male and female mice in the fed and fasted state. TG, TC, FC and FFA concentrations were determined enzymatically. Data are presented as mean values (n=3) ± SEM. *, $p < 0.05$; **, $p \leq 0.01$.

fed	**male n**	**mg/dl TG**	**TC**	**FC**	**mM FFA**
WT	3	122.5 ± 20.1	91.1 ± 3.7	34.3 ± 1.5	n.d.
DKO	3	123.4 ± 18.9	119.7 ± 5.2*	38.3 ± 1.3	
fasted					
WT	3	57.1 ± 2.1	82.1 ± 3.9	20.8 ± 0.6	1.3 ± 0.1
DKO	3	31.1 ± 3.5**	105.5 ± 2.7**	26.7 ± 1.9*	0.9 ± 0.2*
	female n	**mg/dl TG**	**TC**	**FC**	**mM FFA**
WT	3	98.5 ± 10.3	85.6 ± 6.7	26.3 ± 2.8	n.d.
DKO	3	95.9 ± 5.6	97.0 ± 4,2*	24.7 ± 3.0	
fasted					
WT	3	49.1 ± 4.1	69.6 ± 7.3	19.5 ± 1.4	1.9 ± 0.2
DKO	3	33.5 ± 5.1*	88.9 ± 3.7*	22.6 ± 3.4	1.1 ± 0.1*

4.7.2 Lipoprotein profile of DKO mice

To investigate the lipid distribution among lipoprotein subclasses, plasma samples of ON fasted DKO mice and their littermates were subjected to FPLC analysis. The TG content in the VLDL-TG fraction was reduced by 55 % in DKO animals, whereas HDL- cholesterol was increased by 30 % in these mice compared to controls (Figure 76 A, B). LDL- cholesterol was elevated by 45 % and TG were decreased by 21 % (Figure 76 A, B). These results were comparable to those of HSL(-/-) mice (Figure 35) and were expected, since KIAA1363(-/-) mice had an unchanged lipoprotein profile compared to their littermates (Figure 36).

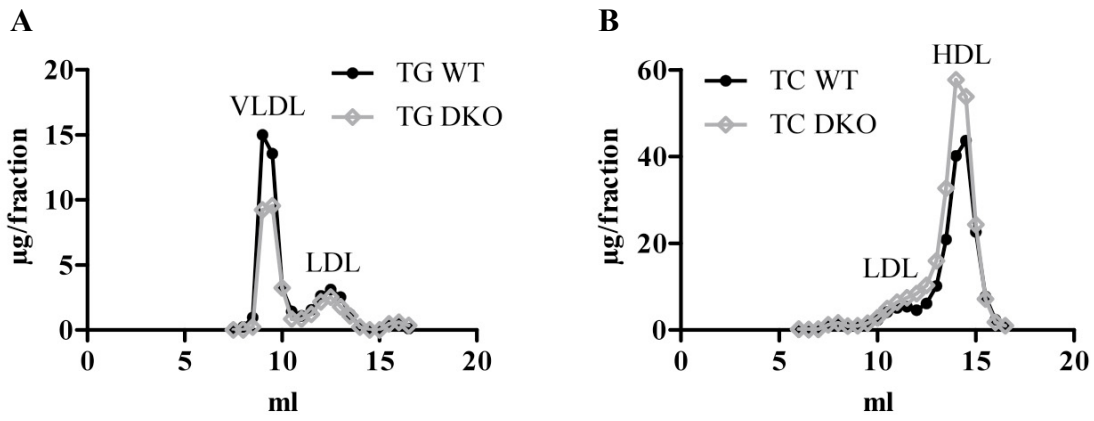

Figure 75: Lipoprotein profile of DKO and control mice. Plasma pools from 4 ON fasted DKO males and 4 controls aged 10 weeks were separated using a Pharmacia FPLC system with a Superose 6 column. FPLC fractions were collected, and TG, TC, and FC concentrations in each fraction were measured enzymatically.

4.5.3 Hydrolase activities of MPM from DKO mice

Enzyme hydrolase activities for CE, TG and AcMAGE were determined in MPM from DKO mice as well as their littermates. Consistent with the data from HSL(-/-) mice, MPM from DKO mice had decreased levels of CE (77 %), TG (34 %) and AcMAGE (13 %) hydrolase activities, respectively (Figure 77 A-C).

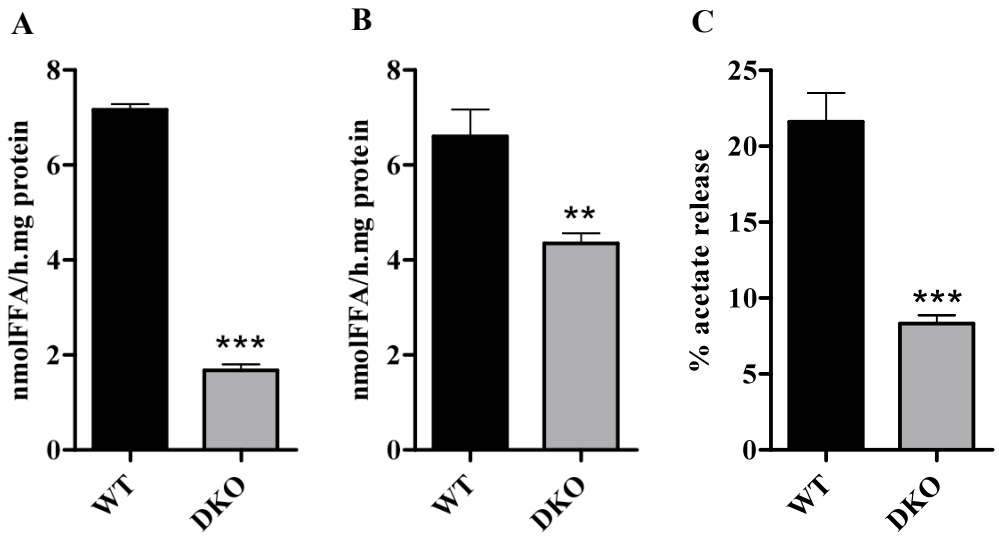

Figure 76: CE, TG and AcMAGE hydrolase activities of macrophages from DKO and WT mice. CE (A), TG (B) and AcMAGE (C) hydrolase activities were determined in whole cell lysates of DKO and WT macrophages of male mice. Data are presented as mean values of 3 mice measured in duplicates. *, $p \leq 0.05$; ***, $p \leq 0.001$.

5. Discussion

Atherosclerosis is a multifactorial disease and the primary cause of heart disease and stroke in westernized societies. Arterial macrophages are able to take up and store tremendous amounts of CE in LD, leading to foam cell formation, which is one of the earliest and causal steps in the initiation and progression of atherosclerosis. These CE stores are mobilized by neutral CE hydrolases, producing unesterified FC that is either secreted to extracellular acceptors or reesterified. Thus, the action of a neutral CE hydrolase in foam cells is very interesting with regard to prevention of foam cell formation.

In first experiments of the present thesis, MPM and foam cells were characterized by confocal laser scanning microscopy. Nile red was used to stain neutral lipids in LD and filipin was taken to label FC in the plasma membrane and lysosomes/endosomes. As expected, MPM almost lacked LD. In contrast, in foam cells the LD were clearly visible also under transmitted light. The plasma membrane was visible in macrophages, as well as more FC and CE were observed in foam cells, probably due to the higher metabolic activity in these cells. The enzymatical determination of the lipid content of MPM and foam cells from male and female C57BL/6 mice confirmed the results from confocal laser scanning microscopy. Foam cells exhibited not only more FC, but also CE, because an excess of FC is toxic for the cells and therefore FC is esterified by ACAT-1. The TG level was also elevated by 40 % in male and 35 % in female foam cells compared to macrophages, which can not be explained by the low TG content of acLDL taken up by these cells. Thus, there must have been active *de novo* biosynthesis of TG taken place. Foam cells from male and female C57BL/6 mice did not show sex-specific differences in their lipid contents.

HSL is very well known to play an important enzymatic role in many murine tissues (88, 136) and is therefore ubiquitously expressed. KIAA1363 is supposed to be an AcMAGE hydrolase in brain, cardiac muscle and kidney (125) and was postulated as a neutral CE hydrolase (124) in MPM and foam cells. In order to verify these findings, I analyzed the male and female murine tissue pattern of these two enzymes on the mRNA level with real time PCR. The highest mRNA expression of HSL was found in WAT and BAT, as expected, because in these tissues it plays an important role as DG hydrolase (105). HSL is also expressed in cardiac muscle (111) and at lower levels in skeletal muscle (137), where it mobilizes TG. HSL is also expressed in testis and adrenals, where it contributes to the CE hydrolase activity (101, 102).

Although HSL is expressed in liver to a minor extent, it was suggested to play a role in the hepatic cholesterol metabolism (108). The HSL mRNA expression in kidney is nearly the same as in liver. The only sex-specific difference was found in brain with a 3-fold higher expression of HSL in females compared to males. The role of HSL in brain is not understood yet. Interestingly mouse brain does not exhibit CE, but ACAT-1 is expressed (138). The cholesterol metabolism in kidney is very important particularly in kidney injury, but nothing about the involved enzymes, especially HSL, is known yet (139). KIAA1363 mRNA is expressed in brain, CM and kidney, where it is supposed to be an AcMAGE hydrolase (125). Almost no mRNA expression was observed in liver, testis, adrenals, WAT, BAT and SM of both sexes.

In MPM and foam cells HSL is expressed at the same level. Numerous conflicting papers have been published about the role of HSL in MPM and foam cells (88, 95, 96, 98, 102, 140, 141). KIAA1363 mRNA expression is very high in MPM and foam cells, where it was recently published as key neutral CE hydrolase, removing cholesterol from these cells (124). HSL and KIAA1363 mRNAs are similarly expressed in MPM and foam cells of male and female mice.

HSL is a serine hydrolase, which was reported to possess lipolytic activities against p-nitrophenyl esters (78), MG, DG, TG, CE (79), RE (80), and steroid esters (81). KIAA1363 was suggested to have CE and TG (124) as well as AcMAGE hydrolase activities (125). After overexpression of the two proteins in COS-7 cells I intended to confirm the already published *in vitro* lipolytic activities of the two enzymes. HSL and KIAA1363 were both able to cleave *p*-nitrophenylvalerate, a very hydrophobic substrate. This was an important evidence for the functional enzyme activity of my recombinant proteins. Furthermore, overexpression of HSL resulted in highly increased CE, TG, DG, and RE hydrolase activities which confirmed published data (79). Very surprisingly, recombinant KIAA1363 was not able to hydrolize CE, TG and DG, but it cleaved RE. These results were also corroborated by the binding of specific fluorescent activity recognition probes (130). To exclude methodological discrepancies the CE hydrolase activity assays were repeated with alternative mixed micelles, including those used by Okazaki et al. (142). Phospholipid-stabilized emulsions are used in lipid hydrolase activity assays to most effectively release [^{3}H]-oleic acid of the respective [^{3}H]-labeled lipid substrates (135, 142). Overexpression of HSL resulted in highly increased neutral CE hydrolase activity under all conditions, whereas no CE hydrolase activity was detected in

lysates of KIAA1363- overexpressing cells. The reason for this apparent discrepancy concerning the CE hydrolase activity of KIAA1363 is unclear and remains unexplained. Overexpression of HSL and KIAA1363 caused an increase in AcMAGE hydrolase activity, which has already been published for KIAA1363 in other cells and tissues (120, 121). From the *in vitro* data I suggest that KIAA1363 is an AcMAGE hydrolase but does not hydrolize CE.

To investigate the physiological consequences of HSL and KIAA1363 deficiency *in vivo*, I used HSL(-/-) (103, 105) and KIAA1363(-/-) mice (122, 125). First of all, I was interested if HSL or KIAA1363 mRNA levels can compensate for the lack of the other gene. Notably, HSL mRNA levels were not altered in KIAA1363(-/-) MPM and foam cells, as well as no difference was found in the gene expression of KIAA1363 in HSL(-/-) mice. I conclude that HSL and KIAA1363 gene expression do not compensate for the lack of the other protein. Moreover, the plasma lipid parameters and the lipoprotein profile of the different genotypes in comparison to their littermates were determined. HSL(-/-) male and female mice revealed decreased TG and FFA levels in the fasted state and elevated CE levels in both the fasted and fed state. These results confirm already published data (103). Due to the impaired DG and TG metabolism of HSL(-/-) mice, plasma levels of FFA were found to be reduced resulting in marked changes in the plasma lipoprotein pattern. The TG content in the VLDL-TG fraction of fasted plasma was reduced, whereas HDL-cholesterol was increased in these mice compared to controls. Studies by Haemmerle et al. (103) have already shown that reduced FFA levels in plasma resulted in decreased cytoplasmic fat stores and VLDL synthesis. In fasted HSL(-/-) animals LPL activities in muscle and WAT was increased, which consequently leads to lower plasma TG levels and may be responsible for elevated HDL-cholesterol (143). No alterations in lipid parameters were observed in KIAA1363(-/-) male and female mice, indicating that KIAA1363 is not an important CE hydrolase *in vivo*.

Next, CE and AcMAGE hydrolase activities in tissues of HSL(-/-) and KIAA1363(-/-) mice were determined. WAT, BAT (102), SM, CM, liver (108), kidney, testis (102, 144), and the brain of HSL(-/-) mice almost totally lacked neutral CE hydrolase activity indicating that HSL is present and active as CE hydrolase in the respective tissues. CE accumulation, however, was only observed in BAT, kidney, and in testis. CE accumulation in testis was already shown in a previous study (102). In the liver, CE concentrations were slightly increased, which is consistent with recently published data showing significant CE accumulation in

HSL(-/-) liver in the fasted but not in the fed state (108). No CE accumulation was observed in WAT, SM, CM, and brain of HSL(-/-) mice. Thus, HSL deficiency in tissues had two distinct effects: in some tissues CE concentrations were increased, in some tissues CE content was unchanged although CE hydrolase activity was almost abolished. These results provide evidence for the presence of alternative CE hydrolase(s) which are not active under conditions optimized for HSL. Unlike HSL, the disruption of KIAA1363 did not affect CE hydrolase activity in any tissue investigated.

In HSL(-/-) MPM and foam cells, neutral CE hydrolase activity was almost abolished. This finding contradicts the study in HSL(-/-) mice by Osuga et al. who showed unchanged neutral CE hydrolysis in HSL(-/-) macrophages (102). Although I repeated CE hydrolase activity assays with substrate micelles described by Osuga et al (102) and Holm and Osterlung (135), the difference in CE hydrolase activity between HSL(-/-) macrophages and control cells remained highly significant. Under all investigated assay conditions KIAA1363(-/-) MPM showed the same CE hydrolase activity as WT MPM. I conclude that KIAA1363 is unlikely to play a major role in cholesterol mobilization in murine tissues, MPM and foam cells.

Although overexpression of HSL resulted in an increase of AcMAGE hydrolase activity, absence of HSL did not alter AcMAGE hydrolase activity in murine cells and tissues. This suggests that HSL normally does not contribute to AcMAGE hydrolysis in mice *in vivo*. In contrast, absence of KIAA1363 in macrophages resulted in significantly decreased AcMAGE hydrolase activity in whole cell lysates, which was due to drastically reduced activity in the membrane fraction. This finding is consistent with previous studies showing that KIAA1363 is an integral membrane protein (120, 121) and provides evidence that KIAA1363 is a major AcMAGE hydrolase in MPM. A reduction in AcMAGE hydrolase activity was also found in KIAA1363(-/-) testis and, in accordance with published data (125), in brain and kidney, but not in the liver of KIAA1363(-/-) mice. In the liver, the KIAA1363 homologue arylacetamide deacetylase may be responsible for AcMAGE hydrolase activity. KIAA1363 might limit PAF levels by diverting AcMAGE to MAGE also in macrophages. There are multiple mechanisms for controlling PAF levels from both biosynthesis (KIAA1363 and other AcMAGE hydrolases) and degradation (PAF acetylhydrolase) pathways. Inhibition of both AcMAGE hydrolases and PAF acetylhydrolase promotes the conversion of AcMAGE to PAF (125). Thus, the contribution of KIAA1363 regulating steady-state levels of ether lipid metabolites may be not only relevant in cancer cells (14), but also in macrophages.

In adipose tissue, HSL(-/-) mice were shown to exhibit a decreased capacity to mobilize FA from DG and TG pools (8,16,17). The present study demonstrates that also HSL(-/-) macrophages have significantly reduced DG and TG hydrolase activities, but intracellular DG and TG concentrations were unaffected. In tissues, it has already been published by Sekiya et al. (108) that the TG hydrolase activity was unchanged comparing livers from HSL(-/-) and WT mice. Grober et al. (110) reported that HSL is responsible for a part of the DG hydrolase activity in murine jejunum and ileum. These data indicate that other TG and DG hydrolase(s) exist to compensate for the lack of HSL in macrophages. As expected KIAA1363(-/-) MPM showed unaltered DG and TG hydrolase activities as well as DG and TG contents.

Although recombinant KIAA1363 exhibits RE hydrolase activity, no effect in the RE hydrolase activity in tissues of KIAA1363(-/-) mice was found. The RE hydrolase activity in MPM in general was very low, but even lower in MPM from KIAA1363(-/-) compared to WT mice. Due to the substantial weak RE hydrolase activity in MPM it is unlikely that KIAA1363 plays a role as RE hydrolase in macrophages. To confirm this assumption, further investigations will have to be done. Regarding HSL, it was recently published by Strom et al (107) that WAT and BAT from HSL(-/-) mice exhibited only negligible RE hydrolase activities compared to tissues from WT mice.

To test whether HSL(-/-) macrophages exhibit alterations in their capacity to mobilize stored CE I measured cholesterol efflux and the intracellular accumulation of acLDL-derived CE. When HSL activity was induced by dibutyryl-cAMP, cholesterol efflux from WT macrophages to the extracellular acceptors HDL_3 and apo-A1 was increased. Without dibutyryl-cAMP in the medium, no differences in the efflux of cholesterol were observed between HSL(-/-) MPM and cells from WT mice. Cyclic AMP activates cAMP-dependent kinase and subsequently leads to phosphorylation and activation of HSL (95, 140, 145). These results indicate that the increased cholesterol efflux by dibutyryl-cAMP in WT macrophages was dependent on the cAMP-mediated induction of HSL. Despite defective cholesterol efflux, the absence of HSL did not affect macrophage LD formation and CE or FC concentrations in both unloaded and acLDL-loaded MPM. The cholesterol efflux from KIAA1363(-/-) MPM and WT MPM was the same, indicating that KIAA1363 plays no role in cholesterol mobilization in MPM.

Next, I checked the FFA, cholesterol and VLDL uptake behaviour of HSL(-/-) MPM. Loading of MPM for 24 h with a [^{3}H]oleic acid/BSA complex resulted in unchanged total uptake of FFA as well as FFA uptake in the different lipid fractions compared to WT MPM. Moreover, the uptake of VLDL was the same in HSL(-/-) and WT MPM. Likewise, similar FC and CE contents were observed when cells were loaded with cholesterol for different time points. Therefore, regardless of the source of cholesterol including acLDL, aggLDL or the CE rich ß-VLDL, the uptake behaviour of HSL(-/-) and WT MPM was the same. The only differences in cholesterol uptake between HSL(-/-) and WT MPM were observed when cells were equilibrated with dibutyryl-cAMP over night; due to the action of stimulated HSL, WT MPM exhibited less CE compared to HSL(-/-) MPM. KIAA1363(-/-) MPM showed the same uptake behaviour as WT MPM. To complete the uptake experiments LPL activity in MPM of all genotypes was measured. Between the knockout mice and their littermates no differences were observed, which confirms the before mentioned results. Interestingly, in WT littermates from HSL(-/-) mice LPL activity was doubled in comparison to WT MPM from the KIAA1363 strain. These differences remain unclarified so far.

Another possibility, why HSL(-/-) MPM exhibited no CE accumulation, was that LAL, located in the lysosomes, might compensate for the lack of the neutral CE hydrolase activity. Thus, I measured the TG and CE hydrolase activities under acid pH conditions. The CE hydrolase activity was the same in all fractions of HSL(-/-) and WT MPM, but the TG hydrolase activity was significantly elevated in HSL(-/-) MPM. This was surprising, since HSL is not the major neutral TG hydrolase in MPM. The acid hydrolase activities were unchanged between KIAA1363(-/-)- and WT macrophages.

Fortunately I obtained an HSL antibody, which is able to block the enzyme activities of HSL (129). Western blot analysis resulted in one specific band at 84 kDa. Assays for TG and CE hydrolase activities were performed with addition of different concentrations of HSL antibody. Fourteen µg/100µg cell protein of HSL antibody were able to block the enzyme activities (against CE and TG) of WT MPM to the same level as HSL(-/-) MPM, leading to the conclusion that this antibody binds in or next to the active site of HSL. AcMAGE hydrolase activity was unaffected by this antibody, confirming that HSL is not an AcMAGE hydrolase in MPM *in vivo*. Importantly, I took this antibody for localization studies in MPM using fluorescence microscopy and transmission electron microscopy (TEM). Both microscopy methods confirmed the specificity of this antibody, since no signals were

detectable in HSL(-/-) MPM. Fluorescence microscopy clearly showed that HSL is located in the cytosol, but not on the LD, suggesting that HSL has to be activated by cAMP to be translocated to the LD. I suggest that HSL is located on LD of macrophage-derived foam cells after phosphorylation as described in WAT (146). The TEM pictures confirmed the results of HSL location in the cytosol and next to the LD.

Since I found KIAA1363 to be an important AcMAGE hydrolase in MPM, I was interested, whether KIAA1363 activity is altered during inflammation. It is already known that attachment of the endotoxin LPS to macrophages leads to liberation of many proinflammatory mediators such as PAF (147). Therefore, WT MPM were loaded with different concentrations of LPS which resulted in concentration dependent downregulation of KIAA1363 mRNA expression. Protein expression was unaffected after 6 h, but downregulated after 24 h, 48 h and 72 h of incubation with LPS. Moreover, the AcMAGE hydrolase activity was significantly reduced after incubation of MPM with 10 ng and 100 ng LPS. From these results I conclude that KIAA1363 enzyme activity is reduced because more AcMAGE is needed for the conversion to PAF during LPS stimulation and is therefore regulated through inflammation processes.

When I started my thesis I thought that both enzymes, HSL and KIAA1363, are CE hydrolases. Thus, I bred HSL(-/-) with KIAA1363(-/-) mice to KIAA1363(-/-)/HSL(-/-) (DKO) mice. This was difficult since HSL(-/-) males are not fertile (102). The lipid parameters as well as the lipoprotein profile of these animals were very similar to HSL(-/-) mice, which might be explained by the fact that KIAA1363(-/-) mice showed unchanged lipid parameters and lipoprotein profiles compared to their littermates. Thus, the DKO mice showed increased TC levels independently of the dietary status and reduced TG and FFA levels in the fasted state. TG in the VLDL fraction were reduced and HDL-cholesterol was elevated in the DKO animals, similar as in HSL(-/-) mice (103). Macrophages of these mice revealed the same decreased enzyme activities (CE, TG and AcMAGE) as HSL(-/-) mice. From these data I conclude that the phenotype of the DKO animals resembles the one of HSL(-/-) mice, at least in whole body and macrophage lipid metabolism.

Taken together, the present study clearly demonstrates that KIAA1363 serves as the principal AcMAGE hydrolase in various tissues and MPM, but does not contribute to neutral CE hydrolase activity. HSL is a potent CE hydrolase in various tissues and macrophages under

the assay conditions used. Absence of HSL-dependent neutral CE hydrolase activity caused CE accumulation in some tissues but did not alter CE content in MPM, WAT, muscle tissues, liver, and brain. I hypothesize that *in vivo* HSL interacts with other, presently unknown lipases in the maintenance of cholesterol homeostasis in macrophages.

Bibliography

1. Berger A. Atherosclerosis. http://wwwnlmnihgov/MEDLINEPLUS/ency/article/000171htm. 2008.
2. Glass CK, Witztum JL. Atherosclerosis. the road ahead. Cell. 2001;104:503-16.
3. Austria S. Todesursachenstatistik Austria. http://wwwstatistikat/web_de/statistiken/bevoelkerung/sterbefaelle/indexhtml. 2006.
4. Blankenhorn DH, Hodis HN. Atherosclerosis--reversal with therapy. West J Med. 1993;159:172-9.
5. Navab M, Berliner JA, Watson AD, Hama SY, Territo MC, Lusis AJ, Shih DM, Van Lenten BJ, Frank JS, Demer LL, Edwards PA, Fogelman AM. The Yin and Yang of oxidation in the development of the fatty streak. A review based on the 1994 George Lyman Duff Memorial Lecture. Arterioscler Thromb Vasc Biol. 1996;16:831-42.
6. Heinecke JW. Oxidants and antioxidants in the pathogenesis of atherosclerosis: implications for the oxidized low density lipoprotein hypothesis. Atherosclerosis. 1998;141:1-15.
7. Cyrus T, Witztum JL, Rader DJ, Tangirala R, Fazio S, Linton MF, Funk CD. Disruption of the 12/15-lipoxygenase gene diminishes atherosclerosis in apo E-deficient mice. J Clin Invest. 1999;103:1597-604.
8. Cybulsky MI, Gimbrone MA, Jr. Endothelial expression of a mononuclear leukocyte adhesion molecule during atherogenesis. Science. 1991;251:788-91.
9. Collins RG, Velji R, Guevara NV, Hicks MJ, Chan L, Beaudet AL. P-Selectin or intercellular adhesion molecule (ICAM)-1 deficiency substantially protects against atherosclerosis in apolipoprotein E-deficient mice. J Exp Med. 2000;191:189-94.
10. Dong ZM, Chapman SM, Brown AA, Frenette PS, Hynes RO, Wagner DD. The combined role of P- and E-selectins in atherosclerosis. J Clin Invest. 1998;102:145-52.
11. Steinberg D, Parthasarathy S, Carew TE, Khoo JC, Witztum JL. Beyond cholesterol. Modifications of low-density lipoprotein that increase its atherogenicity. N Engl J Med. 1989;320:915-24.
12. Han KH, Han KO, Green SR, Quehenberger O. Expression of the monocyte chemoattractant protein-1 receptor CCR2 is increased in hypercholesterolemia. Differential effects of plasma lipoproteins on monocyte function. J Lipid Res. 1999;40:1053-63.
13. Aviram M. Modified forms of low density lipoprotein and atherosclerosis. Atherosclerosis. 1993;98:1-9.
14. Brown MS, Goldstein JL. Lipoprotein metabolism in the macrophage: implications for cholesterol deposition in atherosclerosis. Annu Rev Biochem. 1983;52:223-61.
15. Acton SL, Scherer PE, Lodish HF, Krieger M. Expression cloning of SR-BI, a CD36-related class B scavenger receptor. J Biol Chem. 1994;269:21003-9.
16. Yamada Y, Doi T, Hamakubo T, Kodama T. Scavenger receptor family proteins: roles for atherosclerosis, host defence and disorders of the central nervous system. Cell Mol Life Sci. 1998;54:628-40.
17. Ross R. Atherosclerosis--an inflammatory disease. N Engl J Med. 1999;340:115-26.
18. Hansson GK. Cell-mediated immunity in atherosclerosis. Curr Opin Lipidol. 1997;8:301-11.
19. Gupta S, Pablo AM, Jiang X, Wang N, Tall AR, Schindler C. IFN-gamma potentiates atherosclerosis in ApoE knock-out mice. J Clin Invest. 1997;99:2752-61.
20. Bloch K. Summing up. Annu Rev Biochem. 1987;56:1-19.
21. Brown MS, Goldstein JL. A receptor-mediated pathway for cholesterol homeostasis. Science. 1986;232:34-47.
22. Danielsson H, Gustafsson B. On serum-cholesterol levels and neutral fecal sterols in germ-free rats; bile acids and steroids 59. Arch Biochem Biophys. 1959;83:482-5.

23. Brown DA, London E. Structure and origin of ordered lipid domains in biological membranes. J Membr Biol. 1998;164:103-14.
24. Maxfield FR, Tabas I. Role of cholesterol and lipid organization in disease. Nature. 2005;438:612-21.
25. Bradford RH, Shear CL, Chremos AN, Dujovne C, Downton M, Franklin FA, Gould AL, Hesney M, Higgins J, Hurley DP, et al. Expanded Clinical Evaluation of Lovastatin (EXCEL) study results. I. Efficacy in modifying plasma lipoproteins and adverse event profile in 8245 patients with moderate hypercholesterolemia. Arch Intern Med. 1991;151:43-9.
26. Shepherd J, Cobbe SM, Ford I, Isles CG, Lorimer AR, MacFarlane PW, McKillop JH, Packard CJ. Prevention of coronary heart disease with pravastatin in men with hypercholesterolemia. West of Scotland Coronary Prevention Study Group. N Engl J Med. 1995;333:1301-7.
27. King W. The medical biochemistry page. http://themedicalbiochemistrypageorg/homehtml. 2009.
28. Brown MS, Goldstein JL. Multivalent feedback regulation of HMG CoA reductase, a control mechanism coordinating isoprenoid synthesis and cell growth. J Lipid Res. 1980;21:505-17.
29. Luskey KL, Faust JR, Chin DJ, Brown MS, Goldstein JL. Amplification of the gene for 3-hydroxy-3-methylglutaryl coenzyme A reductase, but not for the 53-kDa protein, in UT-1 cells. J Biol Chem. 1983;258:8462-9.
30. Osborne TF, Gil G, Goldstein JL, Brown MS. Operator constitutive mutation of 3-hydroxy-3-methylglutaryl coenzyme A reductase promoter abolishes protein binding to sterol regulatory element. J Biol Chem. 1988;263:3380-7.
31. Osborne TF, Goldstein JL, Brown MS. 5' end of HMG CoA reductase gene contains sequences responsible for cholesterol-mediated inhibition of transcription. Cell. 1985;42:203-12.
32. Chang TY, Limanek JS, Chang CC. Evidence indicating that inactivation of 3-hydroxy-3-methylglutaryl coenzyme A reductase by low density lipoprotein or by 25-hydroxycholesterol requires mediator protein(s) with rapid turnover rate. J Biol Chem. 1981;256:6174-80.
33. Edwards PA, Lan SF, Tanaka RD, Fogelman AM. Mevalonolactone inhibits the rate of synthesis and enhances the rate of degradation of 3-hydroxy-3-methylglutaryl coenzyme A reductase in rat hepatocytes. J Biol Chem. 1983;258:7272-5.
34. Faust JR, Luskey KL, Chin DJ, Goldstein JL, Brown MS. Regulation of synthesis and degradation of 3-hydroxy-3-methylglutaryl-coenzyme A reductase by low density lipoprotein and 25-hydroxycholesterol in UT-1 cells. Proc Natl Acad Sci U S A. 1982;79:5205-9.
35. Gil G, Faust JR, Chin DJ, Goldstein JL, Brown MS. Membrane-bound domain of HMG CoA reductase is required for sterol-enhanced degradation of the enzyme. Cell. 1985;41:249-58.
36. Liscum L, Finer-Moore J, Stroud RM, Luskey KL, Brown MS, Goldstein JL. Domain structure of 3-hydroxy-3-methylglutaryl coenzyme A reductase, a glycoprotein of the endoplasmic reticulum. J Biol Chem. 1985;260:522-30.
37. Lakshmanan MR, Nepokroeff CM, Ness GC, Dugan RE, Porter JW. Stimulation by insulin of rat liver -hydroxy- -methylglutaryl coenzyme A reductase and cholesterol-synthesizing activities. Biochem Biophys Res Commun. 1973;50:704-10.
38. Simonet WS, Ness GC. Post-transcriptional regulation of 3-hydroxy-3-methylglutaryl-CoA reductase mRNA in rat liver. Glucocorticoids block the stabilization caused by thyroid hormones. J Biol Chem. 1989;264:569-73.
39. Hua X, Yokoyama C, Wu J, Briggs MR, Brown MS, Goldstein JL, Wang X. SREBP-2, a second basic-helix-loop-helix-leucine zipper protein that stimulates transcription by binding to a sterol regulatory element. Proc Natl Acad Sci U S A. 1993;90:11603-7.

40. Yokoyama C, Wang X, Briggs MR, Admon A, Wu J, Hua X, Goldstein JL, Brown MS. SREBP-1, a basic-helix-loop-helix-leucine zipper protein that controls transcription of the low density lipoprotein receptor gene. Cell. 1993;75:187-97.
41. Duncan EA, Brown MS, Goldstein JL, Sakai J. Cleavage site for sterol-regulated protease localized to a leu-Ser bond in the lumenal loop of sterol regulatory element-binding protein-2. J Biol Chem. 1997;272:12778-85.
42. Hua X, Sakai J, Ho YK, Goldstein JL, Brown MS. Hairpin orientation of sterol regulatory element-binding protein-2 in cell membranes as determined by protease protection. J Biol Chem. 1995;270:29422-7.
43. Sakai J, Nohturfft A, Cheng D, Ho YK, Brown MS, Goldstein JL. Identification of complexes between the COOH-terminal domains of sterol regulatory element-binding proteins (SREBPs) and SREBP cleavage-activating protein. J Biol Chem. 1997;272:20213-21.
44. Yang T, Espenshade PJ, Wright ME, Yabe D, Gong Y, Aebersold R, Goldstein JL, Brown MS. Crucial step in cholesterol homeostasis: sterols promote binding of SCAP to INSIG-1, a membrane protein that facilitates retention of SREBPs in ER. Cell. 2002;110:489-500.
45. Ravid T, Doolman R, Avner R, Harats D, Roitelman J. The ubiquitin-proteasome pathway mediates the regulated degradation of mammalian 3-hydroxy-3-methylglutaryl-coenzyme A reductase. J Biol Chem. 2000;275:35840-7.
46. Nohturfft A, Brown MS, Goldstein JL. Topology of SREBP cleavage-activating protein, a polytopic membrane protein with a sterol-sensing domain. J Biol Chem. 1998;273:17243-50.
47. Hua X, Sakai J, Brown MS, Goldstein JL. Regulated cleavage of sterol regulatory element binding proteins requires sequences on both sides of the endoplasmic reticulum membrane. J Biol Chem. 1996;271:10379-84.
48. Sakai J, Duncan EA, Rawson RB, Hua X, Brown MS, Goldstein JL. Sterol-regulated release of SREBP-2 from cell membranes requires two sequential cleavages, one within a transmembrane segment. Cell. 1996;85:1037-46.
49. Wang X, Sato R, Brown MS, Hua X, Goldstein JL. SREBP-1, a membrane-bound transcription factor released by sterol-regulated proteolysis. Cell. 1994;77:53-62.
50. Espenshade PJ, Cheng D, Goldstein JL, Brown MS. Autocatalytic processing of site-1 protease removes propeptide and permits cleavage of sterol regulatory element-binding proteins. J Biol Chem. 1999;274:22795-804.
51. Rawson RB, Zelenski NG, Nijhawan D, Ye J, Sakai J, Hasan MT, Chang TY, Brown MS, Goldstein JL. Complementation cloning of S2P, a gene encoding a putative metalloprotease required for intramembrane cleavage of SREBPs. Mol Cell. 1997;1:47-57.
52. Brown MS, Goldstein JL. The SREBP pathway: regulation of cholesterol metabolism by proteolysis of a membrane-bound transcription factor. Cell. 1997;89:331-40.
53. Hwang D, Rhee SH. Receptor-mediated signaling pathways: potential targets of modulation by dietary fatty acids. Am J Clin Nutr. 1999;70:545-56.
54. Sessler AM, Ntambi JM. Polyunsaturated fatty acid regulation of gene expression. J Nutr. 1998;128:923-6.
55. Smith S. The animal fatty acid synthase: one gene, one polypeptide, seven enzymes. FASEB J. 1994;8:1248-59.
56. Yen CL, Farese RV, Jr. Fat breakdown: a function for CGI-58 (ABHD5) provides a new piece of the puzzle. Cell Metab. 2006;3:305-7.
57. Lass A, Zimmermann R, Haemmerle G, Riederer M, Schoiswohl G, Schweiger M, Kienesberger P, Strauss JG, Gorkiewicz G, Zechner R. Adipose triglyceride lipase-mediated lipolysis of cellular fat stores is activated by CGI-58 and defective in Chanarin-Dorfman Syndrome. Cell Metab. 2006;3:309-19.

58. O`Day. Receptor-Mediated Endocytosis: Cholesterol Uptake and Cholesterolemia. http://wwwerinutorontoca/~w3bio315/lecture18htm. 2009.
59. Rader DJ, Daugherty A. Translating molecular discoveries into new therapies for atherosclerosis. Nature. 2008;451:904-13.
60. Brown MS, Goldstein JL. Familial hypercholesterolemia: defective binding of lipoproteins to cultured fibroblasts associated with impaired regulation of 3-hydroxy-3-methylglutaryl coenzyme A reductase activity. Proc Natl Acad Sci U S A. 1974;71:788-92.
61. Goldstein JL, Brown MS. Binding and degradation of low density lipoproteins by cultured human fibroblasts. Comparison of cells from a normal subject and from a patient with homozygous familial hypercholesterolemia. J Biol Chem. 1974;249:5153-62.
62. Rothblat GH, Mahlberg FH, Johnson WJ, Phillips MC. Apolipoproteins, membrane cholesterol domains, and the regulation of cholesterol efflux. J Lipid Res. 1992;33:1091-7.
63. Chang TY, Chang CC, Cheng D. Acyl-coenzyme A:cholesterol acyltransferase. Annu Rev Biochem. 1997;66:613-38.
64. Bjorkhem I, Andersson O, Diczfalusy U, Sevastik B, Xiu RJ, Duan C, Lund E. Atherosclerosis and sterol 27-hydroxylase: evidence for a role of this enzyme in elimination of cholesterol from human macrophages. Proc Natl Acad Sci U S A. 1994;91:8592-6.
65. Warner GJ, Stoudt G, Bamberger M, Johnson WJ, Rothblat GH. Cell toxicity induced by inhibition of acyl coenzyme A:cholesterol acyltransferase and accumulation of unesterified cholesterol. J Biol Chem. 1995;270:5772-8.
66. Blaner WS. STRA6, a cell-surface receptor for retinol-binding protein: the plot thickens. Cell Metab. 2007;5:164-6.
67. Harrison EH. Mechanisms of digestion and absorption of dietary vitamin A. Annu Rev Nutr. 2005;25:87-103.
68. Herr FM, Ong DE. Differential interaction of lecithin-retinol acyltransferase with cellular retinol binding proteins. Biochemistry. 1992;31:6748-55.
69. Blomhoff R, Helgerud P, Rasmussen M, Berg T, Norum KR. In vivo uptake of chylomicron [3H]retinyl ester by rat liver: evidence for retinol transfer from parenchymal to nonparenchymal cells. Proc Natl Acad Sci U S A. 1982;79:7326-30.
70. Blomhoff R, Blomhoff HK. Overview of retinoid metabolism and function. J Neurobiol. 2006;66:606-30.
71. Senoo H. Structure and function of hepatic stellate cells. Med Electron Microsc. 2004;37:3-15.
72. Blaner WS, Obunike JC, Kurlandsky SB, al-Haideri M, Piantedosi R, Deckelbaum RJ, Goldberg IJ. Lipoprotein lipase hydrolysis of retinyl ester. Possible implications for retinoid uptake by cells. J Biol Chem. 1994;269:16559-65.
73. Hagen E, Myhre AM, Tjelle TE, Berg T, Norum KR. Retinyl esters are hydrolyzed in early endosomes of J774 macrophages. J Lipid Res. 1999;40:309-17.
74. Bastien J, Rochette-Egly C. Nuclear retinoid receptors and the transcription of retinoid-target genes. Gene. 2004;328:1-16.
75. Kielian T, Drew PD. Effects of peroxisome proliferator-activated receptor-gamma agonists on central nervous system inflammation. J Neurosci Res. 2003;71:315-25.
76. Moraes LA, Piqueras L, Bishop-Bailey D. Peroxisome proliferator-activated receptors and inflammation. Pharmacol Ther. 2006;110:371-85.
77. Schug TT, Berry DC, Shaw NS, Travis SN, Noy N. Opposing effects of retinoic acid on cell growth result from alternate activation of two different nuclear receptors. Cell. 2007;129:723-33.
78. Osterlund T, Danielsson B, Degerman E, Contreras JA, Edgren G, Davis RC, Schotz MC, Holm C. Domain-structure analysis of recombinant rat hormone-sensitive lipase. Biochem J. 1996;319 (Pt 2):411-20.

79. Fredrikson G, Stralfors P, Nilsson NO, Belfrage P. Hormone-sensitive lipase of rat adipose tissue. Purification and some properties. J Biol Chem. 1981;256:6311-20.
80. Wei S, Lai K, Patel S, Piantedosi R, Shen H, Colantuoni V, Kraemer FB, Blaner WS. Retinyl ester hydrolysis and retinol efflux from BFC-1beta adipocytes. J Biol Chem. 1997;272:14159-65.
81. Lee FT, Adams JB, Garton AJ, Yeaman SJ. Hormone-sensitive lipase is involved in the hydrolysis of lipoidal derivatives of estrogens and other steroid hormones. Biochim Biophys Acta. 1988;963:258-64.
82. Contreras JA, Karlsson M, Osterlund T, Laurell H, Svensson A, Holm C. Hormone-sensitive lipase is structurally related to acetylcholinesterase, bile salt-stimulated lipase, and several fungal lipases. Building of a three-dimensional model for the catalytic domain of hormone-sensitive lipase. J Biol Chem. 1996;271:31426-30.
83. Holm C. Molecular mechanisms regulating hormone-sensitive lipase and lipolysis. Biochem Soc Trans. 2003;31:1120-4.
84. Holm C, Kirchgessner TG, Svenson KL, Fredrikson G, Nilsson S, Miller CG, Shively JE, Heinzmann C, Sparkes RS, Mohandas T, et al. Hormone-sensitive lipase: sequence, expression, and chromosomal localization to 19 cent-q13.3. Science. 1988;241:1503-6.
85. Holst LS, Langin D, Mulder H, Laurell H, Grober J, Bergh A, Mohrenweiser HW, Edgren G, Holm C. Molecular cloning, genomic organization, and expression of a testicular isoform of hormone-sensitive lipase. Genomics. 1996;35:441-7.
86. Mulder H, Holst LS, Svensson H, Degerman E, Sundler F, Ahren B, Rorsman P, Holm C. Hormone-sensitive lipase, the rate-limiting enzyme in triglyceride hydrolysis, is expressed and active in beta-cells. Diabetes. 1999;48:228-32.
87. Shen WJ, Sridhar K, Bernlohr DA, Kraemer FB. Interaction of rat hormone-sensitive lipase with adipocyte lipid-binding protein. Proc Natl Acad Sci U S A. 1999;96:5528-32.
88. Kraemer FB, Shen WJ. Hormone-sensitive lipase: control of intracellular tri-(di-)acylglycerol and cholesteryl ester hydrolysis. J Lipid Res. 2002;43:1585-94.
89. Yeaman SJ. Hormone-sensitive lipase--a multipurpose enzyme in lipid metabolism. Biochim Biophys Acta. 1990;1052:128-32.
90. Egan JJ, Greenberg AS, Chang MK, Wek SA, Moos MC, Jr., Londos C. Mechanism of hormone-stimulated lipolysis in adipocytes: translocation of hormone-sensitive lipase to the lipid storage droplet. Proc Natl Acad Sci U S A. 1992;89:8537-41.
91. Shen WJ, Patel S, Miyoshi H, Greenberg AS, Kraemer FB. Functional interaction of hormone-sensitive lipase and perilipin in lipolysis. J Lipid Res. 2009.
92. Greenberg AS, Shen WJ, Muliro K, Patel S, Souza SC, Roth RA, Kraemer FB. Stimulation of lipolysis and hormone-sensitive lipase via the extracellular signal-regulated kinase pathway. J Biol Chem. 2001;276:45456-61.
93. Wood SL, Emmison N, Borthwick AC, Yeaman SJ. The protein phosphatases responsible for dephosphorylation of hormone-sensitive lipase in isolated rat adipocytes. Biochem J. 1993;295 (Pt 2):531-5.
94. Goodman DS. Cholesterol ester metabolism. Physiol Rev. 1965;45:747-839.
95. Small CA, Goodacre JA, Yeaman SJ. Hormone-sensitive lipase is responsible for the neutral cholesterol ester hydrolase activity in macrophages. FEBS Lett. 1989;247:205-8.
96. Escary JL, Choy HA, Reue K, Schotz MC. Hormone-sensitive lipase overexpression increases cholesteryl ester hydrolysis in macrophage foam cells. Arterioscler Thromb Vasc Biol. 1998;18:991-8.
97. Okazaki H, Osuga J, Tsukamoto K, Isoo N, Kitamine T, Tamura Y, Tomita S, Sekiya M, Yahagi N, Iizuka Y, Ohashi K, Harada K, Gotoda T, Shimano H, Kimura S, Nagai R, Yamada N, Ishibashi S. Elimination of cholesterol ester from macrophage foam cells by adenovirus-mediated gene transfer of hormone-sensitive lipase. J Biol Chem. 2002;277:31893-9.

98. Escary JL, Choy HA, Reue K, Wang XP, Castellani LW, Glass CK, Lusis AJ, Schotz MC. Paradoxical effect on atherosclerosis of hormone-sensitive lipase overexpression in macrophages. J Lipid Res. 1999;40:397-404.
99. Osuga J, Ishibashi S, Oka T, Yagyu H, Tozawa R, Fujimoto A, Shionoiri F, Yahagi N, Kraemer FB, Tsutsumi O, Yamada N. Targeted disruption of hormone-sensitive lipase results in male sterility and adipocyte hypertrophy, but not in obesity. Proc Natl Acad Sci U S A. 2000;97:787-92.
100. Contreras JA. Hormone-sensitive lipase is not required for cholesteryl ester hydrolysis in macrophages. Biochem Biophys Res Commun. 2002;292:900-3.
101. Kraemer FB, Shen WJ, Natu V, Patel S, Osuga J, Ishibashi S, Azhar S. Adrenal neutral cholesteryl ester hydrolase: identification, subcellular distribution, and sex differences. Endocrinology. 2002;143:801-6.
102. Osuga J, Ishibashi S, Oka T, Yagyu H, Tozawa R, Fujimoto A, Shionoiri F, Yahagi N, Kraemer FB, Tsutsumi O, Yamada N. Targeted disruption of hormone-sensitive lipase results in male sterility and adipocyte hypertrophy, but not in obesity. Proc Natl Acad Sci U S A. 2000;97:787-92.
103. Haemmerle G, Zimmermann R, Strauss JG, Kratky D, Riederer M, Knipping G, Zechner R. Hormone-sensitive lipase deficiency in mice changes the plasma lipid profile by affecting the tissue-specific expression pattern of lipoprotein lipase in adipose tissue and muscle. J Biol Chem. 2002;277:12946-52.
104. Lobo MV, Huerta L, Arenas MI, Busto R, Lasuncion MA, Martin-Hidalgo A. Hormone-sensitive lipase expression and IHC localization in the rat ovary, oviduct, and uterus. J Histochem Cytochem. 2009;57:51-60.
105. Haemmerle G, Zimmermann R, Hayn M, Theussl C, Waeg G, Wagner E, Sattler W, Magin TM, Wagner EF, Zechner R. Hormone-sensitive lipase deficiency in mice causes diglyceride accumulation in adipose tissue, muscle, and testis. J Biol Chem. 2002;277:4806-15.
106. Haemmerle G, Lass A, Zimmermann R, Gorkiewicz G, Meyer C, Rozman J, Heldmaier G, Maier R, Theussl C, Eder S, Kratky D, Wagner EF, Klingenspor M, Hoefler G, Zechner R. Defective lipolysis and altered energy metabolism in mice lacking adipose triglyceride lipase. Science. 2006;312:734-7.
107. Strom K, Gundersen TE, Hansson O, Lucas S, Fernandez C, Blomhoff R, Holm C. Hormone-sensitive lipase (HSL) is also a retinyl ester hydrolase: evidence from mice lacking HSL. FASEB J. 2009.
108. Sekiya M, Osuga J, Yahagi N, Okazaki H, Tamura Y, Igarashi M, Takase S, Harada K, Okazaki S, Iizuka Y, Ohashi K, Yagyu H, Okazaki M, Gotoda T, Nagai R, Kadowaki T, Shimano H, Yamada N, Ishibashi S. Hormone-sensitive lipase is involved in hepatic cholesteryl ester hydrolysis. J Lipid Res. 2008;49:1829-38.
109. Fernandez C, Lindholm M, Krogh M, Lucas S, Larsson S, Osmark P, Berger K, Boren J, Fielding B, Frayn K, Holm C. Disturbed cholesterol homeostasis in hormone-sensitive lipase-null mice. Am J Physiol Endocrinol Metab. 2008;295:E820-31.
110. Grober J, Lucas S, Sorhede-Winzell M, Zaghini I, Mairal A, Contreras JA, Besnard P, Holm C, Langin D. Hormone-sensitive lipase is a cholesterol esterase of the intestinal mucosa. J Biol Chem. 2003;278:6510-5.
111. Kraemer FB, Patel S, Saedi MS, Sztalryd C. Detection of hormone-sensitive lipase in various tissues. I. Expression of an HSL/bacterial fusion protein and generation of anti-HSL antibodies. J Lipid Res. 1993;34:663-71.
112. Langfort J, Ploug T, Ihlemann J, Saldo M, Holm C, Galbo H. Expression of hormone-sensitive lipase and its regulation by adrenaline in skeletal muscle. Biochem J. 1999;340 (Pt 2):459-65.

113. Suzuki J, Shen WJ, Nelson BD, Patel S, Veerkamp JH, Selwood SP, Murphy GM, Jr., Reaven E, Kraemer FB. Absence of cardiac lipid accumulation in transgenic mice with heart-specific HSL overexpression. Am J Physiol Endocrinol Metab. 2001;281:E857-66.
114. Reynisdottir S, Angelin B, Langin D, Lithell H, Eriksson M, Holm C, Arner P. Adipose tissue lipoprotein lipase and hormone-sensitive lipase. Contrasting findings in familial combined hyperlipidemia and insulin resistance syndrome. Arterioscler Thromb Vasc Biol. 1997;17:2287-92.
115. Reynisdottir S, Eriksson M, Angelin B, Arner P. Impaired activation of adipocyte lipolysis in familial combined hyperlipidemia. J Clin Invest. 1995;95:2161-9.
116. Large V, Reynisdottir S, Langin D, Fredby K, Klannemark M, Holm C, Arner P. Decreased expression and function of adipocyte hormone-sensitive lipase in subcutaneous fat cells of obese subjects. J Lipid Res. 1999;40:2059-66.
117. Imbeault P, Vidal H, Tremblay A, Vega N, Nadeau A, Despres JP, Mauriege P. Age-related differences in messenger ribonucleic acid expression of key proteins involved in adipose cell differentiation and metabolism. J Clin Endocrinol Metab. 2001;86:828-33.
118. Nagase T, Kikuno R, Ishikawa KI, Hirosawa M, Ohara O. Prediction of the coding sequences of unidentified human genes. XVI. The complete sequences of 150 new cDNA clones from brain which code for large proteins in vitro. DNA Res. 2000;7:65-73.
119. Jessani N, Liu Y, Humphrey M, Cravatt BF. Enzyme activity profiles of the secreted and membrane proteome that depict cancer cell invasiveness. Proc Natl Acad Sci U S A. 2002;99:10335-40.
120. Chiang KP, Niessen S, Saghatelian A, Cravatt BF. An enzyme that regulates ether lipid signaling pathways in cancer annotated by multidimensional profiling. Chem Biol. 2006;13:1041-50.
121. Nomura DK, Leung D, Chiang KP, Quistad GB, Cravatt BF, Casida JE. A brain detoxifying enzyme for organophosphorus nerve poisons. Proc Natl Acad Sci U S A. 2005;102:6195-200.
122. Nomura DK, Durkin KA, Chiang KP, Quistad GB, Cravatt BF, Casida JE. Serine hydrolase KIAA1363: toxicological and structural features with emphasis on organophosphate interactions. Chem Res Toxicol. 2006;19:1142-50.
123. Casida JE, Nomura DK, Vose SC, Fujioka K. Organophosphate-sensitive lipases modulate brain lysophospholipids, ether lipids and endocannabinoids. Chem Biol Interact. 2008;175:355-64.
124. Okazaki H, Igarashi M, Nishi M, Sekiya M, Tajima M, Takase S, Takanashi M, Ohta K, Tamura Y, Okazaki S, Yahagi N, Ohashi K, Amemiya-Kudo M, Nakagawa Y, Nagai R, Kadowaki T, Osuga J, Ishibashi S. Identification of neutral cholesterol ester hydrolase, a key enzyme removing cholesterol from macrophages. J Biol Chem. 2008;283:33357-64.
125. Nomura DK, Fujioka K, Issa RS, Ward AM, Cravatt BF, Casida JE. Dual roles of brain serine hydrolase KIAA1363 in ether lipid metabolism and organophosphate detoxification. Toxicol Appl Pharmacol. 2008;228:42-8.
126. OpenWetWare. LacZ staining. http://openwetwareorg/wiki/LacZ_staining_of_cells.
127. Folch J, Lees M, Sloane Stanley GH. A simple method for the isolation and purification of total lipides from animal tissues. J Biol Chem. 1957;226:497-509.
128. Sattler W, Puhl H, Hayn M, Kostner GM, Esterbauer H. Determination of fatty acids in the main lipoprotein classes by capillary gas chromatography: BF3/methanol transesterification of lyophilized samples instead of Folch extraction gives higher yields. Anal Biochem. 1991;198:184-90.
129. Pfeifer T. Adenovirus mediated gene transfer and cellular localization of potential cholesteryl ester hydrolases
Graz: Medical University 2007.

130. Schmidinger H, Birner-Gruenberger R, Riesenhuber G, Saf R, Susani-Etzerodt H, Hermetter A. Novel fluorescent phosphonic acid esters for discrimination of lipases and esterases. Chembiochem. 2005;6:1776-81.
131. Birner-Gruenberger R, Susani-Etzerodt H, Waldhuber M, Riesenhuber G, Schmidinger H, Rechberger G, Kollroser M, Strauss JG, Lass A, Zimmermann R, Haemmerle G, Zechner R, Hermetter A. The lipolytic proteome of mouse adipose tissue. Mol Cell Proteomics. 2005;4:1710-7.
132. Holm C, Osterlund T. Hormone-sensitive lipase and neutral cholesteryl ester lipase. In: Doolittle MH, Reue K, editors. Lipase and phospholipase protocols. Totowa: Humana Press Inc.; 1999. p. 109-21.
133. Kratky D, Strauss JG, Zechner R. Tissue-specific activity of lipoprotein lipase in skeletal muscle regulates the expression of uncoupling protein 3 in transgenic mouse models. Biochem J. 2001;355:647-52.
134. Kolb D, Muller M, Zellnig G, Zechmann B. Cadmium induced changes in subcellular glutathione contents within glandular trichomes of Cucurbita pepo L. Protoplasma. 2009.
135. Holm C, Osterlund T. Hormone-sensitive lipase and neutral cholesteryl ester lipase. Methods Mol Biol. 1999;109:109-21.
136. Zechner R, Kienesberger PC, Haemmerle G, Zimmermann R, Lass A. Adipose triglyceride lipase and the lipolytic catabolism of cellular fat stores. J Lipid Res. 2009;50:3-21.
137. Langfort J, Ploug T, Ihlemann J, Holm C, Galbo H. Stimulation of hormone-sensitive lipase activity by contractions in rat skeletal muscle. Biochem J. 2000;351:207-14.
138. Uelmen PJ, Oka K, Sullivan M, Chang CC, Chang TY, Chan L. Tissue-specific expression and cholesterol regulation of acylcoenzyme A:cholesterol acyltransferase (ACAT) in mice. Molecular cloning of mouse ACAT cDNA, chromosomal localization, and regulation of ACAT in vivo and in vitro. J Biol Chem. 1995;270:26192-201.
139. Zager RA, Kalhorn TF. Changes in free and esterified cholesterol: hallmarks of acute renal tubular injury and acquired cytoresistance. Am J Pathol. 2000;157:1007-16.
140. Contreras JA. Hormone-sensitive lipase is not required for cholesteryl ester hydrolysis in macrophages. Biochem Biophys Res Commun. 2002;292:900-3.
141. Okazaki H, Osuga J, Tsukamoto K, Isoo N, Kitamine T, Tamura Y, Tomita S, Sekiya M, Yahagi N, Iizuka Y, Ohashi K, Harada K, Gotoda T, Shimano H, Kimura S, Nagai R, Yamada N, Ishibashi S. Elimination of cholesterol ester from macrophage foam cells by adenovirus-mediated gene transfer of hormone-sensitive lipase. J Biol Chem. 2002;277:31893-9.
142. Hajjar DP, Minick CR, Fowler S. Arterial neutral cholesteryl esterase. A hormone-sensitive enzyme distinct from lysosomal cholesteryl esterase. J Biol Chem. 1983;258:192-8.
143. Levak-Frank S, Hofmann W, Weinstock PH, Radner H, Sattler W, Breslow JL, Zechner R. Induced mutant mouse lines that express lipoprotein lipase in cardiac muscle, but not in skeletal muscle and adipose tissue, have normal plasma triglyceride and high-density lipoprotein-cholesterol levels. Proc Natl Acad Sci U S A. 1999;96:3165-70.
144. Vallet-Erdtmann V, Tavernier G, Contreras JA, Mairal A, Rieu C, Touzalin AM, Holm C, Jegou B, Langin D. The testicular form of hormone-sensitive lipase HSLtes confers rescue of male infertility in HSL-deficient mice. J Biol Chem. 2004;279:42875-80.
145. Stralfors P, Belfrage P. Phosphorylation of hormone-sensitive lipase by cyclic AMP-dependent protein kinase. J Biol Chem. 1983;258:15146-52.
146. Clifford GM, Londos C, Kraemer FB, Vernon RG, Yeaman SJ. Translocation of hormone-sensitive lipase and perilipin upon lipolytic stimulation of rat adipocytes. J Biol Chem. 2000;275:5011-5.
147. Shapiro L, Gelfand JA. Cytokines and sepsis: pathophysiology and therapy. New Horiz. 1993;1:13-22.

Abbreviations

AADA	arylacetamide deacetylase
Abc	ATP-binding cassette transporter
ACAT	acyl coenzyme A: cholesterol acyltransferase
Acc	acyl-CoA carboxylase
AH	acetylhydrolase
acLDL	acetylated low density lipoprotein
AcMAGE	acetyl monoalkylglycerol ether
aggLDL	aggregated low density lipoprotein
Apo	apolipoprotein
APS	ammonium persulfate
AT	annealing temperature
ATGL	adipose triglyceride lipase
ATP	adenosine tri-phospate
BAT	brown adipose tissue
Bp	base pairs
BSA	bovine serum albumin
cAMP	cyclic adenosine mono-phosphate
CCR2	chemokine (C-C motif) receptor 2
CD36	cluster of differentiation 36
cDNA	complementary deoxyribonucleic acid
CE	cholesteryl ester
CETP	cholesteryl ester transfer protein
CM	cardiac muscle
CPM	counts per minute
CPO	chlopyrifos oxon
Cyp7a1	cholesterol 7α-hydroxylase
Cyp27a1	cholesterol 27-hydroxylase
DEPC	diethylpyrocarbonate
DG	diacylglycerol
DMEM	Dulbecco`s modified Eagle’s medium
DMSO	dimethylsulfoxid
DNA	deoxyribonucleic acid

DTT	dithiothreitol
EDTA	ethylenediaminetetraacetic acid
ER	endoplasmic reticulum
ERK	extracellular signal-regulated kinase
EtBr	ethidium bromide
FA	fatty acid
Fabp	fatty acid binding protein
FAS	fatty acid synthase
FAT	fatty acid transporter
FC	free cholesterol
FCS	fetal bovine serum
FFA	free fatty acid
FPLC	fast protein liquid chromatography
FW	forward primer
FXR	farnesoid X receptor
GC	gas chromatography
^{3}H	tritium
H	hours
HDL	high density lipoprotein
HMG-CoA	3-hydroxy-3-methylglutaryl-CoA
HMGCR	3-hydroxy-3-methylglutaryl-CoA reductase
HMGCS	3-hydroxy-3-methylglutaryl-CoA synthase
HSL	hormone sensitive lipase
ICAM-1	inter-cellular adhesion molecule 1
IDL	intermediate density lipoprotein
IL	interleukin
INF	interferon
iNOS	inducible nitric oxide synthase
INSIG	insulin-induced gene
IPP	isopentenylpyrophospate
kDa	kilo Dalton
KO	knockout
15-LO	15-lipoxygenase
LAL	lysosomal acid lipase

LC	liquid chromatography
LD	lipid droplet
LDL	low density lipoprotein
LDLR	low density lipoprotein receptor
LPA	lysophosphatidic acid
LPDS	lipoprotein depleted serum
LPL	lipoprotein lipase
LPS	lipopolysaccharides
LRAT	lecithin retinol acyltransferase
LXR	liver X receptot
LXRE	liver X receptor element
MCP-1	monocyte chemotactic protein-1
M-CSF	macrophage colony-stimulating factor
MG	monoglycerides
MHC	major histocompatibility complex
MIN	minutes
modLDL	modified low density lipoprotein
MOPS	morpholinopropansulfonicacid
MPM	mouse peritoneal macrophages
mRNA	messenger ribonucleic acid
MS	mass spectrometry
NADPH	nicotinamide adenine dinucleotide phosphate
nCEH	neutral cholesteryl ester hydrolase
NEFA	non esterified fatty acids
ON	overnight
OP	organophosphorus
oxLDL	oxidized low density lipoprotein
PAF	platelet activating factor
PBS	phosphate buffered saline
PC	phoshatidylcholine
PCR	polymerase chain reaction
PI	phosphatidylinositol
PKA	protein kinase A
PL	phospholipids

PLTP	phospholipid transfer protein
PNPV	p-Nitrophenylvalerate
PPAR	peroxisome proliferator-activated receptors
PUFA	polyunsaturated fatty acid
RA	retinoic acids
RALD	retinaldehyde
RAR	retinoic acid receptor
RBP	retinol binding protein
RE	retinyl ester
Rev	reverse primer
RNA	ribonucleic acid
ROH	retinol
RT	room temperature
RXR	retinoid X receptor
S	seconds
SCAP	sterol response element-binding protein cleavage- activating protein
SEM	standard error of mean
SD	standard deviation
SDS	sodium dodecyl sulfate
SM	sceletal muscle
SR	scavenger receptor
SRE	sterol response element
SREBP	sterol response element-binding protein
S1P	site-1 protease
S2P	site-2 proteas
TC	total cholesterol
TEMED	tetramethylethylenediamine
TG	triglyceride
TLC	thin layer chromatography
TNF	tumor necrosis factor
VCAM-1	vascular cell adhesion molecule-1
VLDL	very low density lipoprotein
WAT	white adipose tissue

WT	wild type
WTD	western type diet